A STABILIZED MIXED FINITE ELEMENT FORMULATION FOR FINITE STRAIN
DEFORMATION

by

Roxana Cisloiu

BS, Technical University "Gh.Asachi", Iasi, Romania, 1991

MS, West Virginia University, 2001

Submitted to the Graduate Faculty of

the School of Engineering in partial fulfillment

of the requirements for the degree of

Doctor of Philosophy

University of Pittsburgh

2006

UMI Number: 3223950

UMI®

UNIVERSITY OF PITTSBURGH

SCHOOL OF ENGINEERING

This dissertation was presented

by

Roxana Cisloiu

It was defended on

February 27, 2006

and approved by

Dr. Roy D. Marangoni, Associate Professor, Dept. of Mechanical Engineering

Dr. Laura Schaefer, Assistant Professor, Dept. of Mechanical Engineering

Dr. William S. Slaughter, Associate Professor, Dept. of Mechanical Engineering

Dissertation Advisor: Dr. Michael R. Lovell, Associate Professor, Dept. of Industrial
Engineering

ABSTRACT

A STABILIZED MIXED FINITE ELEMENT FORMULATION FOR FINITE STRAIN
DEFORMATION

Roxana Cisloiu, PhD

University of Pittsburgh, 2006

When improving the current state of technology in the finite element method, element formulation is a very important area of investigation. The objective of this dissertation is to develop a robust low-order tetrahedral element that is capable of meshing complicated geometries which cannot be meshed with standard brick elements. This element will be applicable to a large class of nonlinear materials that include nearly incompressible and incompressible materials and capable of analyzing small and large deformation as well as large rotations. Development of such an element will particularly benefit large strain metal-forming applications.

Linear tetrahedral elements are very practical for several reasons including their simplicity and efficiency. Despite their advantages, these elements have known shortcomings in their performance when applied to incompressible or nearly incompressible materials because of their tendency to lock. To overcome this problem a stabilized mixed formulation is proposed for tetrahedral elements that can be utilized in solid mechanics and large deformation problems.

An enhanced strain derived from a bubble function is added to the element to provide the necessary stabilization. The uniqueness of the proposed formulation lies within the fact that it does not require any geometric or material dependent parameters and no specific material model so that the formulation is completely general.

The element was implemented through a user-programmable element into the commercial finite element software, ANSYS. Using the ANSYS platform, the performance of the element was evaluated by different numerical investigations encompassing both small and large deformation, linear and nonlinear materials as well as near and fully incompressible conditions.

The element formulation was tested with several standard metal forming problems such as metal extrusion and punch forging that are known to experience difficulties during large deformations. The results were compared with analytical results or other available finite element results in the literature.

Finally, conclusions are drawn and possible future investigations are discussed such as the application of the new element in 3D rezoning, dynamic problems and anisotropic materials.

TABLE OF CONTENTS

LIST OF TABLES

LIST OF FIGURES

ACKNOWLEDGEMENTS

I have learnt a great deal from those who have taught me and worked with me over these years and I would like to gratefully acknowledge all of them.

First of all, I would like to thank my advisor, Dr. Michael Lovell, for his faith in me, for always encouraging me, for his enthusiastic and expert guidance. Without his support this work could not have been neither started nor completed.

My great appreciation also goes to wonderful people of ANSYS, Inc. and especially to Jin Wang who helped me with great patience at critical and opportune times. I am grateful to him for his thoughtful and creative comments and more generally for exploring with me the boundaries of professional friendship.

Many thanks to the committee members: Dr. Roy Marangoni, Dr. Laura Schaefer and Dr. William Slaughter.

I express my gratitude to the staff of the Mechanical Engineering Department and especially to Glinda Harvey who has been for me, not only the graduate administrator but always a very dear friend.

I am deeply indebted to my long standing friends – Matt Palamara, Sergey Sidorov, Raffaella de Vita, Brian Ennis, Zhaochun Yang, Jim Cordle and Jon Chambers and last, but not least, I should thank to my husband and son for their patience and forbearance whilst I have spent so much of our time working on this degree.

1. 0 INTRODUCTION

1.1 SIGNIFICANCE

Tetrahedral elements are very attractive because the most powerful mesh generators used today produce these elements. They are simple and less sensitive to distortion and their implementation leads to lower memory requirements and computational costs. Because of advances in hardware and parallel computations techniques, more complicated geometries are now being modeled. Meshing of these geometries becomes extremely difficult using quadrilateral and brick elements. The stringent necessity of a finite model that can easily interface with CAD models, together with the fact that triangular and tetrahedral meshes are very robust and fast, has brought about the need for developing high quality tetrahedral elements.

As noted in the literature, none of these elements developed to date perform well in all situations. Herein lies the main motivation of the proposed research. Standard displacement based finite elements lock in two different situations: bending (shear locking) and incompressible or near incompressible materials (volumetric locking). Constant strain tetrahedral elements show severe volumetric locking and stiff behavior in bending. Locking can generally be defined as the tendency for the finite element solution to approach zero because of restrictions in the medium being modeled (shear strain or incompressibility constraints). When expressed in a discrete form, locking is a condition of an over constrained system. In these situations the interpolation functions are incapable of representing the deformations that develop.

The interpolation functions should ensure that any anticipated constraints are handled without over restricting the system. Failure to do so causes solutions to lock which ultimately leads to erroneous results. Displacements are under predicted by factors of 5 to 10, making these elements completely useless [6]. Thus, in bending dominated problems, constant strain elements don't have the capacity to represent the curvature because of their lack of deformation modes resulting in a very stiff answer. This effect can be alleviated if the mesh is refined or if higher order elements are used; both of these solutions are detrimental to the computational time. The most difficult situation that cannot be solved by refining the mesh is the volumetric locking.

Under nearly incompressible (Poisson's ratio close to 0.5 or bulk modulus approaches infinity) and incompressible conditions, the displacements are not accurately predicted. The volumetric strain, which is determined from the derivatives of the displacements, will therefore not be accurately predicted. Any small error in the volumetric strain will transform into a larger error in the stresses and hydrostatic pressures, which in turn will have a detrimental effect on the displacements [4]. This is due to the fact that external loads are at any moment balanced by stresses via the principle of virtual work. To eliminate volumetric locking, two different techniques have evolved [6]. The first uses multi-field elements in which the pressures or the stresses and strain fields are considered as independent variables. The second uses the reduced integration procedures in which certain terms of the internal forces are under integrated. Both of these techniques have their own shortcomings. When multi-field methods are used, the resulting elements possess instabilities in the additional fields. The same shortcoming emerges from the reduced integration techniques as well. Over the last several years different strategies have been developed for reducing and avoiding the volumetric locking and pressure oscillations in finite element solutions.

Unfortunately, very few contributions in the area of element technology were sought to improve the performance of the linear tetrahedral elements. The focus has always been on stabilizing the low-order quadrilateral and hexahedral elements and it seems that only in the last three-four years some attention has been directed towards the simplex elements. Therefore there are very few publications related to the stabilization of triangular and tetrahedral elements and most of them are directed towards fluid elements [1, 7, 9-10, 17, 25, 29, 35-36, 41-42]. Among the few works of stabilizing these elements, some formulations address the problem of small deformations [14-16,30-33] and other apply only to hyperelastic materials [11-12, 27, 44] or J2 plasticity [15, 33, 38]. At present there is no formulation applicable to both general finite strain deformation and to a large class of nonlinear materials.

1.2 MOTIVATION AND OBJECTIVES

The increasing use of automated mesh generators and remeshers has triggered the need for accurate and efficient triangular and tetrahedral elements. This is especially true in the modeling of metal forming processes. At the present time, there is not a meshing program available that can discretize complex geometrical shapes of formed parts without using triangular and tetrahedral elements. Finite element models used in analyses of metal forming processes must be able to represent the nearly incompressible nature of elasto-plastic deformation of materials during forming. For this to be possible, the issue of volumetric locking has to be addressed since it can cause severe artificial stiffness that limits the flow of the material. Because linear triangles and tetrahedral elements developed with mixed formulations still suffer from volumetric locking and pressure instabilities, simulation of metal forming is somewhat limited [39-40].

3

As discussed in 1.1, special stabilizing techniques must be developed to avoid locking in these elements.

In this study a mixed enhanced strain formulation is proposed to specifically address the above issue. Hence, the following objectives will be attained in the present research project:

1. Develop a stabilization technique for the four-node tetrahedral element that will allow large deformation analyses to be performed with a large variety of nonlinear materials and in nearly incompressible and incompressible conditions. The stabilizing procedure will be based on the enhanced strain approach of R.Taylor [47] derived from a bubble function.

2. Implement the new formulation into a user programmable element that interfaces with the commercial finite element software, ANSYS.

3. Perform numerical investigations to assess the convergence and accuracy of the new element.

4. Use the developed elements to simulate metal forming processes.

1.3 NONLINEAR FINITE ELEMENT METHODS

For more than a decade, nonlinear finite element techniques have become popular in the analysis of metal forming, fluid-solid interaction and fluid flow problems. In recent years, the areas of biomechanics and electromagnetics have started to use nonlinear finite elements. Despite these efforts, there are still numerous intractable nonlinear problems for which solutions have not been obtained. A large segment of these problems can be categorized as large deformation problems that are applied to very complicated geometries and highly nonlinear materials.

A problem is defined as nonlinear if the force-displacement relationship depends on the current deformation state. Nonlinearities can arise from three different sources: material, geometry and nonlinear boundary conditions. Material nonlinearity results from the nonlinear relationship between stresses and strains. Nonlinearities caused by boundary conditions or loads can be found in contact and friction problems such as metal forming, gears, crash, and the interference of mechanical components. These problems are nonlinear because instantaneous changes in stiffness occur over time. Geometric nonlinearity results from the nonlinear relationship between strains and displacements on one hand, and the nonlinear relationships between stresses and forces on the other hand. This type of nonlinearity is mathematically well defined but quite difficult to solve numerically and includes problems such as large strain manufacturing, crash and impact phenomenon. As stated in section 1.2, the present research work will focus on a formulation for general finite strain deformation. This type of nonlinearity can be solved by three approaches: Lagrangian Formulation, Eulerian Formulation and Arbitrary Lagrangian-Eulerian Formulation (ALE) [6]. In the Lagrangian method the finite element mesh is attached to the material and moves through space along with it. It usually describes the deformation of structural elements. A shortcoming of this method is that the mesh distortion is as severe as the deformation of the object. Recent advances in adaptive meshing and rezoning have improved this problem. The Lagrangian approach can be classified into two categories: the Total Lagrangian method (TL) and the Updated Lagrangian method (UL). In TL the equilibrium is expressed with respect to the original undeformed state, which is the reference configuration. In the UL the current configuration acts as the reference state. Since the formulation being proposed in the present study applies to large deformations involving element distortions within ANSYS, the Updated Lagrangian formulation will be used.

2.0 LITERATURE REVIEW

2.1 MIXED FORMULATION METHODS

2.1.1 General Aspects

It was emphasized in section 1.1 that the main disadvantage of the low-order triangular and tetrahedral elements is the tendency to lock. One way to overcome volumetric locking is by employing multi-fields elements in which the pressures or stress and strain fields are considered as independent variables, and thus they are interpolated independently of the displacements.

Multi-field elements are formulated based on multi-field weak forms or variational principles, also known as mixed variational principles. These elements are designed only when specific constraints exist, such as incompressibility, and they are ineffective in the absence of such constraints.

In most cases including this study, the hydrostatic pressure is used as an additional independent field. This type of formulation is also known as a mixed u/p formulation. In the mixed u/p formulation, the pressure is obtained at global level instead of being calculated from volumetric strain. In such an approach the solution accuracy is independent of Poisson's ratio or bulk modulus.

The main features of a mixed formulation according to [49] are:

1) The continuity requirements on the shape functions are different. The additional variable can be discontinuous in or between elements as no derivatives of this are present.

2) If the focus is more on the additional variable then an improved approximation can result in a higher accuracy than was obtained for the pure displacement formulation.

3) The equations resulting from mixed formulations often have zero diagonal terms. This constitutes a significant problem since the Gaussian elimination process used in element solution becomes unstable.

4) The additional number of variables enlarges the size of the algebraic problem but this disadvantage can be dealt with by suitable iterative methods.

The greatest concern of these mixed methods that was not mentioned above is their <u>stability</u>. This will be discussed in the next section.

2.1.2 Stability of Mixed Methods: The Patch Test.

The main problem of the mixed methods is choosing the interpolation function for the additional variable, which in our case is the hydrostatic pressure. It was shown mathematically [4] that for certain choices of the shape functions, the mixed formulations do not yield meaningful results.

This mathematical criterion, which expresses the requirement related to the shape functions in mixed formulations, is often called the Ladyzhenskaya-Babuška-Brezzi condition (LBB condition) [4]. To establish if this condition is satisfied for an element is a very difficult task because the formulation of this condition has a very mathematical character. Thus, experts in this area tried to replace this condition with a more simple procedure for determining whether the condition is satisfied. One such condition, called the constraint count condition, has proven to be

very effective in determining if an element performs well in incompressible and nearly incompressible situations [26]. It is not a precise mathematical condition but rather a quick and simple way of verifying an element.

According to [49], if we consider the displacement variable as the primary variable and the additional variable as the constraint variable then the stability of an element can be obtained if this condition is satisfied for any isolated patch on the boundaries of which we constrain the maximum number of primary variables and the minimum number of constraint variables.

If n_u represent the total number of displacement equations after imposing the boundary conditions and n_p represents the total number of incompressibility constraints then the constrained ratio is defined as $r = \dfrac{n_u}{n_p}$. This ratio should mimic the behavior of the ratio between the number of equilibrium equations and the number of incompressibility conditions for the governing system of partial differential equations. In two dimensions the ideal value would be r =2/1=2, and for three dimensions r =3/1=3. A value of r less than the ideal value indicates the tendency to lock. If $r ≤ 1$ there are more constraints of the pressure than there are displacements degrees of freedom available and severe locking is anticipated. A value much larger than the ideal value indicates that not enough incompressibility constraints are present so this condition will be poorly approximated.

Mixed displacement-pressure formulations with equal order of interpolation for both u and p do not pass the Babuška-Brezzi conditions unless special stabilization techniques are used. The main goal in the element technology is to produce more efficient codes and this is possible only if the interpolation spaces of displacement and pressure coincide.

This motivated an extensive research effort to find formulations which would make it possible to circumvent the LBB condition and use equal order interpolation functions. This category is called stabilized mixed methods and is treated extensively in 2.3.

For shortness reasons, only the linear elastic mixed u/p and u/p/ε_v formulations of Zienkwicz and Taylor [49] will be presented in the next sections as they serve as a basis of the mixed enhanced strain formulation developed in this study.

2.1.3 Two-Field Mixed Formulation

The main problem in the application of a pure displacement formulation to incompressible and nearly incompressible problem lies in the determination of the hydrostatic pressure, which is related to the volumetric part of the strain (for isotropic materials). Mixed formulations are based on decomposing the stress tensor into its deviatoric and hydrostatic components.

$$\boldsymbol{\sigma} = \mathbf{s} + \mathbf{pI}$$
$$\sigma_{ij} = s_{ij} + p\delta_{ij} \tag{2.1}$$

where s_{ij} is the deviatoric stress and $p = \dfrac{1}{3} tr(\sigma)$. $\tag{2.2}$

The constitutive relation linking s_{ij} and the strain tensor is supplemented by a constraint equation relating the pressure and the volumetric strain $\varepsilon_v = \varepsilon_{ii} = \delta_{ij}\varepsilon_{ij}$. $\tag{2.3}$

In the case of elastic materials,

$$\varepsilon_v = \frac{p}{K} \tag{2.4}$$

where K is the bulk modulus of the material related with Poisson's ratio by

$$K = \frac{E}{3(1-2\nu)} \tag{2.5}$$

In the incompressible limit, $v=0.5$ and $K=\infty$ and the equation (2.4) becomes

$$\varepsilon_v = 0 \tag{2.6}$$

The deviatoric strain is expressed as $\varepsilon_{ij}^{dev} = \varepsilon_{ij} - \dfrac{1}{3}\delta_{ij}\varepsilon_v$ $\qquad$ (2.7)

Equilibrium and Virtual Work

Many engineering problems can be solved by finding an approximate (finite element) solution for the displacements, deformations, stresses, forces, and other state variables in a solid body that is subjected to a loading history. The exact solution of such a problem requires that both force and moment equilibrium be maintained at all times over any arbitrary volume of the body.

Let V be the volume occupied by a part of the body in the current configuration and S the surface bounding this volume. Let the surface traction at any point on S be the force **t** per unit of current area and let the body force at any point in the volume be **b** per unit current volume. Force equilibrium for the volume is then:

$$\int_S \mathbf{t}dS + \int_V \mathbf{b}dV = 0 \tag{2.8}$$

The true or Cauchy stress matrix $\boldsymbol{\sigma}$ is defined by $\quad \mathbf{t} = \mathbf{n} \cdot \boldsymbol{\sigma}$ $\qquad$ (2.9)

where **n** is the unit outward normal to S at the point. Using (2.9) and applying the Green's theorem we can rewrite (2.8) as

$$\left(\frac{\partial}{\partial x}\right) \cdot \boldsymbol{\sigma} + \mathbf{b} = 0 \tag{2.10}$$

The moment equilibrium equation leads to the results that the true Cauchy stress matrix must be symmetric: $\boldsymbol{\sigma} = \boldsymbol{\sigma}^{\mathbf{T}}$.

The basis for the development of any finite element formulation is the introduction of some locally based spatial approximations to parts of the solution.

To develop such an approximation we replace the equilibrium equation (2.10) by an equivalent "weak form"- a single scalar equation over the entire body which is obtained by multiplying the point wise differential equation by an arbitrary, vector-valued "test function" and integrate it. The test function can be imagined as an arbitrary "virtual" displacement field, $\delta\mathbf{u}$, which is completely arbitrary except that it must obey any prescribed kinematic constraints and have sufficient continuity. The dot product of this test function with the equilibrium equation results in a single scalar equation that is integrated over the entire body to represent the <u>principle of virtual work</u>. This statement has a very simple physical interpretation: the work done by the external forces subjected to any virtual displacement field is equal to the work done by the equilibrating stresses on the deformation of the same displacement field.

$$\int_V \delta\boldsymbol{\varepsilon}^{\mathrm{T}}\boldsymbol{\sigma}\,dV - \int_V \delta\mathbf{u}^{\mathrm{T}}\mathbf{b}\,dV - \int_S \delta\mathbf{u}^{\mathrm{T}}\mathbf{t}\,dS = 0 \tag{2.11}$$

with $\boldsymbol{\sigma} = \mathbf{C}\boldsymbol{\varepsilon}$ as the constitutive relation and the deviatoric part as $s_{ij} = D_{ijkl}\varepsilon_{kl}^{dev}$

Now the **equilibrium equation** is rewritten using (2.1) and treating p as an independent variable

$$\int_V \delta\varepsilon_{ij}s_{ij}\,dV + \int_V \delta\varepsilon_v\,p\,dV - \int_V \delta u_i b_i\,dV - \int_S \delta u_i t_i\,dS = 0, i = 1,2,3 \tag{2.12}$$

and in addition we shall impose a weak form of (2.4), i.e. the **pressure constitutive equation**:

$$\int_V \delta p(\varepsilon_v - \frac{p}{K})\,dV = 0 \tag{2.13}$$

<u>Matrix Formulation</u>

Substituting now the independent approximations of $u, p, \delta u, \delta p$ as

$$\mathbf{u} \approx \mathbf{N}_u\mathbf{u}^{\mathrm{e}}, \delta\mathbf{u} \approx \mathbf{N}_u\delta\mathbf{u}^{\mathrm{e}} \quad \text{and} \quad \mathbf{p} \approx \mathbf{N}_{\mathbf{p}}\mathbf{p}^{\mathrm{e}}, \delta\mathbf{p} \approx \mathbf{N}_{\mathbf{p}}\delta\mathbf{p}^{\mathrm{e}} \tag{2.14}$$

where $\mathbf{N} = \left[N^A N^B, ... N^N\right]^T$ are the interpolation functions for displacements and

$\mathbf{u}^e = \left[\mathbf{u}^A \mathbf{u}^B, ... \mathbf{u}^N\right]^T, \delta\mathbf{u}^e = \left[\delta\mathbf{u}^A \delta\mathbf{u}^B, ... \delta\mathbf{u}^N\right]^T, \mathbf{p}^e = \left[\mathbf{p}^A \mathbf{p}^B, ... \mathbf{p}^N\right]^T, \delta\mathbf{p}^e = \left[\delta\mathbf{p}^A \delta\mathbf{p}^B, ... \delta\mathbf{p}^N\right]^T$

are the displacements, virtual displacements, pressure, and virtual pressures at each node.

If we insert the above relations in the weak form (2.12) and (2.13) and make use of the Lemma of calculus of variations we get the element wise linear equations system:

$$\begin{bmatrix} \mathbf{K}_{uu} & \mathbf{K}_{up} \\ \mathbf{K}_{pu} & \mathbf{K}_{pp} \end{bmatrix}^e \begin{bmatrix} \mathbf{u} \\ \mathbf{p} \end{bmatrix}^e = \begin{bmatrix} \mathbf{R} \\ \mathbf{0} \end{bmatrix}^e \qquad \text{where} \tag{2.15}$$

$$\mathbf{K}_{uu}^e = \int_V \mathbf{B}^T \mathbf{D} \mathbf{B} dV \tag{2.16}$$

is the element stiffness matrix that connects the displacements through the differential operator of the shape functions, **B,** and the deviatoric part of the material constitutive matrix **D,**

$$\mathbf{K}_{up}^e = (\mathbf{K}_{pu}^e)^T = \int_V (\nabla N_u) \mathbf{N}_p dV \tag{2.17}$$

are the mixed terms depending on displacements as well as on the pressures, with

$$\nabla N_u = \left[\mathbf{N}_{,1} \, \mathbf{N}_{,2} ... \mathbf{N}_{,ND}\right]^T \tag{2.18}$$

$$\mathbf{K}_{pp}^e = \int_V \mathbf{N}_p^T \frac{1}{K} \mathbf{N}_p dV \tag{2.19}$$

is the term which depends only on the pressure.

$$\mathbf{R} = \int_V \mathbf{N}_u^T \mathbf{b} dV + \int_S \mathbf{N}_u^T \mathbf{t} dS \tag{2.20}$$

If incompressibility exists, the pressure term becomes zero.

The fundamental problem now relates to finding effective interpolation functions for both displacements and pressures so that accurate finite element solutions are obtained.

2.1.4 Three-Field Mixed Formulation

For many constitutive models such as hyperelasticity that can have multiple deformation states for the same stress level it is more convenient to use a three-field variational form [47, 49].

This formulation is more general and more suitable for anisotropic, inelastic materials and finite deformation problems. It employs approximations of displacement, pressure and strain.

The use of this type of approximation has led to successful lower-order quadrilateral or hexahedral elements that can be used in nearly incompressible cases for a large class of materials.

Assuming an independent approximation for the hydrostatic pressure, p, and the volumetric strain, ε_v, the same problem as in 2.1.3 can be formulated by introducing two constraint equations with two Lagrange multipliers in the principle of virtual work. Thus, if the two constraints are:

$$\varepsilon_v = \varepsilon_x + \varepsilon_y + \varepsilon_z = \mathbf{1}^{\mathrm{T}}\boldsymbol{\varepsilon} \text{ where } \mathbf{1} = [1,1,1,0,0,0]^T \tag{2.21}$$

$$\varepsilon_v = \frac{p}{K} \tag{2.22}$$

the principle of virtual work can be expressed by (2.12) and the two additional weak statements of equations (2.21) and (2.22) written as:

$$\begin{aligned}
&\int_V \delta p(\mathbf{1}^{\mathrm{T}}\boldsymbol{\varepsilon} - \varepsilon_v)dV = 0 \\
&\int_V \delta\varepsilon_v(K\varepsilon_v - p)dV = 0
\end{aligned} \tag{2.23}$$

Then, using finite element approximations for $\boldsymbol{u}$ and p fields from (2.14) and

$$\varepsilon_v \approx N_v \varepsilon_v^e \tag{2.24}$$

a mixed approximation is obtained in the following matrix formulation:

13

$$\begin{bmatrix} \mathbf{K}_{uu} & \mathbf{K}_{up} & 0 \\ \mathbf{K}_{up}^{T} & 0 & -\mathbf{K}_{pv} \\ 0 & -\mathbf{K}_{pv}^{T} & \mathbf{K}_{vv} \end{bmatrix} \begin{bmatrix} \mathbf{u} \\ \mathbf{p} \\ \boldsymbol{\varepsilon}_{v} \end{bmatrix}^{e} = \begin{bmatrix} \mathbf{R} \\ 0 \\ 0 \end{bmatrix}^{e} \tag{2.25}$$

where $\mathbf{K}_{uu}, \mathbf{K}_{up}$ and $\mathbf{R}$ are the same as in (2.16), (2.17) and (2.19) and,

$$\begin{aligned} \mathbf{K}_{pv} &= \int_{V} \mathbf{N}_{v}^{T} \mathbf{N}_{p} dV \\ \mathbf{K}_{vv} &= \int_{V} \mathbf{N}_{v}^{T} \mathbf{K} \mathbf{N}_{v} dV \end{aligned} \tag{2.26}$$

Usually $\mathbf{N}_v$ is identical with $\mathbf{N}_p$ so that $\mathbf{K}_{pv}$ is symmetric positive definite. In the case when $\mathbf{p}$ is continuous and $\boldsymbol{\varepsilon}_v$ is discontinuous the volumetric strain can be eliminated from the third equation leading to a system of equations in only two unknowns, $\mathbf{u}$ and $\mathbf{p}$.

2.2 REVIEW OF STABILIZED MIXED METHODS

Stabilized finite element methods were initially developed for application in the Galerkin finite element method to solve problems in engineering and mathematics that produce numerical approximations that didn't have the stability properties of the continuous problem. Stabilized methods attempt to improve the stability behavior without compromising accuracy.

Incompressible fluid dynamics have always been the front line of research in this area. Several approaches have achieved success and have been extended to the solid mechanics as well. Some of them are demonstrated to be related under specific conditions [30] but they can be generally classified into the following categories:

1) Stabilization by employing finite element approximations enriched with so-called "bubble" functions.

2) Stabilization by adding mesh-dependent perturbation terms, which depend on the residuals of the governing equation.

3) Mixed-enhanced strain stabilization

4) Orthogonal sub-grid scale method (OSGS)

5) Finite increment calculus (FIC)

All the methods, with the exception of 1) and 3), utilize a weighting parameter that is applied to the additional terms. Other approaches are average nodal pressures [21-22], average nodal deformation gradient techniques [15], or composite elements [48] but they are not of great interest to the proposed research since they will be hard to implement into commercial finite element software. Each of these methods will be discussed in the next sections.

2.2.1 Bubble Stabilization

The first effort to stabilize the low–order elements was the "MINI" element introduced by Arnold, Brezzi and Fortin in [3]. This is an attractive linear triangle with a displacement interpolation enhanced with a cubic bubble function. This element has three external degrees of freedom per vertex (two displacements and one pressure) and an equivalent internal node due to the bubble function with two degrees of freedom (displacements) (see Figure 1). The bubble function is a higher order polynomial that vanishes on the boundary of the element and is equal to unity in the center of the triangle. Such a bubble function can be written in terms of area coordinates as:

$$N_e(\xi) = 27\xi_1\xi_2\xi_3 \tag{2.27}$$
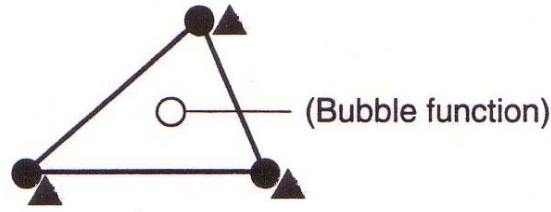
Figure 1. Linear displacement/linear pressure triangle with bubble function

The displacement field with the bubble function can be approximated as:

$$\mathbf{u} \approx \sum_i N_i u_i + N_e u_e \tag{2.28}$$

where u_i are the nodal displacements and u_e are internal parameters. Similarly, the pressures are interpolated as:

$$\mathbf{p} \approx \sum_i N_i p_i \tag{2.29}$$

For the linear triangle and tetrahedral element the shape functions are the area, respectively the

volume coordinates $N_i = \xi_i$ (2.30)

Because the internal parameters are defined separately for each element, a partial solution can

be performed at the element level to obtain a set of equations in terms of external degrees of

freedom as discussed in the mixed u/p formulation.

<u>Advantages</u> of using bubble function:

- Satisfies LBB condition and the mixed patch test

- Few degrees of freedom

- Easy to implement in large strain deformation because it does not require the introduction

  of other parameters

Disadvantages:

- Only marginally stable

- This element might not be robust enough since in many tests the pressure solution still had small amplitude oscillations.

- In transient problems, the accelerations will also involve the bubble mode and will affect the inertial terms.

2.2.2 Stabilization by Adding Mesh-Dependent Terms

The idea of this method is to modify the discrete equations instead of the interpolation functions.

The simplest form of this type of stabilization is to add a non-zero diagonal term through a penalty-like term in the pressure constitutive equation. This was first introduced by Brezzi and Pitkaranta in [11] for stabilizing the finite element approximation of Stokes problem. Numerous other alternatives of this method have been developed [23-25, 29-30, 43-44]. Recalling from section 2.1.3, the splitting of the Cauchy stress into the deviatoric and volumetric parts as:

$$\boldsymbol{\sigma} = \mathbf{s} + \mathbf{pI}$$
$$\sigma_{ij} = s_{ij} + p\delta_{ij} \tag{2.31}$$

and noting that the deviatoric stress is related to the deviatoric strain through the relation:

$$s_{ij} = 2G\varepsilon_{ij}^{dev} = G\left(\frac{\partial u_i}{\partial x_j} + \frac{\partial u_j}{\partial x_i} - \frac{2}{3}\delta_{ij}\frac{\partial u_k}{\partial x_k}\right) \tag{2.32}$$

The equilibrium equations in the absence of inertial forces are:

$$\frac{\partial s_{ij}}{\partial x_j} + \frac{\partial p}{\partial x_i} + b_i = 0 \tag{2.33}$$

Substituting the constitutive equation for the deviatoric part (2.32) into (2.33)

$$G\left(\frac{1}{3}\frac{\partial^2 u_i}{\partial x_j \partial x_i} + \frac{\partial^2 u_j}{\partial x_i \partial x_i}\right) + \frac{\partial p}{\partial x_i} + b_i = 0 \tag{2.34}$$

or in tensor form:

$$G\left(\frac{1}{3}\nabla(\nabla \cdot \mathbf{u}) + \nabla^2 \mathbf{u}\right) + \nabla p + \mathbf{b} = 0$$

where ∇^2 is the Laplacian operator and ∇ is the gradient operator.

The pressure constitutive equation in terms of displacement is:

$$\varepsilon_v = \nabla \cdot \mathbf{u} = \frac{p}{K} \tag{2.35}$$

Taking the divergence of the equilibrium equation (2.34) and using (2.35) we obtain:

$$\left(1 + \frac{4G}{3K}\right)\nabla^2 p + \nabla \cdot \mathbf{b} = 0 \tag{2.36}$$

This equation was used to construct the additional term for the weak form, which would otherwise be zero. Brezzi and Pitkaranta [11] added a weighted form and set the body force to zero for simplicity. Then, they integrated by parts and ignored the boundary terms to obtain a more attractive form of the pressure constitutive equation:

$$\int_V \delta p \left(\mathbf{1}^T \boldsymbol{\varepsilon} - \frac{p}{K}\right) dV + \beta \int_{V_e} \frac{\partial \delta p}{\partial x_i} \frac{\partial p}{\partial x_i} dV = 0 \tag{2.37}$$

From dimensional considerations with the first term, the parameter β should have a value proportional to L^4/F where L is length and F is force.

In the work of Hughes *et al.*[29], β is given in terms of the characteristic element length *h* and a non negative, non dimensional stability parameter, α as:

$$\beta = -\frac{\alpha h^2}{2G} \tag{2.38}$$

This method and alternatives to it have been applied to incompressible linear elasticity and to the Stokes flow [9-10, 12, 23-25, 29-30, 43]. The above formulation was extended to finite deformation by O. Klaas *et al* [31] and applied to a linear displacement, linear pressure tetrahedral element. They provide a formulation for finite elasticity in both reference and current configuration, which is then linearized to allow an implementation in a Newton-Raphson scheme. Their formulation can be used for the hyperelastic materials.

Advantages

- No oscillations in the stress field

- Stress concentrations are well approximated

Disadvantages

- Addition of the non-zero diagonal terms does not have a strong theoretical foundation

- Requires the choice of a parameter

- Depends on the element length (maximum edge length) which also changes under the large deformation assumption

- Depends also on the material through the shear modulus

2.2.3 Mixed Enhanced Strain Stabilization

This method is presented in Zienkiewicz and Taylor [49] and applied by R. Taylor [47] to a low-order tetrahedral element in both small deformation and finite deformation. It uses a three-field approximation involving continuous u, p and discontinuous volume change ε_v together with an enhanced strain formulation. The enhanced strains are added to the regular strains to provide the necessary stabilization for the nearly incompressible case. His formulation starts from the functional and takes into consideration a hyperelastic material for which a strain energy function

exists. This approach though is no longer valid for materials for which we cannot define a strain energy function.

Small deformation case

Splitting the strain into their deviatoric and volumetric components, the mixed strain can be written as:

$$\mathbf{\varepsilon} = \mathbf{\varepsilon}^{\text{dev}} + \frac{1}{3}\mathbf{1}\varepsilon_v \qquad (2.39)$$

The functional, its variation and then linearization are given as:

$$\Pi(\varepsilon,\varepsilon_v,p) = \int_V \left[W(\varepsilon) + p(1^T \varepsilon - \varepsilon_v) \right] dV + \Pi_{ext} = Stationary$$

$$\delta\Pi = \int_V \left[\left(\delta\mathbf{\varepsilon}^{\text{dev}} + \frac{1}{3}\mathbf{1}\delta\varepsilon_v \right)^T \mathbf{\sigma} + \delta p(\mathbf{1}^T\varepsilon - \varepsilon_v) + (\mathbf{1}^T\delta\mathbf{\varepsilon} - \delta\varepsilon_v)p \right] dV + \delta\Pi_{ext} = 0$$

$$d(\delta\Pi) = \int_V \left[\left(\delta\mathbf{\varepsilon}^{\text{dev}} + \frac{1}{3}\mathbf{1}\delta\varepsilon_v \right)^T \mathbf{D} \left(d\mathbf{\varepsilon}^{\text{dev}} + \frac{1}{3}\mathbf{1}d\varepsilon_v \right) + \delta p(\mathbf{1}^T d\varepsilon - d\varepsilon_v) + (\mathbf{1}^T\delta\mathbf{\varepsilon} - \delta\varepsilon_v)dp \right] dV + d\delta\Pi_{ext} = 0$$

Matrix Formulation

The displacement, pressure, and volume change in each element are written using the interpolation functions in terms of volume coordinates, ξ, and corresponding nodal values as:

$$\mathbf{u}(\xi) = \xi_\alpha \hat{\mathbf{u}}^\alpha = \mathbf{N}\hat{\mathbf{u}}$$
$$p(\xi) = \xi_\alpha \hat{p}^\alpha = \mathbf{N}\hat{\mathbf{p}} \qquad (2.40)$$
$$\varepsilon_v(\xi) = \xi_\alpha \hat{\varepsilon}_v^\alpha = \mathbf{N}\hat{\mathbf{\varepsilon}}_v$$

Strains are computed using the strain-displacement matrix as: $\mathbf{\varepsilon}(\xi) = \mathbf{B}_\alpha(\xi)\hat{\mathbf{u}}^\alpha$ (2.41)

An enhanced strain formulation is considered as

$$\mathbf{\varepsilon}_e(\xi) = \mathbf{B}_e(\xi)\hat{\mathbf{u}}^e \qquad (2.42)$$

where $\hat{\mathbf{u}}^e$ are the enhanced strain parameters and $\mathbf{B}_e(\xi)$ is obtained from the derivatives of a

bubble mode $\qquad\qquad\qquad N_e(\xi) = \xi_1\xi_2\xi_3\xi_4$ (2.43)

Thus, the mixed strain is:

$$\varepsilon = \mathbf{I}^{\text{dev}}(\mathbf{B_u}\hat{\mathbf{u}} + \mathbf{B_e}\hat{\mathbf{u}}^{\mathbf{e}}) + \frac{1}{3}\mathbf{1}\varepsilon_v \tag{2.44}$$

Replacing all these approximations in the linearized variation of the functional we obtain a linear system of equations with four unknown increments of displacements, enhanced strain parameters, pressures and volumetric changes.

The tangent tensor is:

$$\mathbf{K} = \begin{bmatrix} \mathbf{K_{uu}} & \mathbf{K_{ue}} & \mathbf{K_{up}} & \mathbf{K_{uv}} \\ \mathbf{K_{ue}}^{\mathbf{T}} & \mathbf{K_{ee}} & \mathbf{K_{ep}} & \mathbf{K_{ev}} \\ \mathbf{K_{up}}^{\mathbf{T}} & \mathbf{K_{ep}}^{\mathbf{T}} & \mathbf{0} & \mathbf{K_{pv}} \\ \mathbf{K_{uv}}^{\mathbf{T}} & \mathbf{K_{ev}}^{\mathbf{T}} & \mathbf{K_{pv}}^{\mathbf{T}} & \mathbf{K_{vv}} \end{bmatrix} \tag{2.45}$$

$$\mathbf{K_{uu}} = \int_{V_e} \mathbf{B_u^T}\mathbf{I_{dev}}\mathbf{DI_{dev}}\mathbf{B_u}dV$$

$$\mathbf{K}_{up} = \int_{V_e} \mathbf{B_u^T}\mathbf{1N}dV$$

$$\mathbf{K_{uv}} = \int_{V_e} \mathbf{B_u^T}\frac{1}{3}\mathbf{I_{dev}}\mathbf{D1N}dV \tag{2.46}$$

$$\mathbf{K}_{pv} = -\int_{V_e} \mathbf{N^T N}dV$$

$$\mathbf{K}_{vv} = \int_{V_e} \mathbf{N^T}\frac{1}{9}\mathbf{1^T}\mathbf{D1N}dV$$

The terms involving the enhanced modes are similar to K_{uu}, K_{up}, K_{uv} but they have $\mathbf{B_e}$ instead of $\mathbf{B_u}$.

Finite Elasticity Case

$$\Pi = \int_V \left[W(\mathbf{C}) + p(J - \varepsilon_v) \right]dV + \Pi_{ext} = Stationary$$

$$\delta\Pi = \int_V \left[\frac{\partial W}{\partial \mathbf{C}} : \delta\mathbf{C} + \delta p(J - \varepsilon_v) + (\delta J - \delta\varepsilon_v)p \right]dV + \delta\Pi_{ext} = 0 \tag{2.47}$$

$$\Delta(\delta\Pi) = \int_V \left[\delta\mathbf{C} : \frac{\partial^2 W}{\partial\mathbf{C}\partial\mathbf{C}} : \Delta\mathbf{C} + \Delta(\delta\mathbf{C}) : \frac{\partial W}{\partial\mathbf{C}} \right] dV + \int_V p\Delta(\delta J) dV + \int_V \delta p(\Delta J - \Delta\varepsilon_v) dV +$$
$$+ \int_V (\delta J - \delta\varepsilon_v)\Delta p \, dV + d\delta\Pi_{ext} = 0$$

The tangent terms resulting from the first two integrals can be split into a constitutive part and a geometric part. The terms involving the enhanced strains will be replaced with the appropriate terms and will have the same form as those involving regular strains.

$$\mathbf{K}^c_{uu} = \int_{V_e} \mathbf{B}^T_u \left[\mathbf{I}_{dev}\mathbf{D}\mathbf{I}_{dev} - \frac{2}{3}\left(\mathbf{1}\sigma^T_{dev} + \sigma_{dev}\mathbf{1}^T\right) + 2\left(\frac{1}{3}\mathbf{1}^T\sigma - \frac{J}{\varepsilon_v}p\right)\mathbf{II} - \left(\frac{2}{9}\mathbf{1}^T\sigma - \frac{J}{\varepsilon_v}p\right)\mathbf{11}^T \right] \mathbf{B}_u dV$$

$$\mathbf{K}^g_{uu} = \int_V \left[\nabla\mathbf{N} : \left(\sigma + \left(\frac{1}{3}\mathbf{1}^T\sigma - \frac{J}{\varepsilon_v}p\right)\mathbf{1}\right)(\nabla\mathbf{N}) \right] \mathbf{I}\varepsilon_v dV$$

$$\mathbf{K}_{up} = \int_{V_e} \mathbf{B}^T_u \mathbf{1}\mathbf{N}J dV$$

$$\mathbf{K}_{uv} = \int_{V_e} \mathbf{B}^T_u \left(\frac{1}{3}\mathbf{I}_{dev}\mathbf{D}\mathbf{1} + \frac{2}{3}\sigma_{dev}\right)\mathbf{N} dV$$

$$\mathbf{K}_{pv} = -\int_{V_e} \mathbf{N}^T\mathbf{N} dV$$

$$\mathbf{K}_{vv} = \int_{V_e} \mathbf{N}^T\left(\frac{1}{9}\mathbf{1}^T\mathbf{D}\mathbf{1} - \frac{1}{9}\mathbf{1}^T\sigma\right)\mathbf{N}\varepsilon_v dV$$

(2.48)

If the interpolation for u and p is continuous in the whole domain and the volumetric change is piece wise continuous, the solution can be performed by using static condensation at the element level. After eliminating u^e and ε_v, a system of equations in incremental nodal displacements and pressures has to be solved.

Advantages

-   Results are free of pressure oscillations

-   Enhanced terms are material and mesh independent

-   Applies to incompressible elastic, hyperelastic materials and to both small and large deformations

Disadvantages

- Increased computational cost due to the introduction of the additional variables but compensated by the possibility of performing static condensation

- Behaves poorer in bending than mixed hexahedral elements with discontinuous pressure and volume change

- Exhibits some locking tendency in bending

2.2.4 Orthogonal Sub-Grid Scale Method

The sub-grid scale approach was proposed first by Hughes [30]. More recently the method of orthogonal sub-grid scale was introduced by Codina [20] and has been applied to incompressible fluid dynamics. Chiumenti et al. extended this method to solid mechanics in the context of incompressible elasticity [19] and J2 plasticity [17-18]. An equal order interpolation is used for both the displacement and pressure. The basic idea of the method is to decompose the continuous fields into a coarse component and a fine component, corresponding to different scales. Since the solution of the problem contains components from both scales it is necessary that the finite element approximation include the effect of both scales. The coarse scale can be solved by a standard finite element interpolation, which cannot solve the fine scale. For the problem to be stable the effect of the fine scale has to be taken into consideration.

Thus, the displacement field can be approximated as;

$$\mathbf{u} = \mathbf{u_h} + \widetilde{\mathbf{u}} \tag{2.49}$$

and the deviatoric stresses can be split into two corresponding contributions as:

$$\mathbf{s} = \mathbf{s_h} + \widetilde{\mathbf{s}} \tag{2.50}$$

This results in the following mixed formulation in the weak form as:

$$\int_V (\delta\mathbf{u_h} + \delta\tilde{\mathbf{u}})(\nabla \cdot (\mathbf{s_h} + \tilde{\mathbf{s}}))dV + \int_V (\delta\mathbf{u_h} + \delta\tilde{\mathbf{u}})\nabla p\, dV + \int_V (\delta\mathbf{u_h} + \delta\tilde{\mathbf{u}})\mathbf{b}\, dV = 0$$

$$\int_V \delta p(\nabla \cdot (\delta\mathbf{u_h} + \delta\tilde{\mathbf{u}}))dV = 0 \tag{2.51}$$

which integrated by parts yields three equations of which one is related to the fine scale:

$$\int_V (\nabla^s \delta\mathbf{u_h})(\mathbf{s_h})dV + \int_V (\nabla^s \delta\mathbf{u_h})(\tilde{\mathbf{s}})dV + \int_V (\nabla \cdot \delta\mathbf{u_h})(p)dV - \int_V (\delta\mathbf{u_h})\mathbf{b}\, dV - \int_V (\delta\mathbf{u_h})\mathbf{t}\, dV = 0$$

$$\int_V (\delta\tilde{\mathbf{u}})(\nabla \cdot \mathbf{s_h})dV + \int_V (\delta\tilde{\mathbf{u}})(\nabla \cdot \tilde{\mathbf{s}})dV + \int_V (\delta\tilde{\mathbf{u}})\mathbf{b}\, dV = 0 \tag{2.52}$$

$$\int_V \delta p(\nabla \cdot \mathbf{u_h})dV + \int_V \delta p(\nabla \cdot \tilde{\mathbf{u}})dV = 0$$

The first equation solves the balance of momentum and includes a stabilization term which depends on the sub-grid stresses. For linear elements this term is zero. The third equation enforces the incompressibility condition and has a stabilization term that depends on the sub-grid scale. The second equation is completely defined in the sub-grid scale and cannot be solved by the finite element mesh. To find the sub-grid displacements that are introduced in the second stabilization term, Codina proposed to look in the space orthogonal to the finite element space.

Such a method has already been applied with success in fluid mechanics. From the second equation, it should be noted that these displacements are driven by the residual of the coarse scale and thus they can be expressed as:

$$\tilde{\mathbf{u}}_e = \tau_e\left(\nabla p - P_h(\nabla p)\right) \tag{2.53}$$

where $\pi_h = P_h(\nabla p)$ is the projection of the gradient of pressure onto the finite element space and τ_e is the same as β from section 2.2.2. Thus the final formulation becomes:

$$\int_V \left(\nabla^s \delta \mathbf{u_h}\right)\left(\mathbf{s_h}\right)dV + \int_V \left(\nabla \cdot \delta \mathbf{u_h}\right)\left(p\right)dV - \int_V \left(\delta \mathbf{u_h}\right)\mathbf{b}\,dV - \int_V \left(\delta \mathbf{u_h}\right)\mathbf{t}\,dV = 0$$

$$\int_V \delta p \left(\nabla \cdot \mathbf{u_h}\right)dV - \sum_{e=1}^{n_{elem}} \tau_e \left(\nabla \delta p \cdot \left[\nabla p - \pi_h\right]\right) = 0 \qquad (2.54)$$

$$\int_V \delta \pi_h \left(\nabla p - \pi_h\right)dV = 0$$

It is important to note that no stabilization term appears in the first equation for low-order elements and the only stabilization term appears in the incompressibility equation.

The tangent stiffness matrix is:

$$\mathbf{K}_e = \begin{bmatrix} K_{uu} & K_{up} & 0 \\ K_{up}^T & -\tau_e K_{pp} & \tau_e K_{up}^T \\ 0 & \tau_e K_{up} & -\tau_e K_{\pi\pi} \end{bmatrix} \qquad (2.55)$$

Advantages:

- Circumvents the strict LBB condition

- Results are free of volumetric locking and pressure oscillations and comparable qualitatively to the mixed quadrilateral and hexahedron.

- Correct failure mechanisms with localized patterns of plastic deformations are obtained which show that the method is not influenced by the mesh directional bias.

Disadvantages:

- The formulation is applicable only for small deformation.

- Requires a parameter depending on element length and shear modulus which makes the formulation hard to extend to finite deformation case.

- Introduces a new field variable, Π_h which is continuous and therefore the static condensation procedure cannot be performed at element level.

2.2.5 Finite Increment Calculus Method

The FIC method is a completely different approach in stabilizing the mixed u/p elements, but yields the same formulation as the previous discussed method (OSGS). The basis of the FIC formulation is the satisfaction of the standard equations of equilibrium in a domain of finite size by expressing the different terms of the differential equation using a Taylor expansion series and retaining the higher order terms.

The resulting equations are enhanced with some additional terms, which introduce the necessary stability to overcome the volumetric locking. This method was first developed by Onate for advective-diffusive and fluid flow problems [33] and was later applied to incompressible solids in [34-36].

This method allows the use of linear triangle and tetrahedral in quasi-incompressible and fully incompressible solid problems. For any problem in mechanics, the equations expressing balance of momentum, mass, heat, etc. can be written in a domain of finite size with h as the characteristic length. By expanding the balance equation in Taylor expansion and retaining the lower order term, we get:

$$r_i - \frac{h_k}{2} \frac{\partial r_i}{\partial x_k} = 0 \tag{2.56}$$

where r_i is the standard form of the i th differential equation for the infinitesimal problem and h_k is the characteristic length of the domain. This method is not useful for obtaining an analytical solution but proves to be very useful for finding an approximate solution, which converges to the analytical one when the grid size tends to zero.

If we consider the mixed u/p formulation as in (2.12) and (2.13) and replacing r_i by the equilibrium equation first and then by the incompressibility equation, we obtain the following:

$$\int_V \delta\varepsilon_{ij} s_{ij} dV + \int_V \delta\varepsilon_v p\, dV - \int_V \delta u_i b_i dV - \int_S \delta u_i t_i dS - \int_V \frac{h_k}{2} \frac{\partial \delta u_i}{\partial x_k} r_i dV = 0$$

$$\int_V \delta p(\varepsilon_v - \frac{p}{K}) dV + \int_V \left(\sum_{i=1}^{n_d} \tau_i r_i \frac{\partial \delta p}{\partial x_i} \right) dV - \int_S \delta p \tau_i n_i r_i dS = 0$$

(2.57)

where τ_i are coefficients referred as intrinsic time parameters with the following value: $\tau_i = \dfrac{3h_i^2}{8G}$,

which is very similar with the heuristically value of $\tau = \dfrac{h^2}{2G}$ chosen in the previous works.

Since the last terms form the first equation and the second equation are not relevant for solid mechanics problems they are omitted in the final formulation. Also introducing the notation

$$r_i = \frac{\partial p}{\partial x_i} + \pi_i$$
$$\pi_i = \frac{\partial s_{ij}}{\partial x_j} + b_i$$ where $\qquad (2.58)$

π_i is the part of the differential equation not containing the pressure gradient This term, once introduced, has to be weakly enforced by means of a Lagrange multiplier ($\delta\pi_i$) yielding the final set of governing equations as:

$$\int_V \delta\varepsilon_{ij} s_{ij} dV + \int_V \delta\varepsilon_v p\, dV - \int_V \delta u_i b_i dV - \int_S \delta u_i t_i dS = 0$$

$$\int_V \delta p(\varepsilon_v - \frac{p}{K}) dV + \int_V \left(\sum_{i=1}^{n_d} \tau_i \frac{\partial \delta p}{\partial x_i} \left[\frac{\partial p}{\partial x_i} + \pi_i \right] \right) dV = 0$$

$$\int_V \delta\pi_i \tau_i \left(\frac{\partial p}{\partial x_i} + \pi_i \right) dV = 0,$$

(2.59)

Matrix formulation is similar with the one obtained in the OSGS methods.

<u>Advantages</u>

- FIC method is based on a very strong theoretical foundation because it emerges naturally from the governing equations

- Results are accurate and free of pressure oscillations

- Can be used in a simpler form by neglecting the effect of the projected pressure gradient terms.

- It is applicable to non-linear dynamics.

<u>Disadvantages</u>

- Stabilization parameters are a function of the material properties and characteristic length

- Extension to finite deformation is impeded by the characteristic length parameters whose consistent definition remains still an open question.

2.2.6 Equivalence between bubble methods and pressure stabilized methods

It can be concluded from the previous sections that the OSGS method produces the same additional terms in the pressure constitutive equation as FIC method and both results are very similar with the terms produced by the pressure stabilized methods with the only difference in the term π, the projected gradient of pressure, which is not so significant for the case of static analyses. Having established that these three methods are similar, the normal question to ask is whether the 'bubble methods' are equivalent or not to these methods. Answering this question will lead us immediately to the most efficient and stable method to adopt for our tetrahedral element. Several authors proved the equivalence between the bubbles and stabilized methods. Hughes [30] establishes a relationship between 'bubble function' methods and stabilized

methods and then of both methods to subgrid scale methods. He also identifies the origin of the τ_i parameters that could have never been explained before as being derived from the element Green's function. Another equivalence proof is offered by R. Pierre in [38] who has shown that by eliminating the cubic bubble using static condensation we recover the stabilized methods.

If we write the displacement field as in the OSGS methods:

$$u(x) = u_h(x) + \widetilde{u}(x) = u_h(x) + \sum \phi_K(x)\widetilde{u}_k \tag{2.60}$$

where u_h is an approximation of u

$\widetilde{u}_k$ are the internal d.o.f. with corresponding bubble function ϕk.

The next simplifying conditions were used for static condensation:

$$\int_\Omega \nabla u_h : \nabla(\phi_k \widetilde{u}_k) dx = 0$$
$$\int_K \nabla(\phi_k \widetilde{u}_k) : \nabla(\phi_k \widetilde{u}_k) dx = A_k \left\| \widetilde{u}_k \right\|^2 \tag{2.61}$$
$$\int_K \nabla(\phi_{k_1} \widetilde{u}_{k_1}) : \nabla(\phi_{k_2} \widetilde{u}_{k_2}) dx = 0$$

By replacing (2.60) in the discrete governing equations (equilibrium and constraint) and using (2.61) we obtain a system of three equations as in the OSGS method out of which the second one refers only to the internal degrees of freedom or 'bubble' parameters. Solving this equation for the bubble parameters and substituting them in the pressure equation by using a very well known formula

$$\int_K \phi_K dx = \frac{9}{20} meas(K) = h_k \tag{2.62}$$

we get the equivalent form of the pressure equation of the 'bubble method' as:

$$\int_K \varepsilon_v \delta p \, dx - h_k \int_K (-\frac{\partial p}{\partial x_i}) \cdot \frac{\partial \delta p}{\partial x_i} \phi_K \, dx =$$

$$= \int_K \varepsilon_v \delta p \, dx + \sum_K C_K h_K^2 \int_K (\frac{\partial p}{\partial x_i}) \cdot \frac{\partial \delta p}{\partial x_i} \, dx = 0$$

(2.63)

It is easy to observe now the by the process of static condensation and under some conditions the method of enriching the displacement field with a cubic bubble function produces the same additional terms in the pressure equation as the pressure stabilized methods. The only difference is that the 'bubble methods' do not produce the projection of pressure gradient that appears in the OSGS and FIC methods.

Therefore, if all methods are equivalent under certain conditions, it seems natural to choose the method that would be the most efficient and easiest to implement.

We chose to implement a mixed u/p enhanced strain approach with the enhanced strain derived from a bubble function for the following reasons:

- Reasonably stable

- Consistent in nonlinear (large deformation) analysis

- No material or mesh dependent parameters

- Computationally efficient (less degrees of freedom per element).

3.0 THEORETICAL DEVELOPMENT

In the present work, a mixed enhanced strain formulation is introduced for a lower-order tetrahedral solid element that is applicable to small and large deformations and large rotations.

The uniqueness of the formulation lies within the fact that no specific geometric or material model parameters are required and no specific material model is chosen which makes the formulation as general as possible. The theoretical formulation is developed from the principle of virtual work and it has a three-field form. The proposed element has a node in each corner with displacement and pressure as external degrees of freedom and a center node with the volumetric strain and displacement as internal degrees of freedom. The stabilization term comes from an enhanced strain derived from a bubble function. Two bubble functions, conforming and nonconforming, are studied for obtaining optimal results. Two formulations, a general three-field formulation and its reduction to a two-field form are presented in the next sections. For efficiency reasons, the reduced two-field form was implemented through a user-programmable element into the commercial finite element software, ANSYS.

3.1 OVERALL APPROACH

Since the proposed formulation is applicable to general finite strain deformation, it has to take into consideration the following factors [6]:

- Geometry changes during deformation; the current configuration is different from the reference configuration and different from the configurations at any other time.

- A large strain definition has to be used.

- Cauchy stress cannot be updated by simply adding its increment due to straining of the material. Cauchy stresses at time t+Δt have to take into account the rigid body rotations.

- Implementation of the non-linear behavior should be based on an incremental approach.

- The equilibrium of the body must be established in the current configuration.

The basic idea of the nonlinear finite element formulation is to linearize the weak form of the governing equations of the problem and to solve these equations for the finite elements discretized domain. This leads to an incremental approach, according to which the solution at each step is obtained from the solution at the previous step. A step is considered a load increment in a static analysis and a time step in transient analysis.

The proposed three-field formulation follows the mixed enhanced strain formulation of Taylor [47] with the difference that it starts from the weak form instead of an energy functional (the weak form is more general-it applies to problems that don't have a variational principle) and uses the Jaumann rate of Cauchy stress with its conjugate deformation rate instead of second Piola-Kirchhoff stress conjugated with Green-Lagrange strain. In his formulations for both small and large deformation problems it is assumed that there exists a stored energy function for the material, expressed in terms of the right Green deformation tensor, which is not always the case.

The present formulation does not assume the existence of such a function but employs a rate form of the constitutive equation which is suitable for both rate-dependent and rate-independent material constitutive laws. This is due to the fact that the Jaumann rate of Cauchy stress is employed as an objective stress rate in the constitutive law. An Updated Lagrangian Jaumann (ULJ) procedure is employed to solve for geometric nonlinearities because of its ability to handle large displacements, large rotations, and large strain analyses. For the finite element implementation, a similar approach to Bathe [6] will be used.

3.2 DEVELOPMENT OF THE THREE-FIELD MIXED ENHANCED FORMULATION

3.2.1 Formulation of the Principle of Virtual Work

Formulating the principle of virtual work constitutes the basis of the theoretical development since obtaining the set of linearized equations is the main goal of an element formulation. They are obtained by differentiating the principle of virtual work and retaining only the linear terms (all higher order terms are ignored). The principle of virtual work, which is the weak form of the equations of equilibrium, is used as the basic equilibrium statement for the proposed formulation [16]. This weak form expresses the equilibrium state in the form of an integral over the entire volume of the body and provides a stronger mathematical basis for studying the approximation than directly discretizing the differential equations of equilibrium and requiring them to be satisfied point wise.

Since the first formulation has three independent variables, displacement, pressure and volumetric strain, the Cauchy stresses have to be modified with the corresponding independent

pressure field and the strains have to be modified with the corresponding independent volumetric strain as [2]:

$$\overline{\sigma_{ij}} = \sigma_{ij}^{dev} + \delta_{ij}\overline{P} = \sigma_{ij} - \delta_{ij}P + \delta_{ij}\overline{P} = \sigma_{ij} + \delta_{ij}(\overline{P} - P) \tag{3.1}$$

$$\overline{\varepsilon}_{ij}^{\ enh} = \varepsilon_{ij,dev}^{\ \ enh} + \frac{1}{3}\delta_{ij}\overline{\varepsilon}^{enh}{}_{v} = \varepsilon_{ij}^{enh} - \frac{1}{3}\delta_{ij}(\varepsilon_{v}^{enh} - \overline{\varepsilon}_{v}) \tag{3.2}$$

where c_{ij} is the Cauchy stress from constitutive law,

σ_{ij}^{dev} is the deviatoric part of the Cauchy stress,

P is the pressure derived from Cauchy stress,

$\overline{P}$ is the interpolated pressure,

ε_{ij}^{enh} is the modified enhanced strain with the stabilizing term from the bubble function

ε_{ij}^{dev} is the deviatoric part of the strain,

$\overline{\varepsilon}_{v}$ is the interpolated volumetric strain and

δ_{ij} is the Kronecker delta.

The internal virtual work can be expressed now as:

$$\delta W_{int} = \int_{V}\overline{\sigma}_{ij}(\overline{\varepsilon}_{ij}^{enh})\delta\varepsilon_{ij}^{enh}dV \tag{3.3}$$

The two constraints imposed by the two additional variables are:

$$\varepsilon_{v} - \overline{\varepsilon}_{v} = 0 \tag{3.4}$$

$$P - \overline{P} = 0 \tag{3.5}$$

The introduction of the two additional field variables has to be weakly enforced in the principle of virtual work by means of two Lagrange multipliers as:

$$\delta W_{int} = \int_{V}\overline{\sigma}_{ij}(\overline{\varepsilon}_{ij}^{enh})\delta\varepsilon_{ij}^{enh}dV + \int_{V}(\varepsilon_{v}^{enh} - \overline{\varepsilon}_{v})\delta\overline{P}dV + \int_{V}(P(\overline{\varepsilon}_{v}^{enh}) - \overline{P})\delta\overline{\varepsilon}_{v}dV \tag{3.6}$$

The augmented principle of virtual work is differentiated again to obtain the incremental principle of virtual work, which yields, by substituting the variables with their finite element approximations, the matrix formulation or the linearized system of equations that has to be solved. During the differentiation process we will obtain the rates of the Cauchy stress and of strains and therefore we need to appropriately define them. This is done in the next section.

3.2.2 Selection of Appropriate Stress and Strain Measures

When a small strain approximation is no longer valid we have to use appropriate measures of stress and strain. The approach that we will follow is to use stress and strain measures that are conjugate so that the principle of virtual work can be expressed as in (3.6).

Many of the materials we wish to model are history dependent and therefore it is common for the constitutive equations to appear in rate form. We therefore need to define the rate of the Cauchy stress for use in the material constitutive law which relates the increments of stress with the increments of strain. One of the objective stresses that can be applied is the Jaumann rate of Cauchy stress expressed by McMeeking and Rice in [32].

The issue that arises when using the second Piola - Kirchhoff stress, which is a materially-based stress, is that it remains constant during the rotation because its components are associated with a material basis. The problem is that the components of the Cauchy stress, σ, are associated with the current directions in space and, therefore, the Cauchy stress rate, $D\sigma$, will be nonzero if there is pure rigid body rotation even though from a constitutive point of view the material is unchanged. Thus, the increment of Cauchy stress, $D\sigma$, must be divided into two different parts: one due to the rigid body motion only and one associated to the rate form of the stress-strain law.

According to [1], if at time t we attach to a material point a set of base vectors, e_i, $i=1, 2, 3$ they cannot stretch but they can spin with the same spin as the material,

$$\mathbf{\Omega} = \frac{1}{2}\left(\frac{\partial \mathbf{v}}{\partial \mathbf{x}} - \frac{\partial \mathbf{v}^\mathbf{T}}{\partial \mathbf{x}} \right) \qquad (3.7)$$

Therefore, their motion can be described as:

$$\dot{\mathbf{e}} = \mathbf{\Omega} \cdot \mathbf{e} \qquad (3.8)$$

Thus, if we consider the Cauchy stress tensor in the current configuration as

$$\mathbf{\sigma} = c_{ij} e_i e_j \qquad (3.9)$$

Taking the time derivative we obtain:

$$\dot{\mathbf{\sigma}} = \dot{\mathbf{\sigma}}^\mathbf{J} + (\mathbf{\Omega} \cdot \mathbf{\sigma} + \mathbf{\sigma} \cdot \mathbf{\Omega}^\mathbf{T}) \qquad (3.10)$$

where $\dot{\mathbf{\sigma}}^\mathbf{J}$ is the rate of Cauchy stress associated with the constitutive response, also called the Jaumann rate of Cauchy stress. The Jaumann stress rate is an objective stress rate tensor that is related to the rate of straining as:

$$\dot{\sigma}^{J}_{ij} = C_{ijkl} D\varepsilon_{kl} = C_{ijkl} d_{kl} \qquad (3.11)$$

with C_{ijkl} as the components of material constitutive tensor,

$$D\varepsilon_{kl} = d_{kl} = \frac{1}{2}\left(\frac{\partial v_k}{\partial x_l} + \frac{\partial v_l}{\partial x_k} \right) \text{as the components of the rate of deformation tensor,}$$

and v_i is the velocity.

Since the Jaumann stress rate is defined in terms of both rate of deformation and past history this equation provides a link between the material model and the overall change in Cauchy stress. Written in indicial notation [28],

$$\dot{\sigma}^{J}_{ij} = \dot{\sigma}_{ij} - \sigma_{ik}\dot{\omega}_{jk} - \sigma_{jk}\dot{\omega}_{ik} \quad \text{where} \qquad (3.12)$$

$$\dot{\omega}_{ij} = \frac{1}{2}\left(\frac{\partial v_i}{\partial x_j} - \frac{\partial v_j}{\partial x_i}\right)$$ is the spin tensor defined in (3.7) written in indicial notation and

$\dot{c}_{ij}$ is the time rate of Cauchy stress.

Then the Cauchy stress rate becomes:

$$Dc_{ij} = C_{ijkl}D\varepsilon_{kl} + c_{ik}D\alpha_{jk} + c_{jk}D\alpha_{ik} \tag{3.13}$$

where $\omega_{ij} = \frac{1}{2}\left(\frac{\partial u_i}{\partial x_j} - \frac{\partial u_j}{\partial x_i}\right)$ are the components of the rotation tensor.

This means that an integration process is always required to evaluate the Cauchy stresses. Thus is suitable for an analysis of path-dependent materials [32].

Under these circumstances the differentiated or linearized principle of virtual work with respect to the current configuration can be used to formulate the Updated Lagrangian Jaumann finite element method. The complete derivation of the differentiation process is presented in the next section and Appendix A.

3.2.3 Linearization of the Principle of Virtual Work

Using the augmented internal virtual work from (3.6) we can formulate the principle of virtual work as: (3.14)

$$\delta W = \delta W_{int} + \delta W_{ext} = \int_V \overline{\sigma}_{ij}(\overline{\varepsilon}_{ij}^{enh})\delta\varepsilon_{ij}^{enh}dV + \int_V (\varepsilon_v^{enh} - \overline{\varepsilon}_v)\delta\overline{P}dV + \int_V (P(\overline{\varepsilon}_v^{enh}) - \overline{P})\delta\overline{\varepsilon}_v dV + \delta W_{ext} = 0$$

Taking the derivative with respect to time of the internal virtual work we get:

$$D\delta W_{int} = \int_V D\overline{\sigma}_{ij}\delta\varepsilon_{ij}^{enh}dV + \int_V \overline{\sigma}_{ij}D\delta\varepsilon_{ij}^{enh}dV + \int_V (D\varepsilon_v^{enh} - D\overline{\varepsilon}_v)\delta\overline{P}dV + \int_V (\varepsilon_v^{enh} - \overline{\varepsilon}_v)D\delta\overline{P}dV +$$
$$+ \int_V D\delta\overline{\varepsilon}_v(P - \overline{P})dV + \int_V (DP - D\overline{P})\delta\overline{\varepsilon}_v dV \tag{3.15}$$

where the differentiation of $D(dV) = \dfrac{\partial Du_k}{\partial x_k}dV = D\varepsilon_v dV$. This term is usually insignificant in

most deformation cases and is ignored. Also this term will yield an unsymmetrical stiffness

matrix [2]. The same observations can be made for the terms involving $D\delta\overline{P}, D\delta\overline{\varepsilon}_v$ which are

very small and can be ignored.

After making these simplifying assumptions, the linearized augmented principle of virtual

work becomes:

$$
D\,\delta W_a = \underbrace{\int_V D\overline{\sigma}_{ij}\,\delta\varepsilon_{ij}^{enh}\,dV + \int_V \overline{\sigma}_{ij}\,D\delta\varepsilon_{ij}^{enh}\,dV}_{A} + \underbrace{\int_V (\frac{1}{3}\delta_{ij}C_{ijkl}\,D\overline{\varepsilon}_{kl}^{enh})\delta\overline{\varepsilon}_v\,dV}_{B} +
$$
$$
+\int_V D\varepsilon_v^{enh}\,\delta\overline{P}\,dV - \int_V D\overline{\varepsilon}_v\,\delta\overline{P}\,dV - \int_V \delta\overline{\varepsilon}_v\,D\overline{P}\,dV
$$
(3.16)

Extending the first two integrals, which are grouped as term A, and using the definition of

Jaumann stress rate from (3.13) we obtain:

$$
A = \int_V D\overline{\sigma}_{ij}\,\delta\varepsilon_{ij}^{enh}\,dV + \int_V \overline{\sigma}_{ij}\,D\delta\varepsilon_{ij}^{enh}\,dV =
$$
$$
= \int_V \{[C_{ijkl}D\overline{\varepsilon}_{kl}^{enh} + \overline{\sigma}_{ik}D\omega_{jk} + \overline{\sigma}_{jk}D\omega_{ik} + \delta_{ij}(D\overline{P} - DP)]\delta\varepsilon_{ij}^{enh} + \overline{\sigma}_{ij}D\delta\varepsilon_{ij}^{enh}\}dV =
$$
$$
= \int_V \delta\varepsilon_{ij}^{enh}C_{ijkl}\left[D\varepsilon_{ij}^{enh} - \frac{1}{3}\delta_{kl}\left(D\varepsilon_v^{enh} - D\overline{\varepsilon}_v\right)\right]dV + \int_V \delta\varepsilon_{ij}^{enh}\left(\overline{\sigma}_{ik}D\omega_{jk} + \overline{\sigma}_{jk}D\omega_{ik}\right)dV +
$$
$$
+\int_V \overline{\sigma}_{ij}D\delta\varepsilon_{ij}^{enh}\,dV + \int_V \delta\varepsilon_v^{enh}\left(D\overline{P} - \frac{1}{3}\delta_{ij}C_{ijkl}D\overline{\varepsilon}_{ij}^{enh}\right)dV =
$$
$$
= \int_V \delta\varepsilon_{ij}^{enh}C_{ijkl}D\varepsilon_{kl}^{enh}\,dV - \int_V \delta\varepsilon_{ij}^{enh}C_{ijkl}\frac{1}{3}\delta_{kl}D\varepsilon_v^{enh}\,dV + \int_V \left[\delta\varepsilon_{ij}^{enh}\left(\overline{\sigma}_{ik}D\omega_{jk} + \overline{\sigma}_{jk}D\omega_{ik}\right) + \overline{\sigma}_{ij}D\delta\varepsilon_{ij}^{enh}\right]dV +
$$
$$
+\int_V \delta\varepsilon_{ij}^{enh}C_{ijkl}\frac{1}{3}\delta_{kl}D\overline{\varepsilon}_v\,dV - \int_V \delta\varepsilon_v^{enh}\frac{1}{3}\delta_{ij}C_{ijkl}D[\varepsilon_{kl}^{enh} - \frac{1}{3}\delta_{kl}(\varepsilon_v^{enh} - \overline{\varepsilon}_v)]dV + \int_V \delta\varepsilon_v^{enh}D\overline{P}\,dV
$$

$$A = \int_V \delta\varepsilon_{ij}^{enh} C_{ijkl} D\varepsilon_{kl}^{enh} dV - \int_V \delta\varepsilon_{ij}^{enh} C_{ijkl} \frac{1}{3}\delta_{kl} D\varepsilon_v^{enh} dV - \int_V \delta\varepsilon_v^{enh} \frac{1}{3}\delta_{ij} C_{ijkl} D\varepsilon_{kl}^{enh} dV +$$

$$+ \int_V \delta\varepsilon_v^{enh} \frac{1}{3}\delta_{ij} C_{ijkl} \frac{1}{3}\delta_{kl} D\varepsilon_v^{enh} dV +$$

$$+ \int_V \left[\delta\varepsilon_{ij}^{enh} \left(\overline{\sigma}_{ik} D\omega_{jk} + \overline{\sigma}_{jk} D\omega_{ik} \right) + \overline{\sigma}_{ij} D\delta\varepsilon_{ij}^{enh} \right] dV +$$

$$+ \int_V \delta\varepsilon_{ij}^{enh} C_{ijkl} \frac{1}{3}\delta_{kl} D\overline{\varepsilon}_v dV - \int_V \delta\varepsilon_v^{enh} \frac{1}{3}\delta_{ij} C_{ijkl} \frac{1}{3}\delta_{kl} D\overline{\varepsilon}_v dV + \int_V \delta\varepsilon_v^{enh} D\overline{P} dV$$

(3.17)

The first four integrals in (3.17) produce the so-called constitutive stiffness term, K_{uu}^c, because it comes from the material constitutive law directly or from the straining; the fifth integral which will be extended in the next section produces the so-called stress stiffness term or geometric stiffness, K_{uu}^{geom} (due to geometric nonlinearities).

$$B = \int_V \left(\frac{1}{3}\delta_{ij} C_{ijkl} D\overline{\varepsilon}_{kl}^{enh} \right) \delta\overline{\varepsilon}_v dV =$$

$$= \int_V \delta\overline{\varepsilon}_v \frac{1}{3}\delta_{ij} C_{ijkl} D[\varepsilon_{kl}^{enh} - \frac{1}{3}\delta_{kl}(\varepsilon_v^{enh} - \overline{\varepsilon}_v)] dV =$$

(3.18)

$$= \int_V \delta\overline{\varepsilon}_v \frac{1}{3}\delta_{ij} C_{ijkl} D\varepsilon_{kl}^{enh} dV - \int_V \delta\overline{\varepsilon}_v \frac{1}{3}\delta_{ij} C_{ijkl} \frac{1}{3}\delta_{kl} D\varepsilon_v^{enh} dV + \int_V \delta\overline{\varepsilon}_v \frac{1}{3}\delta_{ij} C_{ijkl} \frac{1}{3}\delta_{kl} D\overline{\varepsilon}_v dV$$

Rewriting (3.16) using the obtained formulas for terms A and B we get the linearized principle of virtual work as:

$$D\delta W_a = \int_V \delta\varepsilon_{ij}^{enh} C_{ijkl} D\varepsilon_{kl}^{enh} dV - \int_V \delta\varepsilon_{ij}^{enh} C_{ijkl} \frac{1}{3}\delta_{kl} D\varepsilon_v^{enh} dV - \int_V \delta\varepsilon_v^{enh} \frac{1}{3}\delta_{ij} C_{ijkl} D\varepsilon_{kl}^{enh} dV +$$

$$+ \int_V \delta\varepsilon_v^{enh} \frac{1}{3}\delta_{ij} C_{ijkl} \frac{1}{3}\delta_{kl} D\varepsilon_v^{enh} dV +$$

$$+ \int_V \left[\delta\varepsilon_{ij}^{enh} \left(\overline{\sigma}_{ik} D\omega_{jk} + \overline{\sigma}_{jk} D\omega_{ik} \right) + \overline{\sigma}_{ij} D\delta\varepsilon_{ij}^{enh} \right] dV +$$

$$+ \int_V \delta\varepsilon_{ij}^{enh} C_{ijkl} \frac{1}{3}\delta_{kl} D\overline{\varepsilon}_v dV - \int_V \delta\varepsilon_v^{enh} \frac{1}{3}\delta_{ij} C_{ijkl} \frac{1}{3}\delta_{kl} D\overline{\varepsilon}_v dV + \int_V \delta\varepsilon_v^{enh} D\overline{P} dV +$$

(3.19)

$$+ \int_V \delta\overline{\varepsilon}_v \frac{1}{3}\delta_{ij} C_{ijkl} D\varepsilon_{kl}^{enh} dV - \int_V \delta\overline{\varepsilon}_v \frac{1}{3}\delta_{ij} C_{ijkl} \frac{1}{3}\delta_{kl} D\varepsilon_v^{enh} dV + \int_V \delta\overline{\varepsilon}_v \frac{1}{3}\delta_{ij} C_{ijkl} \frac{1}{3}\delta_{kl} D\overline{\varepsilon}_v dV +$$

$$+ \int_V D\varepsilon_v^{enh} \delta\overline{P} dV - \int_V D\overline{\varepsilon}_v \delta\overline{P} dV - \int_V \delta\overline{\varepsilon}_v D\overline{P} dV$$

The final expression for the linearized internal virtual work is:

$$
D\delta W_a = \int_V (\delta\varepsilon_{ij}^{enh} C_{ijkl} D\varepsilon_{kl}^{enh} - \delta\varepsilon_{ij}^{enh} C_{ijkl} \frac{1}{3}\delta_{kl} D\varepsilon_v^{enh} - \delta\varepsilon_v^{enh} \frac{1}{3}\delta_{ij} C_{ijkl} D\varepsilon_{kl}^{enh} +
$$

$$
+ \delta\varepsilon_v^{enh} \frac{1}{3}\delta_{ij} C_{ijkl} \frac{1}{3}\delta_{kl} D\varepsilon_v^{enh})dV + + \int_V \left[\delta\varepsilon_{ij}^{enh}\left(\overline{\sigma}_{ik} D\omega_{jk} + \overline{\sigma}_{jk} D\omega_{ik}\right) + \overline{\sigma}_{ij} D\delta\varepsilon_{ij}^{enh}\right]dV +
$$

$$
+ \int_V \delta\varepsilon_v^{enh} D\overline{P}dV + \int_V (\delta\varepsilon_{ij}^{enh} - \frac{1}{3}\delta\varepsilon_v^{enh})C_{ijkl} \frac{1}{3}\delta_{kl} D\overline{\varepsilon}_v dV + \tag{3.20}
$$

$$
+ \int_V D\varepsilon_v^{enh} \delta\overline{P}dV - \int_V D\overline{\varepsilon}_v \delta\overline{P}dV + + \int_V \delta\widetilde{\varepsilon}_v \frac{1}{3}\delta_{ij} C_{ijkl}(D\varepsilon_{kl}^{enh} - \frac{1}{3}\delta_{kl} D\varepsilon_v^{enh})dV -
$$

$$
- \int_V \delta\widetilde{\varepsilon}_v D\overline{P}dV + \int_V \delta\widetilde{\varepsilon}_v \frac{1}{3}\delta_{ij} C_{ijkl} \frac{1}{3}\delta_{kl} D\overline{\varepsilon}_v dV
$$

The derivation of the geometric stiffness term (second integral) can be found in Appendix A. The final result for this term is:

$$
\overline{\sigma}_{ik} D\omega_{jk} \delta\varepsilon_{ij} + \overline{\sigma}_{jk} D\omega_{ik} \delta\varepsilon_{ij} + \overline{\sigma}_{ij} D\delta\varepsilon_{ij} = \overline{\sigma}_{ij}\left(\frac{\partial Du_k}{\partial x_j}\frac{\partial \delta u_k}{\partial x_i} - 2\delta\varepsilon_{ik} D\varepsilon_{jk}\right) \tag{3.21}
$$

Returning now to the linearized principle of virtual work and replacing the nonlinear geometric term with the above formula written in terms of enhanced strains, we obtain the final formulation:

$$
D\delta W_a = \int_V (\delta\varepsilon_{ij}^{enh,dev} C_{ijkl} D\varepsilon_{kl}^{enh,dev})dV + \int_V \left[\overline{\sigma}_{ij}\left(\frac{\partial Du_k}{\partial x_j}\frac{\partial \delta u_k}{\partial x_i} - 2\delta\varepsilon_{ik}^{enh} D\varepsilon_{jk}^{enh}\right)\right]dV +
$$

$$
+ \int_V \delta\varepsilon_v^{enh} D\overline{P}dV + \int_V \delta\varepsilon_{ij}^{enh,dev} C_{ijkl} \frac{1}{3}\delta_{kl} D\overline{\varepsilon}_v dV +
$$

$$
+ \int_V D\varepsilon_v^{enh} \delta\overline{P}dV - \int_V D\overline{\varepsilon}_v \delta\overline{P}dV + \tag{3.22}
$$

$$
+ \int_V \delta\widetilde{\varepsilon}_v \frac{1}{3}\delta_{ij} C_{ijkl}(D\varepsilon_{kl}^{enh,dev})dV - \int_V \delta\widetilde{\varepsilon}_v D\overline{P}dV + \int_V \delta\widetilde{\varepsilon}_v \frac{1}{3}\delta_{ij} C_{ijkl} \frac{1}{3}\delta_{kl} D\overline{\varepsilon}_v dV
$$

From here it can be seen that each of the integrals produces the specific stiffness term associated with the corresponding variable yielding a symmetric system of incremental equations.

40

3.3 REDUCTION OF THE THREE-FIELD TO A TWO-FIELD FORMULATION

For efficiency reasons and easiness of implementation, the above formulation was reduced to a mixed displacement pressure form.

For the two-field form the principle of virtual work has to be modified accordingly by taking out the constraint $\varepsilon_v^{enh} - \bar{\varepsilon}_v = 0$ that corresponds to the volumetric strain variable as:

$$\delta W_{\text{int}} = \int_V \bar{\sigma}_{ij}(\bar{\varepsilon}_{ij}^{enh})\delta\varepsilon_{ij}^{enh}dV + \int_V (P(\bar{\varepsilon}_v^{enh}) - \bar{P})\delta\bar{\varepsilon}_v dV \tag{3.23}$$

and by expressing the interpolated volumetric strain from the second term as a function of the interpolated pressure as:

$$\delta\bar{P} = \frac{1}{3}\delta_{ij}\bar{\sigma}_{ij} = \frac{1}{3}\delta_{ij}C_{ijkl}\delta\bar{\varepsilon}_{kl}^{enh} = \frac{1}{3}\delta_{ij}\left(\delta\varepsilon_{kl}^{enh,dev} + \frac{1}{3}\delta_{kl}\delta\bar{\varepsilon}_v^h\right) =$$
$$= \frac{1}{3}\delta_{ij}C_{ijkl}\delta\varepsilon_{kl}^{enh,dev} + \frac{1}{3}\delta_{ij}C_{ijkl}\frac{1}{3}\delta_{kl}\delta\bar{\varepsilon}_v = \frac{1}{3}\delta_{ij}C_{ijkl}\delta\varepsilon_{kl}^{enh,dev} + K\delta\bar{\varepsilon}_v \Rightarrow \tag{3.24}$$

$$\delta\bar{\varepsilon}_v = \frac{\delta\bar{P}}{K} - \frac{1}{3K}\delta_{ij}C_{ijkl}\delta\varepsilon_{kl}^{enh,dev} = \frac{\delta\bar{P}}{K} - \frac{1}{3K}\delta_{ij}C_{ijkl}\delta\varepsilon_{kl}^{enh} + \delta\varepsilon_v^{enh} \ , \tag{3.25}$$

where $K = \frac{1}{9}\delta_{ij}C_{ijkl}\delta_{kl}$ is the instantaneous bulk modulus.

Under these circumstances the linearized principle of virtual work for the mixed u/p formulation becomes:

$$D\delta W_{\text{int}} = \int_V D\overline{\sigma}_{ij}\delta\varepsilon_{ij}^{enh}dV + \int_V \overline{\sigma}_{ij}D\delta\varepsilon_{ij}^{enh}dV + \int_V \delta\widetilde{\varepsilon}_v(DP - D\overline{P})dV =$$

$$= \int_V \delta\varepsilon_{ij}^{enh}C_{ijkl}D\varepsilon_{kl}^{enh}dV + \int_V \left[\delta\varepsilon_{ij}^{enh}\left(\overline{\sigma}_{ik}D\omega_{jk} + \overline{\sigma}_{jk}D\omega_{ik}\right) + \overline{\sigma}_{ij}D\delta\varepsilon_{ij}^{enh}\right]dV +$$

$$+ \int_V \delta\varepsilon_v^{enh}D\overline{P}dV - \int_V \delta\varepsilon_v^{enh}DPdV +$$

$$+ \int_V (DP - D\overline{P})\left(\frac{\delta\overline{P}}{K} - \frac{1}{3K}\delta_{ij}C_{ijkl}\delta\varepsilon_{kl}^{enh} + \delta\varepsilon_v^{enh}\right)dV = \qquad (3.25)$$

$$= \int_V (\delta\varepsilon_{ij}^{enh}C_{ijkl}D\varepsilon_{kl}^{enh}dV - DP\frac{\delta_{ij}}{3K}C_{ijkl}\delta\varepsilon_{kl}^{enh})dV + \int_V DP\frac{\delta\overline{P}}{K}dV - \int_V D\overline{P}\frac{\delta\overline{P}}{K}dV +$$

$$+ \int_V D\overline{P}\frac{\delta_{ij}}{3K}C_{ijkl}\delta\varepsilon_{kl}^{enh}dV + \int_V \left[\delta\varepsilon_{ij}^{enh}\left(\overline{\sigma}_{ik}D\omega_{jk} + \overline{\sigma}_{jk}D\omega_{ik}\right) + \overline{\sigma}_{ij}D\delta\varepsilon_{ij}^{enh}\right]dV$$

But, $DP = \dfrac{1}{3}\delta_{ij}C_{ijkl}D\varepsilon_{kl}^{enh}$ $\qquad (3.26)$

If we substitute (3.26) in (3.25) we get:

$$D\delta W_{\text{int}} = \int_V \left(\delta\varepsilon_{ij}^{enh}C_{ijkl}D\varepsilon_{kl}^{enh} - \frac{1}{9K}\delta\varepsilon_{ij}^{enh}C_{ijmn}^T\delta_{mn}\delta_{op}C_{opkl}D\varepsilon_{kl}^{enh}\right)dV +$$

$$+ \int_V \overline{\sigma}_{ij}\left(\frac{\partial Du_k}{\partial x_j}\frac{\partial \delta u_k}{\partial x_i} - 2\delta\varepsilon_{ik}^{enh}D\varepsilon_{jk}^{enh}\right)dV - \int_V D\overline{P}\frac{1}{K}\delta\overline{P}dV + \qquad (3.27)$$

$$+ \int_V \frac{1}{3K}\delta_{ij}C_{ijkl}D\varepsilon_{kl}^{enh}\delta\overline{P}dV + \int_V D\overline{P}\frac{1}{3K}\delta_{ij}C_{ijkl}\delta\varepsilon_{kl}^{enh}dV$$

The above formula represents the final expression for the rate of internal virtual work from which the incremental system of equations can be deduced by substituting the variables with their finite element interpolations. For this to be possible, (3.27) has to be converted in a matrix formulation which can be easily implemented in a FORTRAN program that interfaces with ANSYS solver capabilities.

3.4 UPDATED LAGRANGIAN JAUMANN FORMULATION

In ANSYS an Updated Lagrangian Jaumann (ULJ) procedure is employed to solve geometric nonlinearities and therefore the same procedure will be used in the proposed formulation and implementation. According to [6], this is a typical formulation for large displacements, large rotations, and large strain analyses. The ULJ formulation is applicable to general elastic-plastic analyses and it is very effective in large strain analysis, because the stress and strain measures used are those to describe the material response in a natural way. According to this procedure the variables at time *t* are considered solved and known and they are used to calculate the solution at time *t+Δt* by solving a set of linearized simultaneous equations. ANSYS uses the Newton-Raphson method as an iterative numerical algorithm for solving the nonlinear equilibrium equations. Details regarding the nonlinear iterative algorithm will be given in chapter 4.

Introduction of this nonlinear procedure at this point is useful only for setting the current configuration (*t+Δt*) as the time when all the stiffness matrices together with internal forces are evaluated. The basic equations employed in the U.L.J. formulation are the Jaumann stress rate equation defined according to (3.13) and the incremental virtual work equation (3.27) from which we can obtain the following two equations:

Equilibrium equation

$$
\int_{t+\Delta t V^{(i-1)}} \delta_{t+\Delta t}\varepsilon_{ij}\left({}^{t+\Delta t}C_{ijmn}^{(k-1)} - \frac{1}{9K}{}^{t+\Delta t}C_{ijmn}^{(k-1)}\delta_{mn}\delta_{op}{}^{t+\Delta t}C_{opkl}^{(k-1)} \right)D_{t+\Delta t}\varepsilon_{kl}d^{t+\Delta t}V^{(k-1)} +
$$

$$
\int_{t+\Delta t V^{(i-1)}} {}^{t+\Delta t}\overline{\sigma}_{ij}^{(k-1)} : \left(\frac{\partial Du_k}{\partial^{t+\Delta t}x_j}\frac{\partial \delta u_k}{\partial^{t+\Delta t}x_i} - 2\delta_{t+\Delta t}\varepsilon_{ik}D_{t+\Delta t}\varepsilon_{jk} \right)d^{t+\Delta t}V^{(k-1)} +
\tag{3.28}
$$

$$
+ \int_{d^{t+\Delta t}V^{(k-1)}} {}^{t+\Delta t}DP^{(k-1)}\frac{\delta_{ij}}{3K}{}^{t+\Delta t}C_{ijkl}^{(k-1)}\delta_{t+\Delta t}\varepsilon_{kl}d^{t+\Delta t}V^{(k-1)} = {}^{t+\Delta t}F_{ext} - {}^{t+\Delta t}F_u^{(i-1)}
$$

Constraint Equation

$$\int_{t+\Delta t V^{(k-1)}} \frac{\acute{c}_{ij}}{3K}{}^{t+\Delta t}C_{ijkl}^{(k-1)}D_{t+\Delta t}\varepsilon_{kl}\delta_{t+\Delta t}\overline{P}d^{t+\Delta t}V^{(k-1)} - \int_{d^{t+\Delta t}V^{(k-1)}} {}^{t+\Delta t}D\overline{P}\frac{1}{K}\delta_{t+\Delta t}\overline{P}d^{t+\Delta t}V^{(k-1)} = 0 - {}^{t+\Delta t}F_p^{(k-1)} \qquad (3.29)$$

where ${}^{t+\Delta t}C_{ijkl}^{(k-1)}$ is the incremental material property tensor at time $t+\Delta t$, referred to the

configuration at time $t+\Delta t$; ${}^{t+\Delta t}\overline{\sigma}_{ij}^{(k-1)}$ is the modified Cauchy stress at time $t+\Delta t$; and ${}^{t+\Delta t}D\varepsilon_{ij}$

and ${}^{t+\Delta t}D\overline{P}$ are the incremental strains and pressures which are referred to the configuration at

time $t+\Delta t$. All the quantities with (k-1) superscript mean that they are evaluated at $t+\Delta t$ using the

value of the displacements obtained from the previous iteration.

Since we are interested in finding the solution in current configuration in terms of the solution

of previous configuration the key term that will provide this is the deformation gradient tensor.

3.5 ENHANCED DEFORMATION GRADIENT

In most structural problems we are interested in finding the deformation of the structure

throughout the loading history in terms of a reference configuration that is given. Suppose a

particle is located at position X initially and moves to position x. The location of the particle in

current configuration is related to the location in the reference configuration by the displacement

u and is given by**:**

$$\mathbf{x} = \mathbf{X} + \mathbf{u} \qquad (3.30)$$

The deformation gradient matrix is defined as:

$$\mathbf{F} = \frac{\partial \mathbf{x}}{\partial \mathbf{X}} = \frac{\partial (\mathbf{X} + \mathbf{u})}{\partial \mathbf{X}} = \mathbf{I} + \frac{\partial \mathbf{u}}{\partial \mathbf{X}} \qquad (3.31)$$

Since the proposed formulation is based on enhancing the deformation mode such that it will prevent volumetric locking it is necessary to relate this deformation mode to a modification of the deformation gradient. This approach has been applied successfully by Taylor [47] to tetrahedral elements.

The incremental deformation gradient can expressed as:

$$\Delta F = {}^{t+\Delta t}_{t} F = \begin{bmatrix} \dfrac{\partial^{t+\Delta t} x_1}{\partial^t x_1} & \dfrac{\partial^{t+\Delta t} x_1}{\partial^t x_2} & \dfrac{\partial^{t+\Delta t} x_1}{\partial^t x_3} \\[3mm] \dfrac{\partial^{t+\Delta t} x_2}{\partial^t x_1} & \dfrac{\partial^{t+\Delta t} x_2}{\partial^t x_2} & \dfrac{\partial^{t+\Delta t} x_2}{\partial^t x_3} \\[3mm] \dfrac{\partial^{t+\Delta t} x_3}{\partial^t x_1} & \dfrac{\partial^{t+\Delta t} x_3}{\partial^t x_2} & \dfrac{\partial^{t+\Delta t} x_3}{\partial^t x_3} \end{bmatrix}$$ (3.32)

or in indicial notation

$$\Delta F_{ij} = \frac{\partial^{t+\Delta t} x_i}{\partial^t x_j} = \frac{\partial \left({}^t x_i + Du_i \right)}{\partial^t x_j} = \delta_{ij} + \frac{\partial Du_i}{\partial^t x_j}$$ (3.33)

The enhanced deformation gradient is enhanced with a term, $\Delta \overline{F}$, obtained from the derivatives of the bubble function as:

$$\Delta F_{ij}^{enh} = \Delta F_{ij} + \Delta \overline{F}_{ij}$$ (3.34)

The total enhanced deformation gradient from the initial configuration to the current configuration is computed in terms of deformation gradient at previous time step and incremental deformation gradient as:

$${}^{t+\Delta t}_{0} F^{enh} = {}^{t+\Delta t}_{t} \Delta F^{enh} \cdot {}^{t}_{0} F^{enh}$$ (3.35)

The volume has to be modified consistently as:

$$dV^{t+\Delta t} = \left| {}^{t+\Delta t}_{0} F^{enh} \right| dV^0 = \left| \Delta F^{enh} \right| \cdot dV^t$$ (3.36)

3.6 FINITE ELEMENT APPROXIMATION. MATRIX FORMULATION

The finite element approximation for the developed formulation is based on assuming a linear interpolation for both the displacement and pressure fields. Generally, the interpolation can be written as:

$$\mathbf{a} = \mathbf{N}^\alpha \mathbf{a}^\alpha \tag{3.37}$$

where $\mathbf{a}$ is a vector-valued function at any point; $\mathbf{N}^\alpha$ is a set of interpolation functions also called shape functions and $\mathbf{a}^\alpha$ is a set of nodal variables.

If we use an isoparametric concept for our four-node tetrahedral element then the coordinates of any point in the tetrahedron can be expressed as:

$$\mathbf{x} = \sum_{\alpha=1}^{4} \mathbf{N}^\alpha(\xi)\mathbf{x}^\alpha = \mathbf{N}\mathbf{x} \tag{3.38}$$

and the same shape functions are used to define the displacement and pressure variables as:

$$\mathbf{u}(\xi) = \sum_{\alpha=1}^{4} \mathbf{N}^\alpha(\xi)\mathbf{u}^\alpha = \mathbf{N}\mathbf{u}$$

$$\overline{P}(\xi) = \sum_{\alpha=1}^{4} \mathbf{N}^\alpha(\xi)\overline{P}^\alpha = \mathbf{N}\overline{\mathbf{P}} \tag{3.39}$$

3.6.1 Shape Functions

The 4-node tetrahedral element is defined by a set of volume coordinates, $\xi_1, \xi_2, \xi_3, \xi_4$ which represent the ratio of the shaded volume to the total volume (see Figure 2)
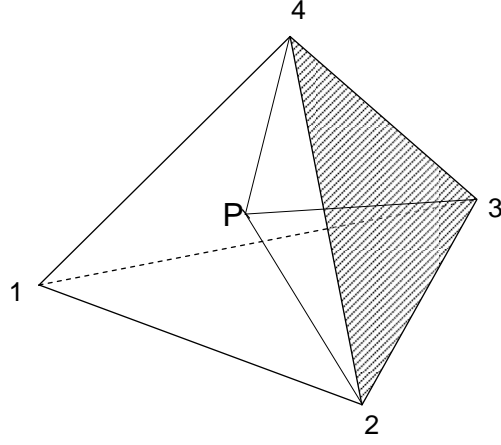
Figure 2. Volume Coordinates

Using the volume coordinates, the position in each tetrahedron is given by:

$$
\begin{aligned}
x &= \xi_1 x_1 + \xi_2 x_2 + \xi_3 x_3 + \xi_4 x_4 \\
y &= \xi_1 y_1 + \xi_2 y_2 + \xi_3 y_3 + \xi_4 y_4 \\
z &= \xi_1 z_1 + \xi_2 z_2 + \xi_3 z_3 + \xi_4 z_4 \\
1 &= \xi_1 + \xi_2 + \xi_3 + \xi_4
\end{aligned}
\tag{3.40}
$$

and the shape functions for the linear tetrahedron are simply the volume coordinates. Each of them is unity for one node and zero at the others and varies linearly everywhere.

$$
\begin{aligned}
N_1 &= \xi_1 \\
N_2 &= \xi_2 \\
N_3 &= \xi_3 \\
N_4 &= \xi_4 = 1 - \xi_1 - \xi_2 - \xi_3
\end{aligned}
\tag{3.41}
$$

It is well known that due to the Babuška-Brezzi condition (or inf-sup condition)[4] the choice of identical shape functions for both displacement and pressure variables is not allowed unless we add stabilization terms to the variational formulation or enrich the space of displacements with a bubble function as in the MINI element [3].

Taylor [47] showed that it is also possible to consider the term added to the strains and deleted the bubble function from the displacement terms. As a solution to this problem an enhanced strain was constructed from the derivative of a bubble function and it was added to provide the

47

necessary stabilization. Our element is based on the same approach and therefore it will have a node in each corner and an internal node located in the center. Two bubble functions, conforming and nonconforming, are studied for an optimal selection.

Conforming Bubble Functions

These functions are a family of high order polynomials that are zero on the boundary of the element. A standard conforming bubble function is the cubic bubble function. The cubic bubble function was used in the development of MINI element and also in the available literature related to triangular and tetrahedral elements [5, 9-10, 12, 23-25, 29-30]. If, for any tetrahedral element we denote the volumetric coordinates by ξ_i, i=1,2,3,4, the conforming bubbles are according to [39]:

$$N_e^c = 64\xi_1\xi_2\xi_3(1-\xi_1-\xi_2-\xi_3) \tag{3.42}$$

This bubble function was used by Taylor [47] in the formulation of his mixed-enhanced tetrahedral element. Taylor's results indicate that the conforming bubble function in (3.52) does not eliminate all oscillations for problems where strong pressure gradients occur. Accordingly, in this research, we will also consider other choice for bubble functions.

Non-Conforming Bubble Functions

R. Pierre showed in 1995 [39], that the conforming bubbles satisfy the LBB condition as long as the mesh is regular. He demonstrated that this happens only if the triangle is equilateral. Hence, he proposed an optimal bubble function for which the local stabilizing effect is the greatest.

This optimal bubble function is a quadratic non-conforming one which means that it does not vanish on the perimeter but it is unity in the center node. This function is defined for any tetrahedron as:

$$N_e^q = 2 - 4\sum_{i=1}^{4} \xi_i^2 \tag{3.43}$$

This function was also used in our formulation due to the following <u>advantages</u>:

- It has the highest stabilizing factor, especially in three dimensions..

- Since it is a quadratic function it will yield linear strains which are fully consistent with the linear interpolations of u and p.

- Implies a lower computational cost due to the fact that we use a quadratic function instead of a cubic (2D) or a quartic one (3D).

- Numerical integration is also less costly.

- In every other aspect the nonconforming bubble is as simple to use as the conforming one.

3.6.2 Matrix Formulation

Using the same interpolation functions for all variables, the displacements and pressures can be represented as:

$$\begin{aligned}
&\mathbf{u}(\xi) = \xi_\alpha \mathbf{u}^\alpha, \overline{P}(\xi) = \xi_\alpha \overline{P}^\alpha \\
&\delta\mathbf{u}(\xi) = \xi_\alpha \delta\mathbf{u}^\alpha, \delta\overline{P}(\xi) = \xi_\alpha \delta\overline{P}^\alpha \\
&D\mathbf{u}(\xi) = \xi_\alpha D\mathbf{u}^\alpha, D\overline{P}(\xi) = \xi_\alpha D\overline{P}^\alpha
\end{aligned} \tag{3.44}$$

where the nodal displacements and pressures together with their variations and increments are:

$$\begin{aligned}
&\mathbf{u}^\alpha = \left[\mathbf{u}^1 \mathbf{u}^2 \mathbf{u}^3 \mathbf{u}^4\right]^T, \overline{\mathbf{P}}^\alpha = \left[\overline{P}^1 \overline{P}^2 \overline{P}^3 \overline{P}^4\right]^T \\
&\delta\mathbf{u}^\alpha = \left[\delta\mathbf{u}^1 \delta\mathbf{u}^2 \delta\mathbf{u}^3 \delta\mathbf{u}^4\right]^T, \delta\overline{\mathbf{P}}^\alpha = \left[\delta\overline{P}^1 \delta\overline{P}^2 \delta\overline{P}^3 \delta\overline{P}^4\right]^T \\
&D\mathbf{u}^\alpha = \left[D\mathbf{u}^1 D\mathbf{u}^2 D\mathbf{u}^3 D\mathbf{u}^4\right]^T, D\overline{\mathbf{P}}^\alpha = \left[D\overline{P}^1 D\overline{P}^2 D\overline{P}^3 D\overline{P}^4\right]^T
\end{aligned} \tag{3.45}$$

and the discretized strains are expressed with the help of an enhanced strain-displacement matrix $\mathbf{B}^{enh}$ as :

$$
\begin{aligned}
\boldsymbol{\varepsilon}^{enh} &\approx \mathbf{B}^{enh}_{\alpha}\mathbf{u}^{\alpha} \\
\delta\boldsymbol{\varepsilon}^{enh} &\approx \mathbf{B}^{enh}_{\alpha}\delta\mathbf{u}^{\alpha} \\
D\boldsymbol{\varepsilon}^{enh} &\approx \mathbf{B}^{enh}_{\alpha}D\mathbf{u}^{\alpha}
\end{aligned}
\tag{3.46}
$$

The enlarged strain-displacement matrix has three additional columns corresponding to the three additional internal displacements and it has to be evaluated with respect to the current configuration. It has the form: $\qquad$ (3.47)

$$
{}_{t+\Delta t}B^{enh} =
\left[
\begin{array}{ccc:ccc}
\dfrac{\partial N_1}{\partial^{t+\Delta t}x_1} & 0 & 0 & \dfrac{\partial N_e}{\partial^{t+\Delta t}x_1} & 0 & 0 \\[2mm]
0 & \dfrac{\partial N_1}{\partial^{t+\Delta t}x_2} & 0 & 0 & \dfrac{\partial N_e}{\partial^{t+\Delta t}x_2} & 0 \\[2mm]
0 & 0 & \dfrac{\partial N_1}{\partial^{t+\Delta t}x_3} & 0 & 0 & \dfrac{\partial N_e}{\partial^{t+\Delta t}x_3} \\[2mm]
\dfrac{\partial N_1}{\partial^{t+\Delta t}x_2} & \dfrac{\partial N_1}{\partial^{t+\Delta t}x_1} & 0 & \dfrac{\partial N_e}{\partial^{t+\Delta t}x_2} & \dfrac{\partial N_e}{\partial^{t+\Delta t}x_1} & 0 \\[2mm]
0 & \dfrac{\partial N_1}{\partial^{t+\Delta t}x_3} & \dfrac{\partial N_1}{\partial^{t+\Delta t}x_2} & 0 & \dfrac{\partial N_e}{\partial^{t+\Delta t}x_3} & \dfrac{\partial N_e}{\partial^{t+\Delta t}x_2} \\[2mm]
\dfrac{\partial N_1}{\partial^{t+\Delta t}x_3} & 0 & \dfrac{\partial N_1}{\partial^{t+\Delta t}x_1} & \dfrac{\partial N_e}{\partial^{t+\Delta t}x_3} & 0 & \dfrac{\partial N_e}{\partial^{t+\Delta t}x_1}
\end{array}
\right]
\quad \alpha = 1,4
$$

Evaluation of the Cartesian derivatives of the shape functions at time $t+\Delta t$ can be done using the derivatives at time t and incremental deformation gradient defined in (3.32):

$$
\frac{\partial N_{\alpha}}{\partial^t x_j} = \frac{\partial N_{\alpha}}{\partial^{t+\Delta t}x_k}\cdot\frac{\partial^{t+\Delta t}x_k}{\partial^t x_j} = \frac{\partial N_{\alpha}}{\partial^{t+\Delta t}x_k}\cdot({}^{t+\Delta t}_{t}\Delta F^{enh}_{kj}) \Rightarrow \frac{\partial N_{\alpha}}{\partial^{t+\Delta t}x_j} = ({}^{t+\Delta t}_{t}\Delta F^{enh}_{kj})^{-T}\cdot\frac{\partial N_{\alpha}}{\partial^t x_j}
\tag{3.48}
$$

Using the above finite element approximations and by placing the variations in the left hand side and the increments in the right hand side, each of the integrals from (3.27) yields the specific stiffness matrix associated with the corresponding variable as:

1. Constitutive stiffness matrix:

$$\mathbf{K}_{uu}^{enh,c} = \int_V \mathbf{B}_{enh}^{\mathbf{T}} (\mathbf{C} - \frac{1}{9K}\mathbf{C}^T \cdot \mathbf{I} \cdot \mathbf{I} \cdot \mathbf{C})\mathbf{B}_{enh}dV \tag{3.49}$$

2. Displacement pressure stiffness matrices:

$$\mathbf{K}_{up}^{enh} = (\mathbf{K}_{pu}^{enh})^{\mathbf{T}} = \int_V \frac{1}{3K_t}\mathbf{B}_{enh}^{\mathbf{T}} \ \mathbf{C}^{\mathbf{T}} \cdot \mathbf{I} \cdot \mathbf{N}dV \tag{3.50}$$

3. Pressure stiffness matrix:

$$\mathbf{K}_{pp} = \int_V -\frac{1}{K}\mathbf{N}^{\mathbf{T}} \cdot \mathbf{N}dV \tag{3.51}$$

where the Voigt matrix notation was used (each second rank tensor is written as a vector and each fourth rank tensor as a matrix).

According to this notation we have:

$$\boldsymbol{\sigma} = \begin{bmatrix} \sigma_{xx} & \sigma_{yy} & \sigma_{zz} & \sigma_{xy} & \sigma_{yz} & \sigma_{zx} \end{bmatrix}^T \tag{3.52}$$

$$\boldsymbol{\varepsilon} = \begin{bmatrix} \varepsilon_{xx} & \varepsilon_{yy} & \varepsilon_{zz} & 2\varepsilon_{xy} & 2\varepsilon_{yz} & 2\varepsilon_{zx} \end{bmatrix}^T \tag{3.53}$$

$$\mathbf{I} = \begin{bmatrix} 1 & 1 & 1 & 0 & 0 & 0 \end{bmatrix}^T \tag{3.54}$$

The elastic moduli are written also in terms of a matrix as:

$$C = \begin{bmatrix}
C_{11} & C_{12} & C_{13} & C_{14} & C_{15} & C_{16} \\
C_{21} & C_{22} & C_{23} & C_{24} & C_{25} & C_{26} \\
C_{31} & C_{31} & C_{33} & C_{34} & C_{35} & C_{36} \\
C_{41} & C_{42} & C_{43} & C_{44} & C_{45} & C_{46} \\
C_{51} & C_{52} & C_{53} & C_{54} & C_{55} & C_{56} \\
C_{61} & C_{62} & C_{63} & C_{64} & C_{65} & C_{66}
\end{bmatrix} \tag{3.55}$$

When large deformations are expected the geometric stiffness matrix is added to the constitutive stiffness matrix to form the final stiffness matrix which is a square symmetric matrix having the dimension of the total number of degrees of freedom.

Converting the formulation of this term into a matrix having the same size as the constitutive stiffness matrix is a rather complicated task since the Voigt notation cannot be used in this case due to the discrepancies in the sizes of the matrices. The procedure used in this work is outlined in the next paragraph.

4. Geometric stiffness matrix:

$$\mathbf{K}_{uu}^{enh,g} = \int_V \left[\mathbf{N}_{,i}^{enh}\right]\left[\overline{\boldsymbol{\sigma}}_{\mathbf{ij}}\right]\left[\mathbf{N}_{,j}^{enh}\right]dV \; - \; \int_V \left[\mathbf{B}_{\mathbf{ki}}^{\mathbf{T},enh}\right]\left[\overline{\boldsymbol{\sigma}}_{ij}\right]\left[\mathbf{B}_{kj}^{enh}\right]dV \tag{3.56}$$

where $\left[\mathbf{N}_{,i}^{enh}\right]$ is the enhanced matrix formed by the derivatives of the shape functions together with the derivatives of the bubble function, obtained by writing the gradient of the virtual displacement matrix as a vector of nine components as follows:

$$\left\{\frac{\partial \delta u_i}{\partial^{t+\Delta t}x_j}\right\} = \left\{\frac{\partial \delta u_1}{\partial x_1}\; \frac{\partial \delta u_1}{\partial x_2}\; \frac{\partial \delta u_1}{\partial x_3}\; \frac{\partial \delta u_2}{\partial x_1}\; \frac{\partial \delta u_2}{\partial x_2}\; \frac{\partial \delta u_2}{\partial x_3}\; \frac{\partial \delta u_3}{\partial x_1}\; \frac{\partial \delta u_3}{\partial x_2}\; \frac{\partial \delta u_3}{\partial x_3}\right\}^T = \left[\frac{\partial N_\alpha}{\partial x_j}\right]\left\{\delta u_i^{\alpha,enh}\right\} \tag{3.57}$$

where

$$\left\{\delta u_i^{\alpha,enh}\right\} = \left\{\delta u_1^1 \quad \delta u_2^1 \quad \delta u_3^1 \quad \delta u_1^2 \quad \delta u_2^2 \quad \delta u_3^2 \quad \delta u_1^3 \quad \delta u_2^3 \quad \delta u_3^3\; \delta u_1^4 \quad \delta u_2^4 \quad \delta u_3^4 \quad \delta u_1^e \quad \delta u_2^e \quad \delta u_3^e\right\}$$

is the enhanced vector of degrees of freedom formed by the twelve external displacement degrees of freedom and the three internal displacement degree of freedom.

Using the above arrangement of vectors the matrix of the derivatives of shape functions can be written as a 9x15 matrix as:

$$\left[\frac{\partial N^{enh}{}_\alpha}{\partial x_j}\right] = \begin{bmatrix} \dfrac{\partial N_1}{\partial x_1} & 0 & 0 & & & & & & \dfrac{\partial N_e}{\partial x_1} \\[2mm] \dfrac{\partial N_1}{\partial x_2} & 0 & 0 & & & & & & \dfrac{\partial N_e}{\partial x_2} \\[2mm] \dfrac{\partial N_1}{\partial x_3} & 0 & 0 & & & & & & \dfrac{\partial N_e}{\partial x_2} \\[2mm] 0 & \dfrac{\partial N_1}{\partial x_1} & 0 & & & & & & \dfrac{\partial N_e}{\partial x_1} \\[2mm] 0 & \dfrac{\partial N_1}{\partial x_2} & 0 & & & & & & \dfrac{\partial N_e}{\partial x_2} \\[2mm] 0 & \dfrac{\partial N_1}{\partial x_3} & 0 & & & & & & \dfrac{\partial N_e}{\partial x_3} \\[2mm] 0 & 0 & \dfrac{\partial N_1}{\partial x_1} & & & & & & \dfrac{\partial N_e}{\partial x_1} \\[2mm] 0 & 0 & \dfrac{\partial N_1}{\partial x_2} & & & & & & \dfrac{\partial N_e}{\partial x_2} \\[2mm] 0 & 0 & \dfrac{\partial N_1}{\partial x_3} & \alpha=1,4 & & & & & \dfrac{\partial N_e}{\partial x_3} \end{bmatrix} \quad (3.58)$$

The Cauchy stress matrix that appears in both terms is written as a 9x9 diagonal matrix as:

$$[\bar{\sigma}_{ij}](9x9) = \begin{bmatrix} \bar{\sigma}_{11} & \bar{\sigma}_{12} & \bar{\sigma}_{13} & 0 & 0 & 0 & 0 & 0 & 0 \\ \bar{\sigma}_{21} & \bar{\sigma}_{22} & \bar{\sigma}_{23} & 0 & 0 & 0 & 0 & 0 & 0 \\ \bar{\sigma}_{31} & \bar{\sigma}_{32} & \bar{\sigma}_{33} & 0 & 0 & 0 & 0 & 0 & 0 \\ 0 & 0 & 0 & \bar{\sigma}_{11} & \bar{\sigma}_{12} & \bar{\sigma}_{13} & 0 & 0 & 0 \\ 0 & 0 & 0 & \bar{\sigma}_{21} & \bar{\sigma}_{22} & \bar{\sigma}_{23} & 0 & 0 & 0 \\ 0 & 0 & 0 & \bar{\sigma}_{31} & \bar{\sigma}_{31} & \bar{\sigma}_{33} & 0 & 0 & 0 \\ 0 & 0 & 0 & 0 & 0 & 0 & \bar{\sigma}_{11} & \bar{\sigma}_{12} & \bar{\sigma}_{13} \\ 0 & 0 & 0 & 0 & 0 & 0 & \bar{\sigma}_{21} & \bar{\sigma}_{22} & \bar{\sigma}_{23} \\ 0 & 0 & 0 & 0 & 0 & 0 & \bar{\sigma}_{31} & \bar{\sigma}_{32} & \bar{\sigma}_{33} \end{bmatrix} \quad (3.59)$$

The same procedure is used for the second term of the geometric stiffness matrix.

The linear system of equations in matrix format will be:

$$\begin{bmatrix} K^{enh}_{uu} & K^{enh}_{up} \\ K^{enh}_{pu} & K_{pp} \end{bmatrix} \begin{bmatrix} Du^{enh} \\ D\bar{P} \end{bmatrix} = \begin{bmatrix} F^{ext} - F^{enh}_u \\ 0 - F_p \end{bmatrix} \quad (3.60)$$

where $K^{enh}_{uu} = K^{enh,c}_{uu} + K^{enh,g}_{uu}$ is a square matrix of size 15x15, $\quad (3.61)$

Du^{enh} is the vector of external and internal degrees of freedom of size 15,

F_u^{enh} is the internal force resulting from the equilibrium equation and,

F_p^{h} is the internal force resulting from the constraint equation.

5. Internal Forces

From the first term of the principle of virtual work the internal force due to the displacement degrees of freedom can be computed as:

$$F_u^{enh} = \int_V (B^{enh})^T \cdot \overline{\sigma} dV \tag{3.62}$$

where $\overline{\sigma} = \sigma + I(\overline{P} - P)$ is the modified Cauchy stress at time $t+\Delta t$ obtained from the strain increment using the Jaumann stress rate and integrated numerically over the substep.

From the second term of the principle of virtual work,

$$\int_V (\varepsilon_v^{enh} - \overline{\varepsilon}_v) \delta \overline{P} dV ,$$

we can compute the fictitious internal force due to the mixed u/p formulation as:

$$\begin{aligned}
F_p &= \int_V \left(D\varepsilon_v - \frac{D\overline{P}}{K} + \frac{\delta_{ij}}{3K} C_{ijkl} D\varepsilon_{kl} - D\varepsilon_v \right) \delta \overline{P} dV = \\
&= \int_V \left(-D\overline{P}\frac{1}{K} + \frac{\delta_{ij}}{3K} C_{ijkl} D\varepsilon_{kl} \right) \delta \overline{P} dV = \\
&= \int_V (DP - D\overline{P}) \delta \overline{P} \frac{1}{K} dV = \int_V (DP - D\overline{P}) \mathbf{N} \cdot \frac{1}{K} dV
\end{aligned} \tag{3.63}$$

where $DP = P^{t+\Delta t} - P^t = \frac{1}{3}\left(\sigma_1^{t+\Delta t} + \sigma_2^{t+\Delta t} + \sigma_3^{t+\Delta t}\right) - \frac{1}{3}\left(\sigma_1^t + \sigma_2^t + \sigma_3^t\right)$ \hfill (3.64)

and the Cauchy stresses at time t are stored from the previous substep.

4.0 ELEMENT IMPLEMENTATION ASPECTS

The finite element method is accompanied by a large number of numerical procedures such as numerical integration, numerical algorithms for solving nonlinear problems, methods for solving a linear system of equations and other methods not related to the scope of our research topic. Since the commercial finite element code ANSYS will be used for implementation, all the numerical methods related to this code will be used.

4.1 INTEGRATION RULES

In the case of distorted elements and non-linear behavior numerical integration is needed. For the proposed tetrahedral element a four point Gauss numerical integration rule was used.

$$\int_V f(\xi)dV = \frac{1}{6}\sum_{l=1}^{n} w_i f(\xi_i)dV \tag{4.1}$$

The factor 1/6 was required because the weighting coefficients always add up unity whereas the volume of the tetrahedron in volume coordinates equals 1/6. The weighting factors and the location of the Gauss integration points are listed in Table1 and shown in Figure 3.
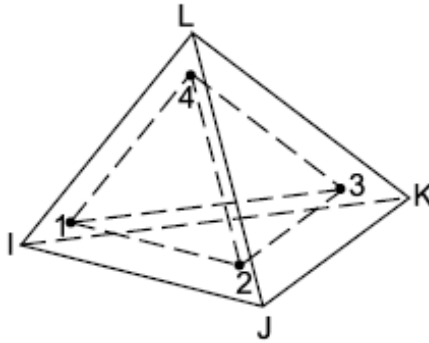
Figure 3. Integration Point Location for Tetrahedral Element [2]

Table 1. Numerical Integration for Tetrahedral Element [2]

Type	Integration Point Location	Weighting Factor
4 corner points	$\xi_1 = 0.585410196624968$ $\xi_2 = \xi_3 = \xi_4 = 0.138196601125010$ Permute ξ_1, ξ_2, ξ_3, ξ_4 for other locations	0.250000000000000

Since stiffness matrices and internal forces are all expressed as integrals over the volume of the element we need an expression for the volume of the tetrahedral element. This is given by the determinant of the Jacobian transformation matrix between volume and Cartesian coordinates as:

$$dV = |Jac| = \frac{1}{6} \begin{vmatrix} \dfrac{\partial x_1}{\partial \xi_1} & \dfrac{\partial x_1}{\partial \xi_2} & \dfrac{\partial x_1}{\partial \xi_3} \\ \dfrac{\partial x_2}{\partial \xi_1} & \dfrac{\partial x_2}{\partial \xi_2} & \dfrac{\partial x_2}{\partial \xi_3} \\ \dfrac{\partial x_3}{\partial \xi_1} & \dfrac{\partial x_3}{\partial \xi_2} & \dfrac{\partial x_3}{\partial \xi_3} \end{vmatrix}$$

(4.2)

which can be derived from:

$$\begin{bmatrix} x_1 \\ x_2 \\ x_3 \end{bmatrix} = \begin{bmatrix} x_1^1 & x_1^2 & x_1^3 & x_1^4 \\ x_2^1 & x_2^2 & x_2^3 & x_2^4 \\ x_3^1 & x_3^2 & x_3^3 & x_3^4 \end{bmatrix} \begin{bmatrix} \xi_1 \\ \xi_2 \\ \xi_3 \\ \xi_4 \end{bmatrix}$$

(4.3)

where x_i^α are the Cartesian coordinates of node α.

This volume is a signed quantity which means that it is positive if the corner nodes are numbered in a special way. To avoid problems with negative volumes, a special subroutine was inserted at the beginning of the user element subroutine in which the volumes for each element were calculated and checked for negative values.

If the volume was found to be negative the sign was changed and stored so it would be accessible at each iteration. Inside the Gauss integration loop the element volume was always multiplied with the sign saved.

4.2 NONLINEAR ITERATIVE ALGORITHM

It was shown in chapter 3 that by using an Updated Lagrangian Formulation the element matrices and load vectors were derived. They can be arranged as a linear system of equations of the form expressed in (3.61) or in an expanded form as:

$$
\begin{bmatrix}
\mathbf{K}_{uu}(12\text{x}12) & \mathbf{K}_{ue}(12\text{x}3) & \mathbf{K}_{up}(12\text{x}4) \\
\mathbf{K}_{eu}(3\text{x}12) & \mathbf{K}_{ee}(3\text{x}3) & \mathbf{K}_{ep}(3\text{x}4) \\
\mathbf{K}_{pu}(4\text{x}12) & \mathbf{K}_{pe}(4\text{x}3) & \mathbf{K}_{pp}(4\text{x}4)
\end{bmatrix}_{(19,19)}
\begin{bmatrix}
\mathbf{Du}(12) \\
\mathbf{Du}_e(3) \\
\mathbf{D\bar{p}}(4)
\end{bmatrix}_{(19)}
=
\begin{bmatrix}
\mathbf{F}^{ext} - \mathbf{F}_u(12) \\
\mathbf{F}_e(3) \\
\mathbf{F}_p(4)
\end{bmatrix}_{(19)}
\qquad (4.4)
$$

where the second row and second column in the element stiffness matrix are actually the last three rows and last three columns of the enhanced stiffness matrix. In other words K_{ue}, K_{pe}, K_{ee} matrices are just parts of the enhanced $K_{uu}(15,15)$ matrix. The sizes of the partitioned matrices and vectors are shown in the parentheses.

Since the proposed interpolations for $\boldsymbol{u}$ and $\bar{p}$ are continuous in the whole domain, and the enhanced strain parameters are introduced only internally in the element, the solution can be performed in two steps. In the first step the internal displacements $\boldsymbol{u}_e$ are eliminated at the element level by static condensation. In the second step the reduced stiffness matrix obtained from the first step, together with the residuals, are assembled into the global equations to be solved using the Newton- Raphson iterative algorithm.

4.2.1 Static Condensation Procedure

In order to solve for the internal displacements, we first need to swap the rows and columns corresponding to the internal parameters with the rows and columns corresponding to the pressure variables. This is done so the final element arrays will have only the displacement and pressure degrees of freedom. The final size of the stiffness matrix, load vector and the vector of the external degrees of freedom has to be 12+4=16. The following steps were performed in the static condensation procedure:

1. Introduce one row and one column of zeros in the 16th place of the enhanced stiffness matrix which will be now (20, 20).

2. Swap the rows and columns corresponding to u_e and $\overline{p}$ such that the internal parameters will be arranged the last and the pressures in the middle. The last row and the last column of the matrix will be all zeros and will be eliminated together with the residuals. The system will now have the form:

$$\begin{bmatrix} \mathbf{K}_{uu}(12\mathbf{x}12) & \mathbf{K}_{up}(12\mathbf{x}4) & \mathbf{K}_{ue}(12\mathbf{x}3) \\ \mathbf{K}_{pu}(4\mathbf{x}12) & \mathbf{K}_{pp}(4\mathbf{x}4) & \mathbf{K}_{pe}(4\mathbf{x}3) \\ \mathbf{K}_{eu}(3\mathbf{x}12) & \mathbf{K}_{ep}(3\mathbf{x}4) & \mathbf{K}_{ee}(3\mathbf{x}3) \end{bmatrix} \begin{bmatrix} \mathbf{Du}(12) \\ \mathbf{D\overline{p}}(4) \\ \mathbf{Du}_e(3) \end{bmatrix} = \begin{bmatrix} \mathbf{F}^{ext} - \mathbf{F}_u \\ \mathbf{0} - \mathbf{F}_p \\ \mathbf{0} - \mathbf{F}_e \end{bmatrix} \qquad (4.5)$$

3. Partition the matrices as:

$$\begin{bmatrix} \mathbf{K}_{11}(16\mathbf{x}16) & \mathbf{K}_{12}(16\mathbf{x}3) \\ \mathbf{K}_{21}(3\mathbf{x}16) & \mathbf{K}_{ee}(3\mathbf{x}3) \end{bmatrix} \begin{bmatrix} \mathbf{Du}_{final} \\ \mathbf{Du}_e \end{bmatrix} = \begin{bmatrix} \mathbf{F}_1 \\ -\mathbf{F}_e \end{bmatrix} \qquad (4.6)$$

$$\mathbf{K}_{11} = \begin{bmatrix} \mathbf{K}_{uu}(12\mathbf{x}12) & \mathbf{K}_{up}(12\mathbf{x}4) \\ \mathbf{K}_{pu}(4\mathbf{x}12) & \mathbf{K}_{pp}(4\mathbf{x}4) \end{bmatrix} \qquad (4.7)$$

$$\mathbf{K}_{12} = \begin{bmatrix} \mathbf{K}_{ue}(12\mathbf{x}3) \\ \mathbf{K}_{pe}(4\mathbf{x}3) \end{bmatrix} \qquad (4.8)$$

$$K_{21} = \left[K_{eu}(3x12) \quad K_{ep}(3x4) \right] \tag{4.9}$$

$$Du_{final} = \begin{bmatrix} Du \\ D\bar{p} \end{bmatrix} \tag{4.10}$$

$$F_1 = \begin{bmatrix} F^{ext} - F_u \\ -F_p \end{bmatrix} \tag{4.11}$$

4. Store $(K_{ee})^{-1} * K_{21}, (K_{ee})^{-1} * F_e$ and retrieve them at the beginning of the next iteration to calculate the iterative value of the internal displacement degrees of freedom.

$$Du^{iter}_e = -\left[K_{ee} \right]^{-1}(F_e - K_{21} \cdot Du^{iter}) \tag{4.12}$$

The increment of the internal displacements is obtained as an accumulation of each iteration value and is stored if the iteration converged.

$$Du_e^{substep} = \sum Du_e^{iter} \tag{4.13}$$

5. Substitute in the first equation to get the final stiffness matrix of size (16,16):

$$K_{final} \cdot Du_{final} = (K_{11} - K_{12} * K_{ee}^{-1} * K_{21}) \cdot Du_{final} = F_{1final} \tag{4.14}$$

6. Calculate reduced internal force as: $F_{1final} = F_1 - (K_{ee})^{-1} * F_e$ (4.15)

7. From here the assembly of final element matrix and residual into global equations proceeds to find out the incremental values of nodal displacements and pressures.

4.2.2 Newton – Raphson Procedure

The basic approach in an incremental step-by-step solution is to assume that the solution at time t is known and to solve for the solution at time $t+\Delta t$ using the balance between the externally applied forces F^{ext} and the restoring forces that correspond to element stresses [6]:

$$^{t+\Delta t}\mathbf{F}^{ext} = {}^{t+\Delta t}\mathbf{F}^{int} \qquad (4.16)$$

where

$$^{t+\Delta t}\mathbf{F}^{int} = {}^{t}\mathbf{F} + \mathbf{F} \qquad (4.17)$$

and $\mathbf{F}$ is the increment in nodal point forces that can be approximated using a tangent stiffness matrix ${}^{t}\mathbf{K}$ which corresponds to the geometric and material conditions at time t .

$$\mathbf{F} = {}^{t}\mathbf{K}\mathbf{Du} \qquad (4.18)$$

where Du is the vector of incremental nodal point displacements.

Thus we obtain,

$$^{t}\mathbf{K}\mathbf{Du} = {}^{t+\Delta t}\mathbf{F}^{ext} - {}^{t}\mathbf{F} \qquad (4.19)$$

Solving for $\mathbf{Du}$ we can calculate an approximation to the displacements at time $t+\Delta t$ as:

$$^{t+\Delta t}\mathbf{u} = {}^{t}\mathbf{u} + \mathbf{Du} \qquad (4.20)$$

From the above expression, the strains, stresses and nodal point forces can be calculated at time $t+\Delta t$, and the procedure can move to the next time increment. Since this procedure may be very unstable the widely used full Newton-Raphson iteration technique (stiffness matrix is updated at each iteration) is utilized in ANSYS to solve the global system.

The equations used in the Newton-Raphson iteration are:

$$^{t+\Delta t}\mathbf{K}^{(i-1)}\mathbf{Du}^{(i)} = {}^{t+\Delta t}\mathbf{F}^{ext} - {}^{t+\Delta t}\mathbf{F}^{(i-1)}$$

$$^{t+\Delta t}\mathbf{u}^{(i)} = {}^{t+\Delta t}\mathbf{u}^{(i-1)} + \mathbf{Du}^{(i)}$$

(4.21)

with the initial conditions:

$$^{t+\Delta t}\mathbf{u}^{(0)} = {}^{t}\mathbf{u}$$

$$^{t+\Delta t}\mathbf{K}^{(0)} = {}^{t}\mathbf{K}$$

$$^{t+\Delta t}\mathbf{F}^{(0)} = {}^{t}\mathbf{F}$$

(4.22)

The general algorithm for a substep at iteration (i) is illustrated in Figure 4 and can be described as follows[2]:

1. Assume $\mathbf{u_0}$ which is usually the converged solution from previous time step and for the first iteration of the first substep is just zero.

2. Compute the updated element stiffness matrix, strains and stresses, which in inelastic analysis are obtained by an integration process, and using (3.63) compute the restoring load.

3. Check equilibrium and if the restoring load is not equal (or at least to within some tolerance) to the applied force then compute $\mathbf{Du}^{(i)}$ using first equation of (4.20).

4. Update the displacement to obtain the next approximation using second equation of (4.20).

5. Repeat steps 2 to 4 until convergence is achieved.
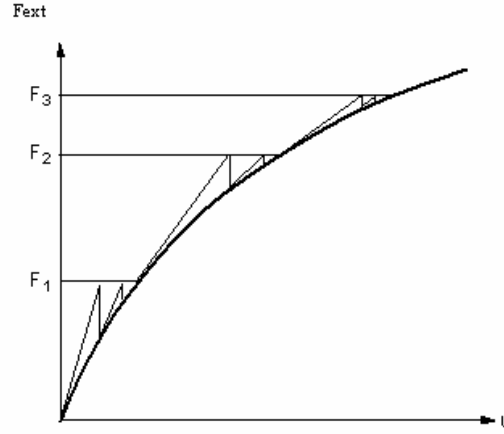
Figure 4. Newton-Raphson Procedure[2]

Convergence in our case is assumed when

$$\|R\| < \varepsilon_R R_{ref} \quad \text{and} \quad \left\|\left(Du^{(i)}\right)\right\| < \varepsilon_u u_{ref} \text{ and } \quad \left\|\left(D\overline{P}^{(i)}\right)\right\| < \varepsilon_p P_{ref} \tag{4.23}$$

where $\mathbf{R} = \mathbf{F}^{ext} - \mathbf{F}^{int}$ is the residual vector and ε_R, ε_u, ε_p are tolerances and the corresponding

R_{ref}, u_{ref}, P_{ref} are reference values and the norm used is the Euclidean norm that is the scalar

measure of the magnitude of the vector as:

$$\|R\| = \sqrt{\sum R_i^2} \tag{4.24}$$

The tolerance used for the out-of-balance convergence for displacement degree of freedom is

0.05 and 0.000125 for the pressure degree of freedom. The default out-of-balance reference

value used was $\left\|\mathbf{F}^{ext}\right\|$, for displacement $\|\mathbf{u}\|$ and for pressure a reference value of 1 was used.

4.3 STRESS AND STRAIN UPDATE ALGORITHM

When a Newton-Raphson iterative algorithm is applied to a history-dependent problem, as in our

case, the nonconverged solution obtained from the iteration process is usually not on the actual

path and thus, the strain and stress which are history-dependent variables have to be integrated over the increment each iteration [1]. They cannot be computed as the sum of the integrations performed in each iteration. We assume though that the primary variables are varying linearly over the increment.

In our formulation the strain is defined as the integral of the strain rate. This integration has to take into account the fact that the principal axes of strain rotate during the deformation.

Therefore the strain at the beginning of the increment must be rotated with the amount of rigid body rotation that occurs during that increment. This is done using the Hughes-Winget [27] algorithm. According to Hughes-Winget, any tensor associated with a rate constitutive equation is integrated as:

$$\mathbf{a_{t+\Delta t}} = \mathbf{\Delta R} \cdot \mathbf{a_t} \cdot \mathbf{\Delta R^T} + \mathbf{\Delta \breve{a}(D\varepsilon)} \tag{4.25}$$

where **a** is the tensor, $\mathbf{\Delta \breve{a}}$ is the increment associated with the material's constitutive behavior which depends on the strain increment, $\mathbf{D\varepsilon}$, defined by the central difference formula as:

$$D\varepsilon = sym(\frac{\partial Du}{\partial x_{t+\Delta t/2}}) \tag{4.26}$$

where

$$x_{t+\Delta t/2} = \frac{1}{2}(x_t + x_{t+\Delta t}) \tag{4.27}$$

and $\mathbf{\Delta R}$ is the rotation matrix computed from the polar decomposition of the deformation gradient at the midpoint configuration:

$$\Delta F_{1/2} = \Delta R_{1/2} \cdot \Delta U_{1/2} \tag{4.28}$$

The displacement increment at midpoint configuration,

$$\frac{\partial \mathbf{Du}}{\partial \mathbf{x}_{t+\Delta t/2}} = \frac{\partial \mathbf{Du}}{\partial \mathbf{x}_{t+\Delta t}} \cdot \frac{\partial \mathbf{x}_{t+\Delta t}}{\partial \mathbf{x}_{t+\Delta t/2}}$$ (4.29)

is computed from the increment of deformation gradient evaluated at the midpoint configuration:

$$\frac{\partial \mathbf{x}_{t+\Delta t}}{\partial \mathbf{x}_{t+\Delta t/2}} = (\frac{\partial \mathbf{x}_{t+\Delta t/2}}{\partial \mathbf{x}_{t+\Delta t}})^{-1} = \left(\frac{\partial (\mathbf{x}_{t+\Delta t} - \frac{1}{2}\mathbf{Du})}{\partial \mathbf{x}_{t+\Delta t}}\right)^{-1} = \left(\mathbf{I} - \frac{1}{2}(\frac{\partial \mathbf{Du}}{\partial \mathbf{x}_{t+\Delta t}})\right)^{-1}$$ (4.30)

and $\dfrac{\partial \mathbf{Du}}{\partial \mathbf{x}_{t+\Delta t}} = \mathbf{B}^{\mathbf{enh}}{}_{t+\Delta t} \cdot \mathbf{Du}$ (4.31)

yielding

$$\frac{\partial \mathbf{Du}}{\partial \mathbf{x}_{t+\Delta t/2}} = \frac{\partial \mathbf{Du}}{\partial \mathbf{x}_{t+\Delta t}} * (\mathbf{I} - \frac{1}{2}\frac{\partial \mathbf{Du}}{\partial \mathbf{x}_{t+\Delta t}})^{-1}$$ (4.32)

If $^{t+\Delta t}\mathbf{U}^{(i-1)}$ and the strains, $^{t+\Delta t}\boldsymbol{\varepsilon}^{(i-1)}$, are known then we proceed to calculate the stresses $^{t+\Delta t}\boldsymbol{\sigma}^{(i-1)}$ which in inelastic analysis are obtained by the above described integration process as in (4.25).

5.0 NUMERICAL INVESTIGATIONS OF LINEAR INCOMPRESSIBLE MATERIALS

The mixed enhanced strain formulation proposed was implemented through a user-programmable element into the commercial finite element software ANSYS. Using the ANSYS platform, the performance of the stabilized formulation was tested considering several 3D problems using the newly developed tetrahedral element. The results of problems were compared to either analytical results in the literature or well known solutions with mixed hexahedral elements with B-bar formulation [2]. The user-programmable element was implemented with four key options such that four formulations are allowed. This was done to show the improvement of the proposed formulation as compared to the pure displacement and mixed u/p without stabilization formulations. The four formulations were: mixed u/p enhanced stabilized with cubic bubble function, mixed enhanced with quadratic bubble function, mixed u/p without stabilization and pure displacement.

Four different tests were developed for linear elastic materials, each of them being carried out at different Poisson's ratios and different mesh sizes: homogeneous deformation tests, thick-walled cylinder under pressure, Cook's membrane problem and two cantilever beam tests for testing the capability of the element in bending. Two different meshes were used in these problems. Whenever the problem permitted (bending tests), the mesh was created by generating, in three directions, blocks of six tetrahedral elements such that the comparison with the hexahedral elements would be more meaningful. In this manner, the number of nodes was the

same in both hexahedral and tetrahedral meshes. It is important to note, however, that the number of elements in the tetrahedral meshes is six times greater than the number of hexahedral elements that were modeled. Therefore, some minor differences in element solutions were expected since the mesh size has an influence on the strain and stress values.

5.1 HOMOGENEOUS DEFORMATION TESTS

Two homogeneous deformation tests were carried out to check the capability of the element to sustain constant strain states. The patch tests were also a very useful tool for the finite element developer to assess the correctness of their formulation and eventual mistakes in programming.

1. Uniaxial compression test

The finite element model for this test represents a cube with side length of 1 made up of six tetrahedral elements. Three of its adjacent faces are restrained to move only in their own planes. The cube is subjected to 4 forces ($F_1=F_7=-1/6$ and $F_5=F_4=-1/3$) that provide a uniform compressive stress of 1 MPa. The material properties used are E=1e6 MPa and $\upsilon=0.3$. The expected results are: stress in the direction of loading is -1.0 MPa and strain in the same direction is -1.e-5. Results of the homogeneous deformation using the enhanced mixed u/p with both bubble functions are matching the expected ones and are identical. Therefore only results corresponding to the quadratic bubble functions are shown in Figure 5.

(a) Stress in loading direction   (b) Strain in loading direction
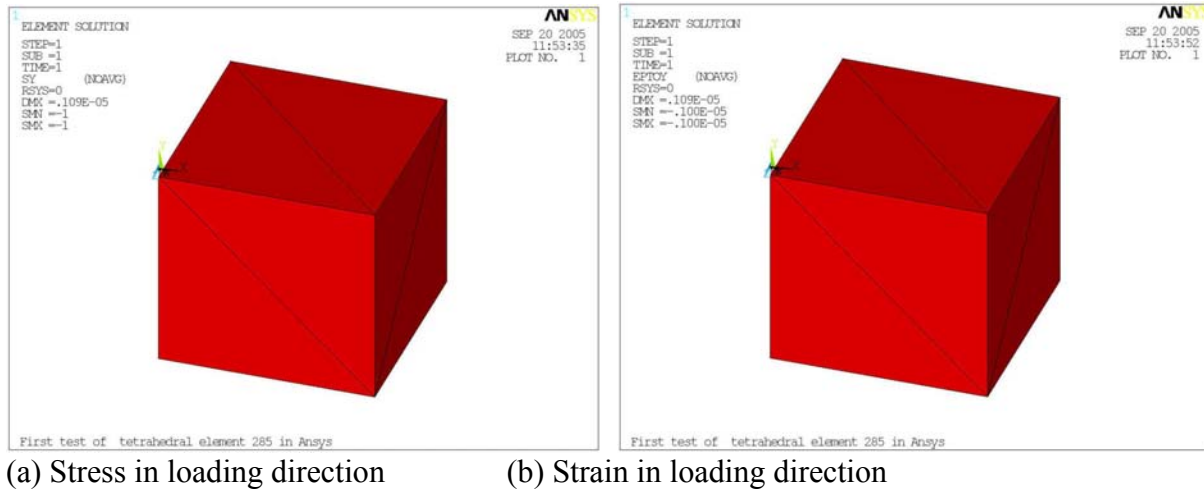
Figure 5. Stress and strain in the direction of loading for the uniaxial compression test

2. **Homogeneous deformation of a unit cube formed of 25-tetrahedra under linear applied displacement field**

The finite element model consists of a 1x1x1 block meshed with 25 tetrahedral elements and subjected to a linearly varying displacement field applied to all nodes as given by the following:

$u = 1.0 + 2.0*x + 1.5*y + 0.5*z$
$v = 0.75 + 2.5*x + 1.0*y + 0.75*z$
$z = 0.5 + 1.5*x + 0.75*y + 1.5*z$

The material properties are E=1.e6MPa and the finite element model is presented in Figure 6.
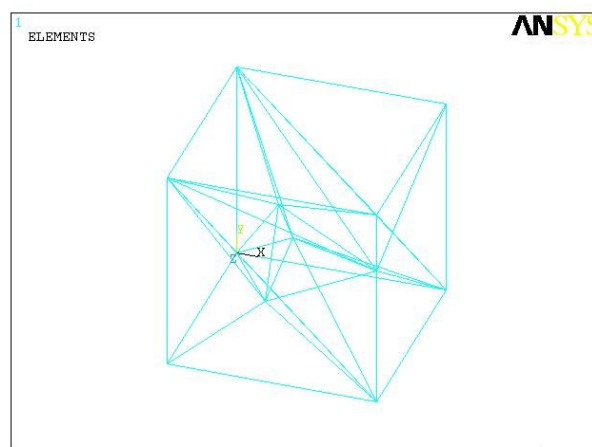
Figure 6. Finite element model of unit cube formed by 25-tetrahedra

67

The computed strains and stresses for this deformation field should be:
$\varepsilon_{xx} = 2.0, \varepsilon_{yy} = 1.0, \varepsilon_{zz} = 1.5$,
$\varepsilon_{xy} = 4.0, \varepsilon_{yz} = 1.5, \varepsilon_{zx} = 2.0$
$\sigma_{xx} = 3400000.0, \sigma_{yy} = 2600000.0, \sigma_{zz} = 3000000.0$,
$\sigma_{xy} = 1600000.0, \sigma_{yz} = 600000.0, \sigma_{zx} = 800000.0$

The mixed enhanced tetrahedral element passed this patch test since the results obtained are exactly as those expected. A part of the output files with strains and stresses for a few selected elements together with expected strains and stresses is presented in Appendix B.

5.2 EXPANSION OF A THICK-WALL CYLINDER UNDER PRESSURE

This test was proposed by R. Taylor in [47] to assess the behavior of a similar strain enhanced tetrahedral element in nearly incompressible materials.

Description of the test

An infinitely long thick walled cylinder with inner radius of 3 units and outer radius of 9 units is subjected to an internal pressure of 1 unit. Due to the axisymmetric nature of the problem, the finite element model can be represented by a wedge of a 5 degree angle sector and a unit thickness. The material properties considered are linear elastic with E = 1.e6 and Poisson's ratios were varied from 0, 0.25, 0.3, 0.49, 0.499 and 0.4999 to evaluate the robustness of the formulation. The mesh is unstructured and the number of divisions per radial direction was varied from N=10, 20 to 30 elements. Results of each formulation are compared with the theoretical results and errors are reported in Tables 2, 3 and 4.

Table 2. Radial displacements for the thick wall cylinder, N=10

Poisson Ratio	Theory	Mixed u/p enhanced Tetra	Error (%)	Mixed u/p	Error(%)	Pure Displace ment	Error (%)
0.0000	3.7500	3.7275	0.5994	3.7274	0.6015	3.7235	0.7058
0.2500	4.4531	4.4242	0.6489	4.4237	0.6594	4.4124	0.9134
0.3000	4.5825	4.5520	0.6642	4.5513	0.6805	4.5365	1.0029
0.4900	5.0399	5.0008	0.7747	4.9701	1.3841	4.7941	4.8760
0.4990	5.0602	5.0204	0.7850	4.8935	3.2927	3.7532	25.8278
0.4999	5.0623	5.0224	0.7876	4.6940	7.2738	1.1884	76.5242
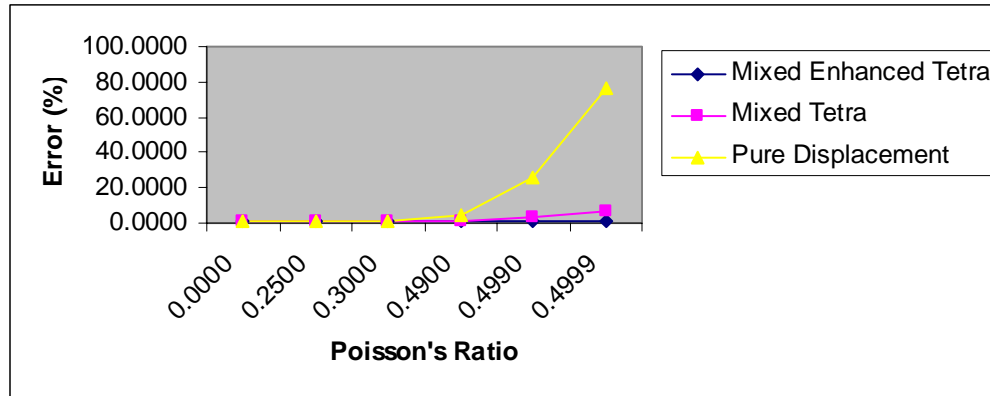
Table 3. Radial displacements for the thick wall cylinder, N=20

Poisson Ratio	Theory	Mixed u/p enhanced Tetra	Error (%)	Mixed u/p	Error(%)	Pure Displace ment	Error (%)
0.0000	3.7500	3.7381	0.3157	3.7382	0.3147	3.7374	0.3348
0.2500	4.4531	4.4388	0.3196	4.4390	0.3151	4.4370	0.3614
0.3000	4.5825	4.4568	0.3197	4.4568	0.3131	4.5654	0.3711
0.4900	5.0399	5.0255	0.2856	5.0305	0.1861	4.9800	1.1878
0.4990	5.0602	5.0462	0.2763	5.0408	0.3834	4.5809	9.4714
0.4999	5.0623	5.0482	0.2767	5.0035	1.1612	2.5048	50.5199
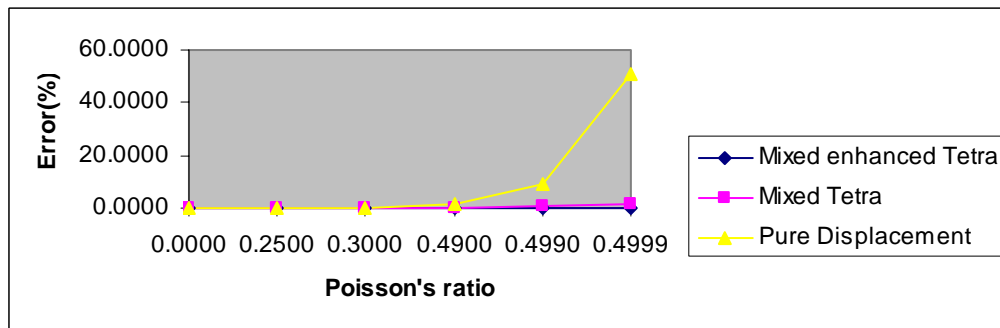
Table 4. Radial displacements for the thick wall cylinder, N=30

Poisson Ratio	Theory	Mixed u/p enhanced Tetra	Error (%)	Mixed u/p	Error(%)	Pure Displacement	Error (%)
0.0000	3.7500	3.7746	0.1431	3.7446	0.1418	3.7444	0.1481
0.2500	4.4531	4.4470	0.1361	4.4472	0.1303	4.4464	0.1498
0.3000	4.5825	4.4576	0.1246	4.5767	0.1263	4.5755	0.1528
0.4900	5.0399	5.0328	0.1391	5.0341	0.1143	5.0021	0.7496
0.4990	5.0602	5.0528	0.1459	5.0413	0.3727	4.7522	6.0857
0.4999	5.0623	5.0547	0.1484	5.0088	1.0566	3.1105	38.5547
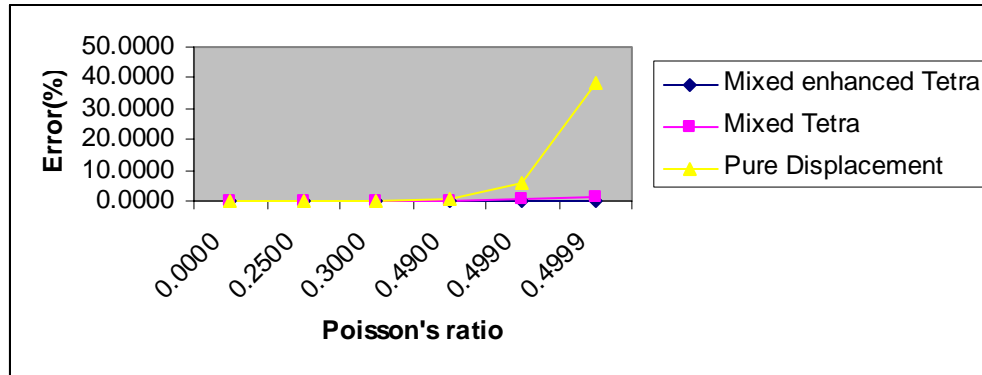
Results and Discussions

Tables 2, 3 and 4 show results of radial displacements at a node located on the inner radius for all the Poisson's ratios considered and for all formulations together with the errors with respect to the theoretical results. Contour plots of radial and tangential stresses for the case of N=20 for all three formulations are shown in Figure 7.

The choice of the bubble function is insignificant since results show that both of them eliminate volumetric locking and stabilize the element in the same manner. This can be assessed from the comparisons with the exact solutions for displacements, radial and tangential stresses.

Pure displacement formulation shows clear evidence of volumetric locking and the mixed u/p formulation improves the behavior in the incompressible limit.

The error in the displacements is greatly reduced but still shows some volumetric locking because of high values of stresses as compared to the theoretical stresses.

As it can be seen from tables, the enhanced mixed u/p tetrahedral element shows errors less than 1% in radial displacement for both compressible and almost incompressible linear elastic materials. The improvement with respect to the other two formulations, is more obvious for υ=0.4999 where the pure displacement formulation gives errors ranging between 38 and 76 % depending on the mesh size and respectively the mixed u/p formulation gives errors ranging between 1-7%. For compressible materials all formulations behave similarly which is expected.

Plots of stress distribution in radial(x) and tangential(y) directions presented in Figure 7(a-f) show that the mixed u/p and pure displacement formulations produce spurious and incorrect patterns with high stress values. In contrast to these formulations, the stress distributions of the stabilized mixed u/p tetrahedral are free of oscillations and the pattern shows clearly the variation of stresses as a function of radii. The reference values of stresses for this particular problem of an infinitely long cylinder were calculated analytically and they were found to be:

$$\sigma_{rr}\big|_{r=r_i} = -1, \sigma_{\theta\theta}\big|_{r=r_i} = 0.25$$
$$\sigma_{rr}\big|_{r=r_0} = 0, \sigma_{\theta\theta}\big|_{r=r_0} = 1.25$$

As it can be seen form Figure 7, the stabilized tetrahedral predicted stresses are in good agreement with the above theoretical ones; the radial stresses are within 4 % and the tangential stresses are within 10% while the mixed u/p and pure displacement formulations' errors are increasing over 100% and 500% respectively.

Another remark in favor of stabilized tetrahedral element is related to the fact that the errors are not varying too much from one Poisson's ratio to another which proves that the developed element is robust.
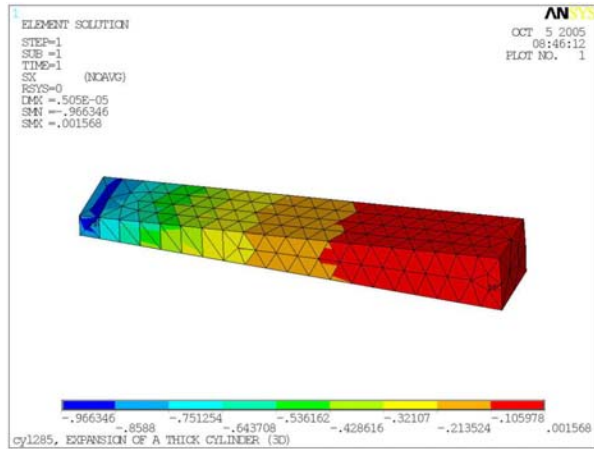
(a) Stabilized Mixed u/p Tetrahedral, radial stress
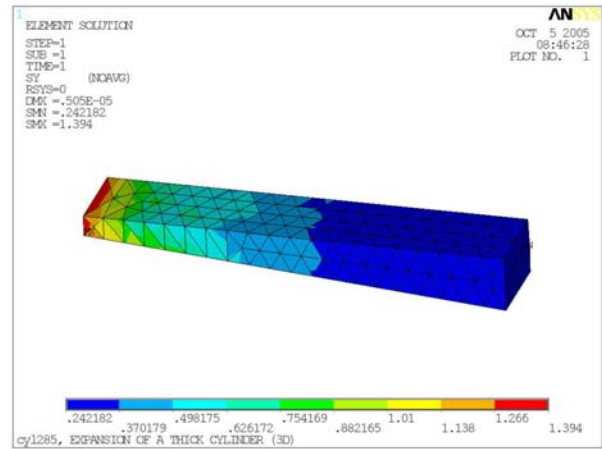
(d) Stabilized Mixed u/p Tetrahedral, tangential stress
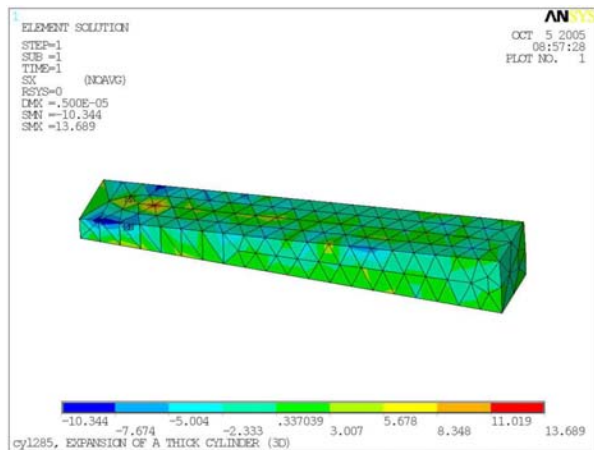
(b) Mixed u/p Tetrahedral, radial stress
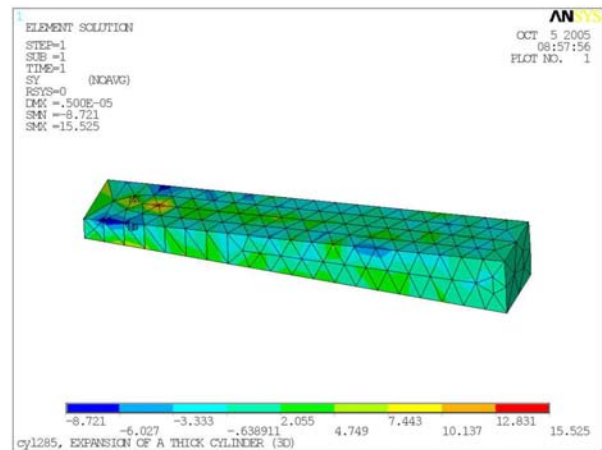
(e) Mixed u/p Tetrahedral, tangential stress
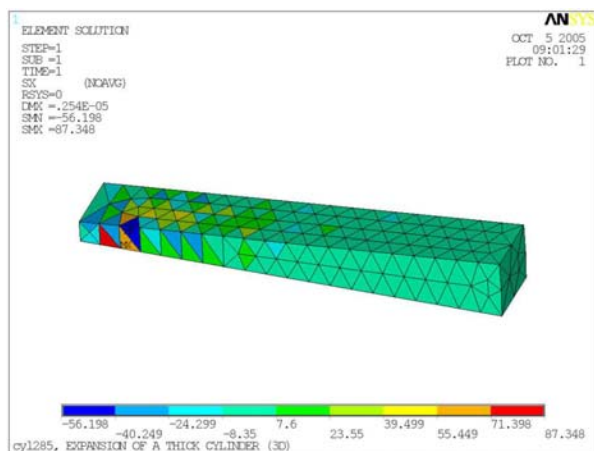
(c) Pure Displacement Tetrahedral, radial stress
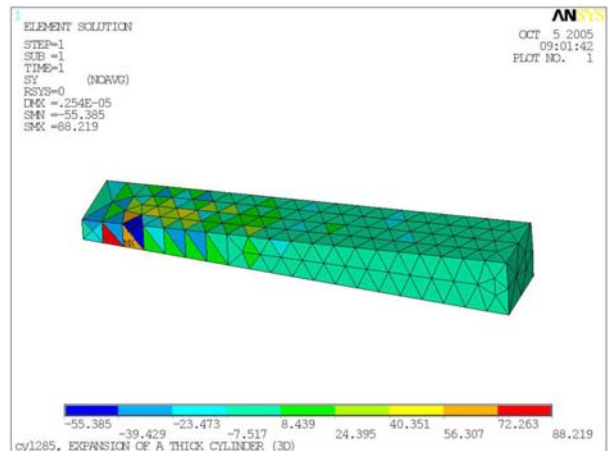
(f) Pure Displacement Tetrahedral, tangential stress

Figure 7. Thick walled cylinder stresses for N=20

5.3 COOK'S PROBLEM

This problem has been frequently used to assess finite elements under combined bending and shear. The problem represents a tapered panel clamped on one side while a shearing load acts on the opposite side (see Figure 8). The thickness was considered t =1 mm and a state of plane strain was simulated by restraining the plate to deform in the thickness direction. Material properties used are E=1000MPa and Poisson's ratio was varied again between 0.3 and 0.4999.

Three mesh sizes were studied having N=10, 20 and 30 elements per edge.
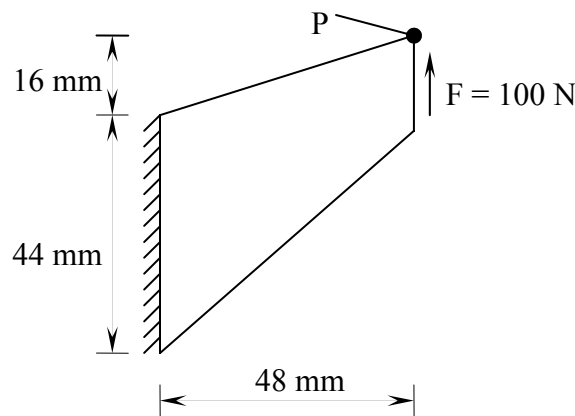
Figure 8. Cook's problem geometry

Results and Discussions

The results are compared for stabilized mixed u/p, mixed u/p and pure displacement formulations with the results of the well known mixed hexahedral elements with mixed enhanced formulation available in ANSYS. These elements are known to behave correctly in incompressibility and shear locking conditions.

Tables 5 and 6 represent the vertical displacement of the top corner node P, the axial stresses for all formulations and the errors with respect to the hexahedral elements. Figures 9, 10 and 11 show contour plots of the normal stresses in x and y direction and shear stresses for all formulations for the mesh size N=20 and Poisson ratio υ=0.4999.

The pure displacement formulation exhibits severe locking behavior as the error in the displacement of point P reaches 42 % and the stresses are highly overestimated. The mixed u/p elements show improved accuracy in displacements (error is just 1.7%) but the stresses show spurious distribution and are overestimated.

The stabilized tetrahedral elements approach very closely the hexahedral element solution in both displacements and stress distribution. They yield accurate results even on coarse meshes with just 0.16% error in displacements and within 5% error in stresses. Also they yield a smooth stress distribution for all the situations considered. The difference that can be noted in axial compressive stresses   when compared to the hexahedral elements is due to the unstructured mesh that was used for the tetrahedral elements which produces highly distorted elements at the left top corner.

As for the shear stresses, the mixed u/p and stabilized mixed u/p yield similar results and distribution patterns which are very close to the hexahedral results. This is explained by the fact that the shear component of the stresses does not contain the volumetric part and therefore is not affected by the increasing pressures developed in cases of volumetric locking.

Table 5. Cook's problem, vertical displacement of top corner node for different mesh sizes

Mesh Size	Hexahedral element	Stabilized Tetrahedral	Error (%)	Mixed u/p Tetrahedral	Error(%)	Pure Displacement Tetrahedral	Error(%)
N=10	29.81	29.378	1.472	28.248	5.262	19.82	33.5
N=20	30.41	30.365	0.16	29.885	1.739	17.43	42.668
N=30	30.63	30.975	1.11	30.657	0.073	17.74	42.09

Table 6. Cook's problem, axial tensile stress for different mesh size

| Mesh Size	Hexahedral element	Stabilized Tetrahedral	Error (%)	Mixed u/p Tetrahedral	Error(%)	Pure Displacement Tetrahedral	Error(%)
N=10	224.24	252.96	12.5	713.586	89.3	7473	Too large
N=20	221.4	229.77	3.6	341.365	54.3	28528	Too large
N=30	222.4	227.4	2.25	298.08	34.2	17178	Too large
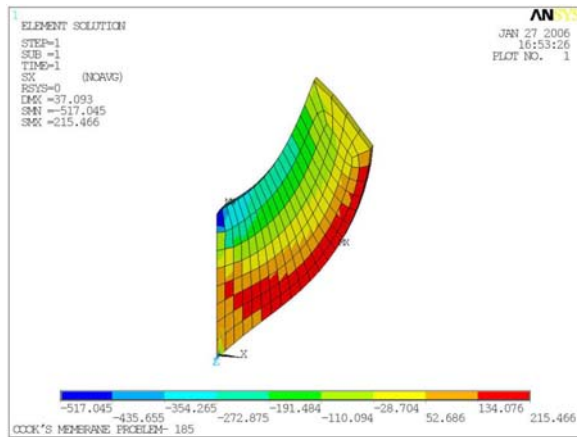
(a) Mixed u/p enhanced strain hexahedral
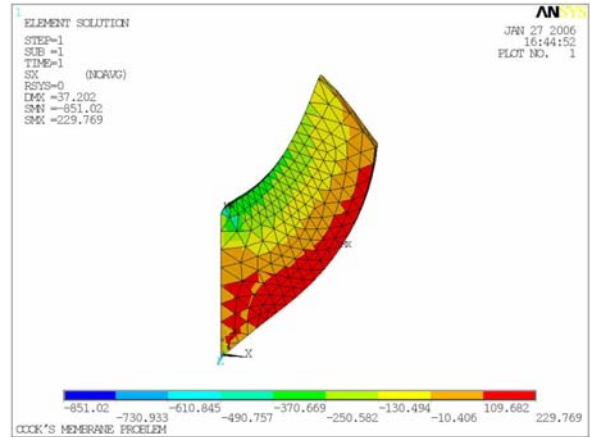
(b) Stabilized mixed u/p tetrahedral
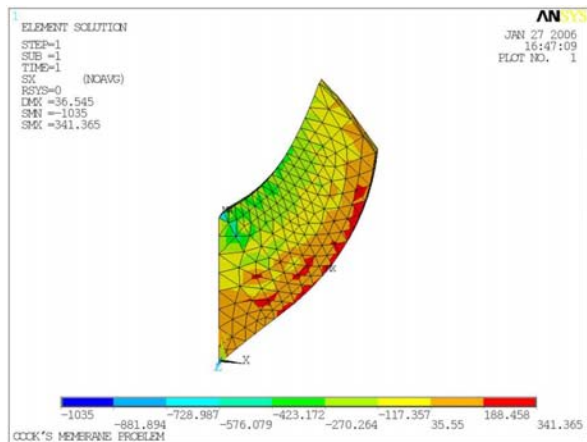
(c) Mixed u/p tetrahedral
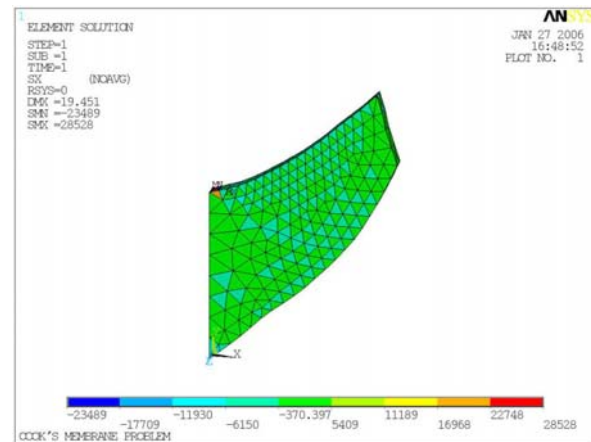
(d) Pure Displacement Tetrahedral

Figure 9. Cook's Problem: Normal Stress in x direction
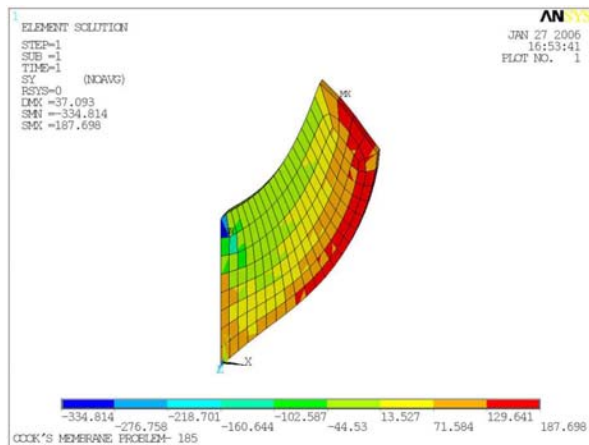
(a) Mixed u/p enhanced strain hexahedral
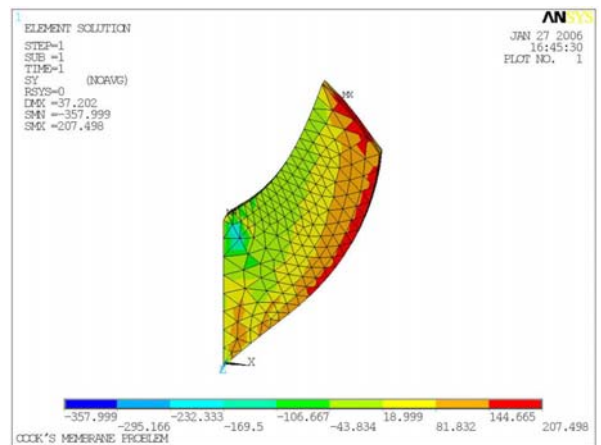
(b) Stabilized mixed u/p tetrahedral
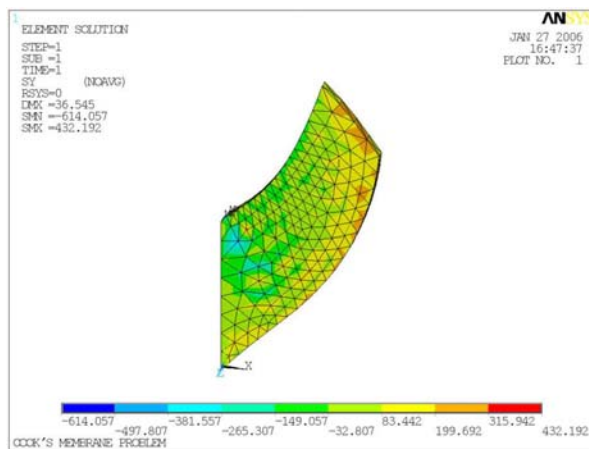
(c) Mixed u/p tetrahedral
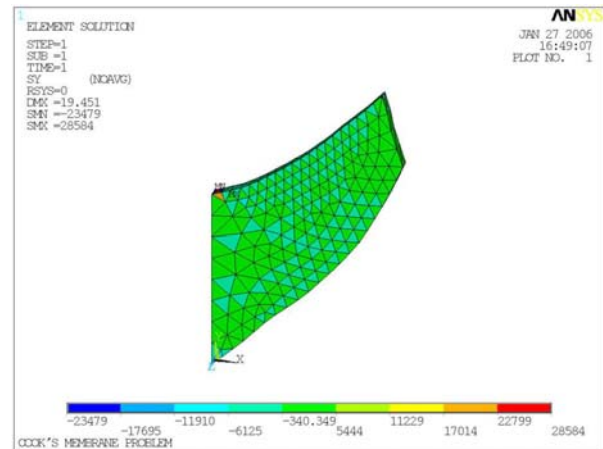
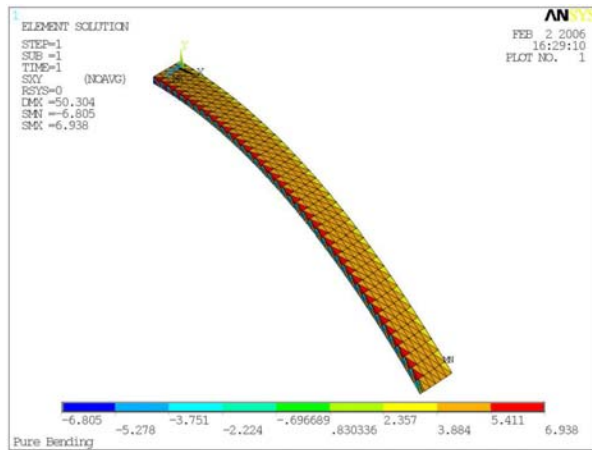(d) Pure Displacement Tetrahedral

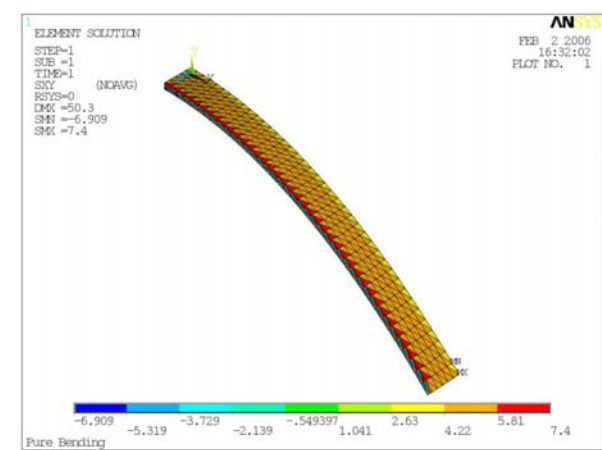**Figure 10. Cook's Problem: Normal Stress in y direction**
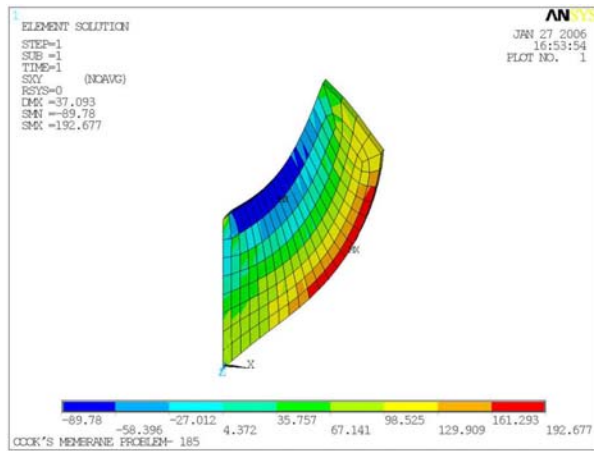
(a) Mixed u/p enhanced strain hexahedral
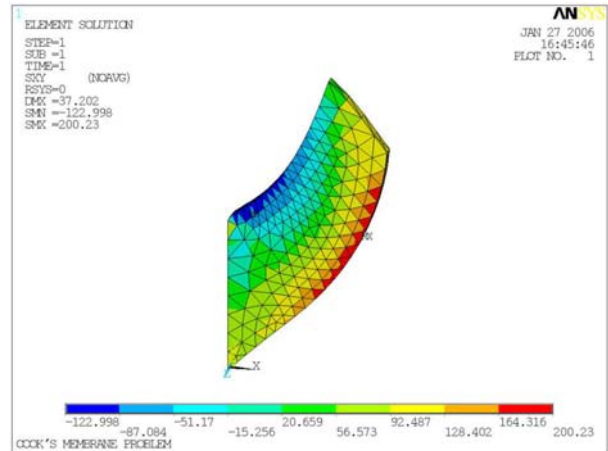
(b) Stabilized mixed u/p tetrahedral
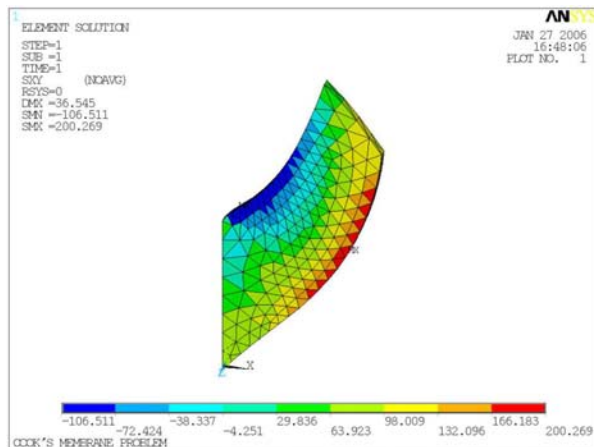
(c) Mixed u/p tetrahedral
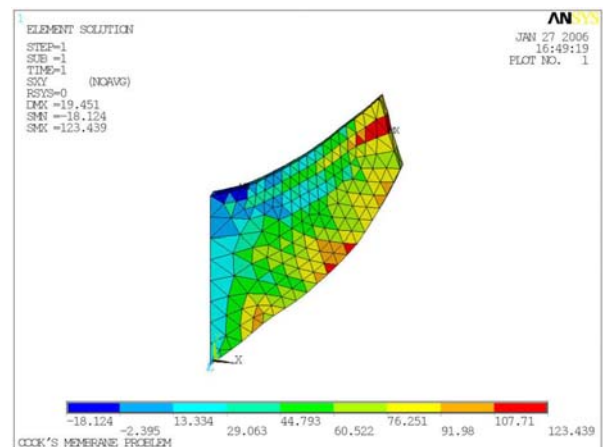
(d) Pure Displacement tetrahedral

Figure 11. Cook's Problem: Shear Stresses

5.4 TEST OF BENDING CAPABILITY

A pure bending test of the newly developed tetrahedral element was performed to assess its bending capabilities in small deformation linear elastic problems. Since we are interested in assessing the performance in shear locking and volumetric locking, only results for Poisson's ratios of $v=0.3$ and $v=0.49999$ are reported. Results of maximum deflections, shear and axial stresses are compared with the mixed u/p hexahedral element results with mixed enhanced strain.

This element is well known for its stability and good performance in both shear and volumetric locking.

Description of the test

The test represents a cantilever beam with a rectangular cross section with width of 10 mm and thickness of 2 mm and length of 100 mm clamped at the left end. A bending moment is applied through two opposite displacement loads along the right edges (top and bottom) such that an extreme pure bending case is simulated. The material properties are taken as E =1000 MPa and Poisson's ratio was considered 0.3 and 0.49999. The mesh used was structured for direct comparison with hexahedral elements. Geometry and finite element model are shown in Figure12.

Contour plots of normal and shear stresses for $v=0.3$, N=6 are shown in Figures 13 and 14 and for $v=0.49999$ are shown in Figure 15 and 16.
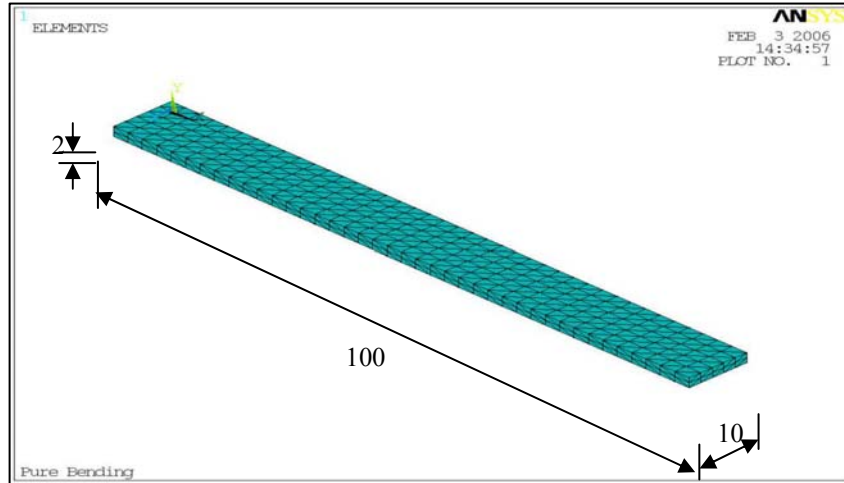
Figure 12. Finite element model of the pure bending test

Results and Discussions

From the two sets of plots it can be deduced that the tetrahedral element's performance in shear locking is not as good as it is in volumetric locking for this extreme case of pure bending. Even though the displacements are within errors of 1 % and the normal stresses are acceptable, the shear stresses have larger values than those obtained using mixed enhanced strain hexahedral elements. The shear stress distribution also shows evidence of locking. When both shear and incompressibility constraints exist, the stabilized tetrahedral brings some improvement as compared to the mixed u/p and pure displacement formulation that is completely locked as it can be seen from Figure 15. This remark helps us conclude that the stabilized tetrahedron is performing poorer than the mixed u/p enhanced strain hexahedral element in pure bending problems. It is though necessary to note that in bending dominant problems, as it was seen for Cook's problem, this limitation disappears and the performance is significantly improved.
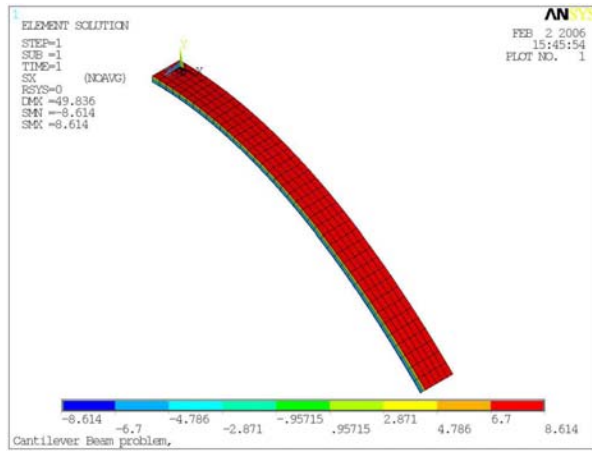
(a) Mixed u/p enhanced strain hexahedral
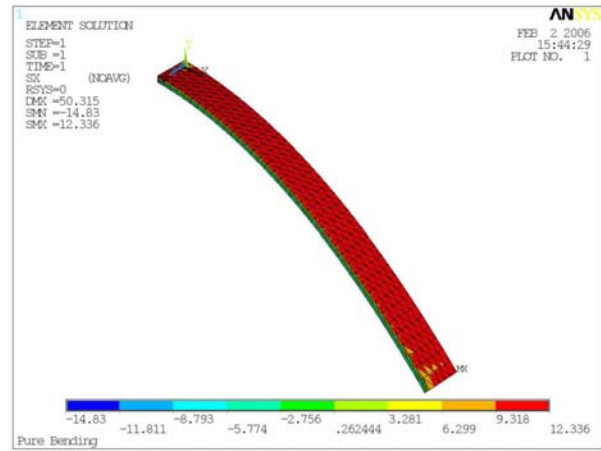
(b) Stabilized Mixed u/p Tetrahedral
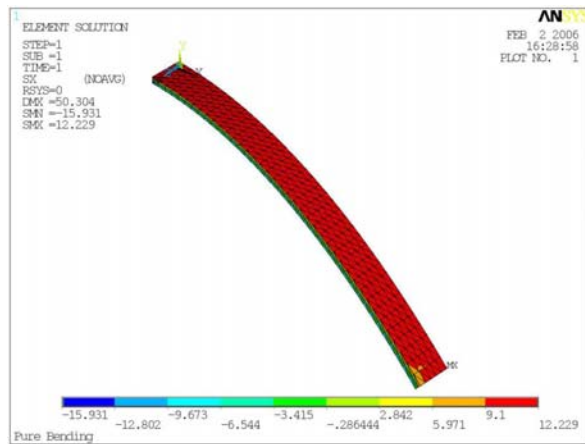
(c) Mixed u/p Tetrahedral
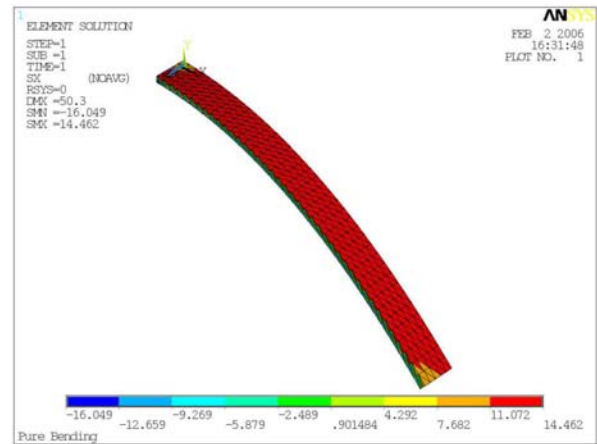
(d) Pure Displacement Tetrahedral

Figure 13. Pure Bending Test: Axial Stress for ν=0.3
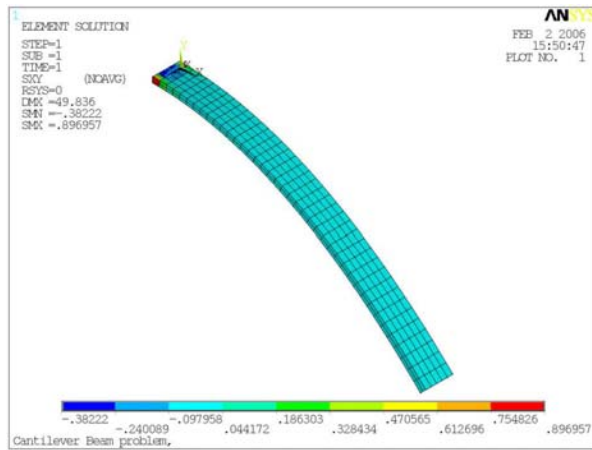
(a) Mixed u/p enhanced strain hexahedral
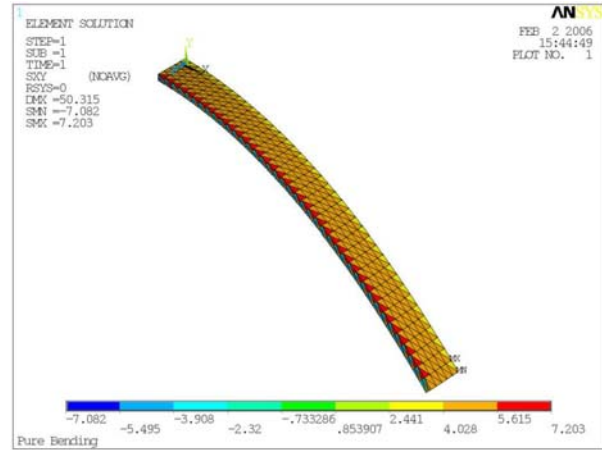
(b) Stabilized mixed u/p tetrahedral

(c) Mixed u/p tetrahedral

(d) Pure Displacement tetrahedral

Figure 14. Pure Bending Test: Shear Stress for ν=0.3
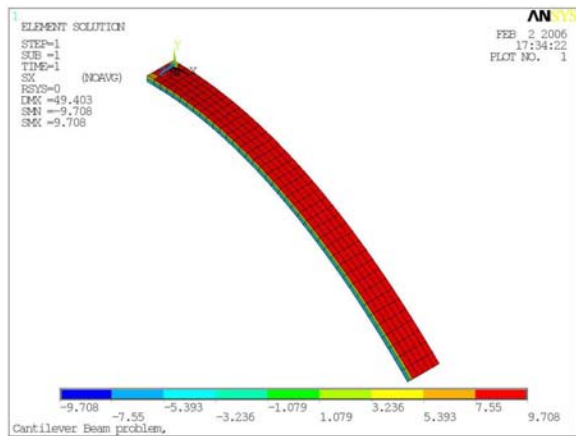
(a)Mixed enhanced strain Hexahedral
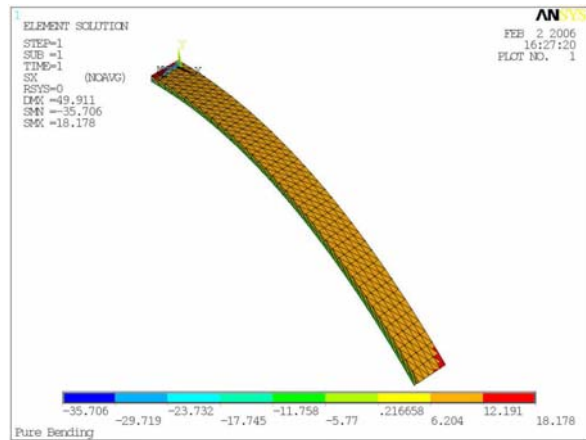
(b) Stabilized mixed Tetrahedral
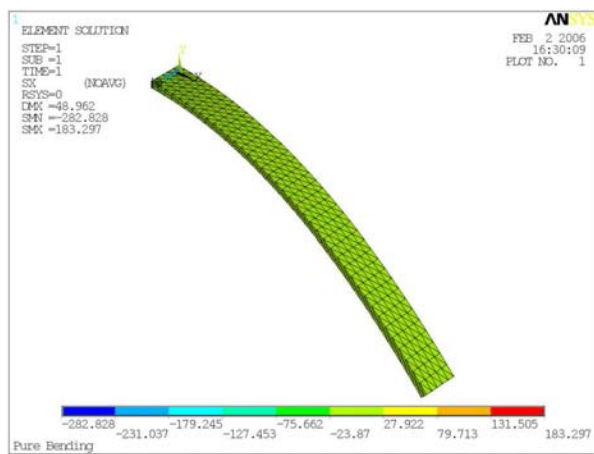
(c) Mixed u/p Tetrahedral
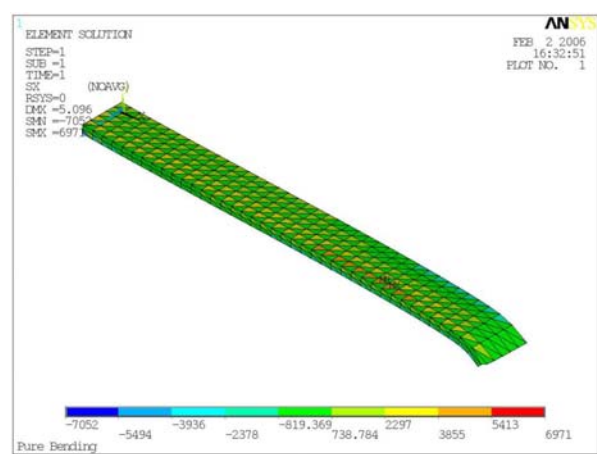
(d) Pure Displacement Tetrahedral

Figure 15. Pure Bending Test: Axial Stress for ν=0.49999.
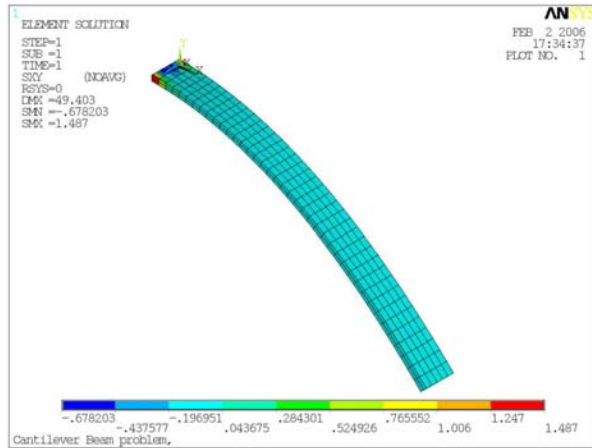
(a) Mixed enhanced strain Hexahedral
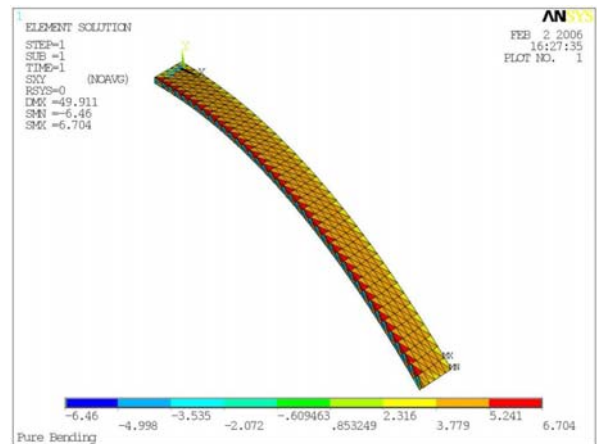
(b) Stabilized Mixed u/p Tetrahedral
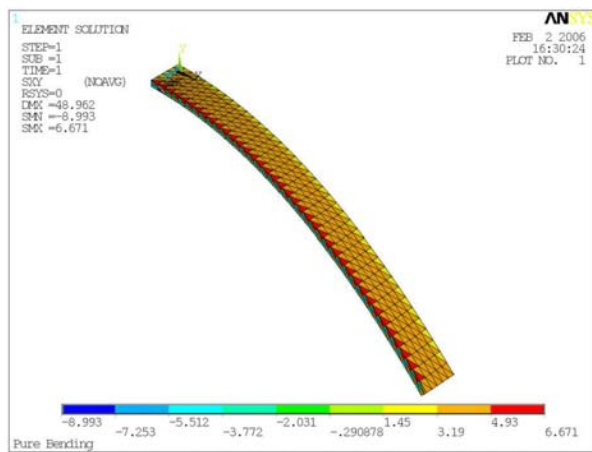
(c) Mixed u/p Tetrahedral
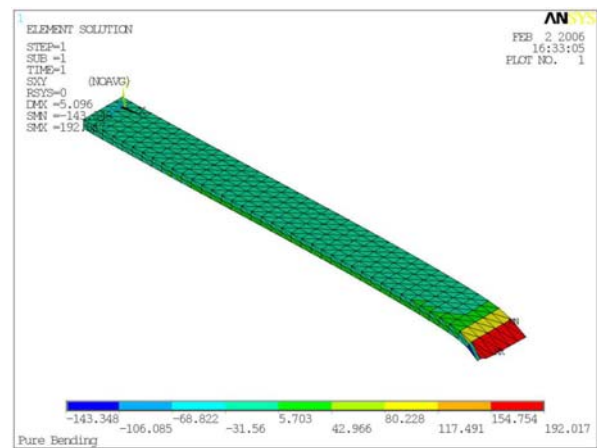
(d) Pure Displacement Tetrahedral

Figure 16. Pure Bending Test: Shear Stress for ν=0.49999.

84

6.0 NUMERICAL INVESTIGATIONS OF NONLINEAR MATERIALS IN LARGE DEFORMATIONS

The behavior of the proposed formulation in large deformations and large rotations using nonlinear materials will be illustrated in a number of benchmark problems with emphasis on simulations of metal forming problems. These are usually very difficult nonlinear problems due to both excessive element distortions and contact conditions together with the presence of the incompressibility constraint. Performance of the stabilized mixed u/p tetrahedral element was tested against the performance of the mixed u/p hexahedral element with B-bar formulation for problems where volumetric locking is prevalent or with enhanced strain in bending dominated problems. As in the previous chapter the behavior of the stabilized formulation was again compared to those of mixed u/p without stabilization and pure displacement for assessing the improved performance that the stabilization brings. It is important to note that analyses were carried out using both the cubic and the quadratic bubble functions. Since identical results were obtained for each bubble function, only the cubic bubble function results are presented in this section.

6.1 NONLINEAR HOMOGENEOUS DEFORMATION TESTS

The same two tests described in chapter 5.1 for linear testing were used to verify the correctness of coding for the finite strain deformation case. These patch tests were passed in the geometrically nonlinear case and brief results are presented in the next section.

1. Uniaxial Compression Test.

Two materials were used for this test. The first material used for the uniaxial compression test is multi linear isotropic (MISO) defined by a four point stress-strain curve with the following properties: E=100e4, ν=0.3. The stress/strain curve of the elasto-plastic material is shown in Figure 17. The applied load is a uniform pressure in vertical direction such that the final height will be reduced to 50%.

Results are compared to the mixed u/p hexahedral with B-bar formulation and again with the other two formulations, the mixed u/p without stabilization and the pure displacement.
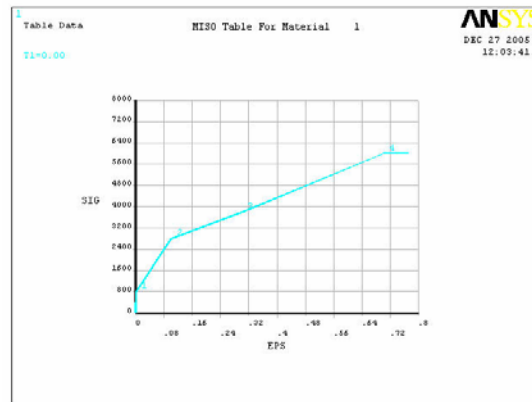
Figure 17. Stress-Strain curve of MISO material

The predicted strain results in the loading direction are presented in Figure 18. The contour plots (see Figure 18 and 19) show both the undeformed geometry and the deformed geometry. They show a homogeneous deformation as it was expected and the displacements, stresses, strains and pressures of the stabilized tetrahedral are in excellent agreement with the hexahedral element. The displacements and strains of the mixed u/p without stabilization are very different from the reference model and even from the pure displacement formulation which performs as better as the stabilized formulation for this special case of deformation.
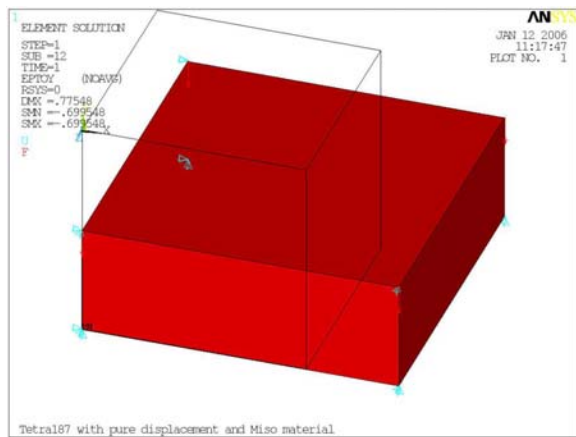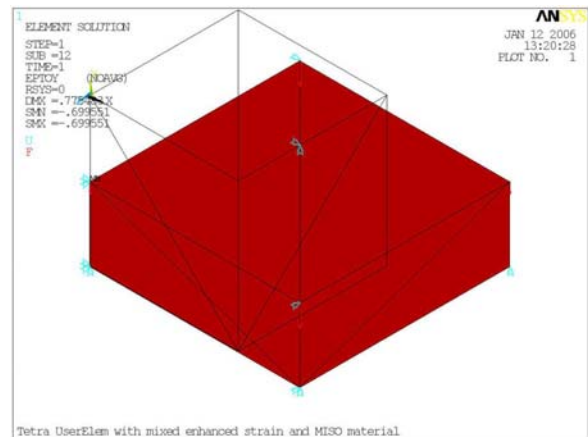
(a) Mixed u/p Hexahedral Element
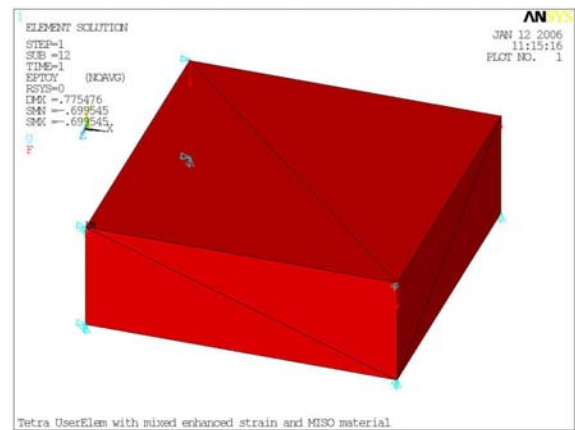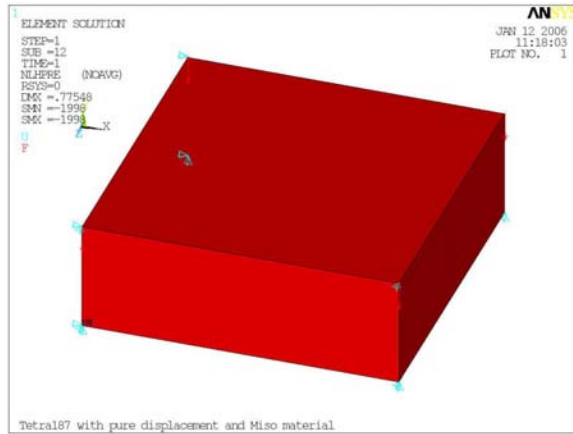
(b) Stabilized Mixed Linear Tetrahedral
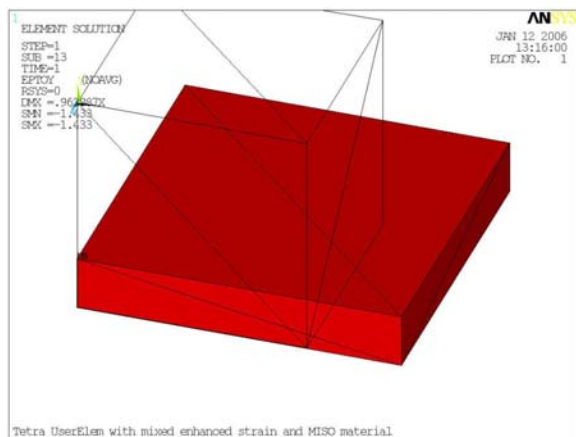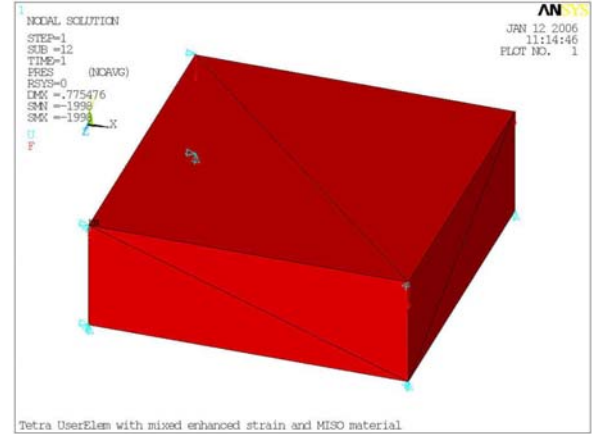
(c) Mixed u/p Tetrahedral

(d) Pure Displacement Tetrahedral

Figure 18. Nonlinear Uniaxial Compression Test: Strain in loading direction.

| (a) Mixed u/p hexahedral | (b) Stabilized Mixed Tetrahedral |

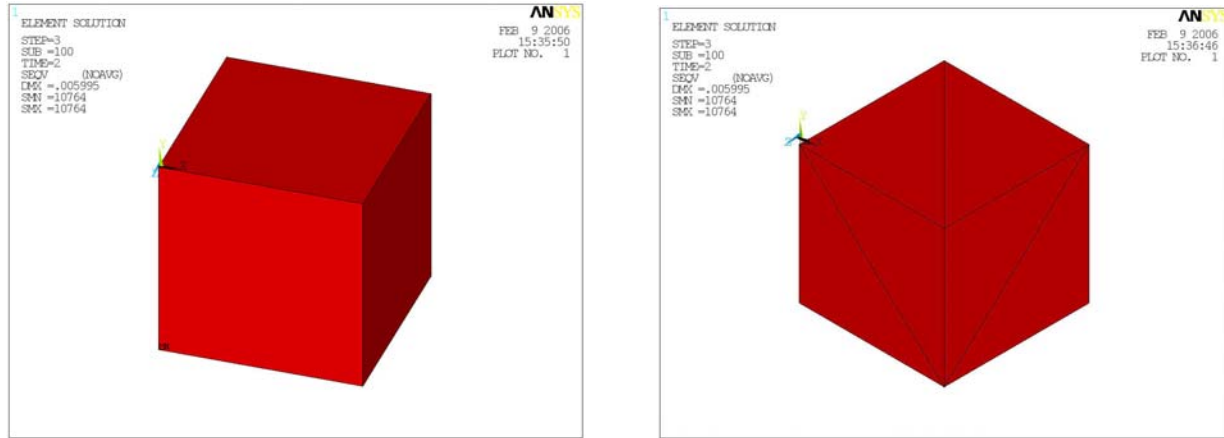**Figure 19. Nonlinear Uniaxial Compression Test: Hydrostatic Pressure.**

The second material is modeled by a rate dependent visco-plasticity model in which the yield strength is introduced by an overstress power law (PERZYNA model) and the static yield strength is defined by using a bilinear isotropic model. The parameters introduced in the model are: E=2.0e5, ν=0.3, σ_0 = 9000, m (strain rate hardening parameter) = 0.2,

γ (Viscosity parameter)=0.4 according to the model $\sigma_y = \sigma_0 \cdot \left(1 + \left(\dfrac{\dot{\varepsilon}_{eqv}^{pl}}{\gamma}\right)^m\right)$

The same boundary conditions as before are maintained and a uniform pressure in the vertical direction is applied in three load steps as follows:

1. Apply a stress equal to the yield stress (9000).

2. Apply a stress equal to 10800.

3. Keep a constant stress at 10800.

Figure 20 shows the equivalent stress for the stabilized tetrahedral compared to the hexahedral element with mixed u/p and B-bar formulation. As it can be observed the results are identical and they show a constant deformation.

(a) Mixed u/p Hexahedral (B-bar)   (b) Stabilized Mixed Tetrahedral

**Figure 20. Rate-Dependent Uniaxial Compression Test: Equivalent Stress**

2. Homogeneous deformation of a unit cube formed of 25-tetrahedra under linear applied displacement field

The same geometry as in the linear case (see section 5.1) was tested now with a bilinear isotropic material and compared to a constant pressure tetrahedral (SOLID 187 in ANSYS). The material properties are taken as follows: E=100 e4, ν=0.3, σ_y =800 and E_T = 10000.

A linear displacement field is applied as:

$$u = (1.0 + 2.0*x + 1.5*y + 0.5*z)*0.45$$
$$v = (0.75 + 2.5*x + 1.0*y + 0.75*z)*0.45$$
$$z = (0.5 + 1.5*x + 0.75*y + 1.5*z)*0.45$$

Figure 21 shows the equivalent stress for the deformed geometry at the last step together with the initial geometry. As it can be seen the stabilized tetrahedral element passes the constant deformation test and the results are identical with the ones for constant pressure tetrahedral.
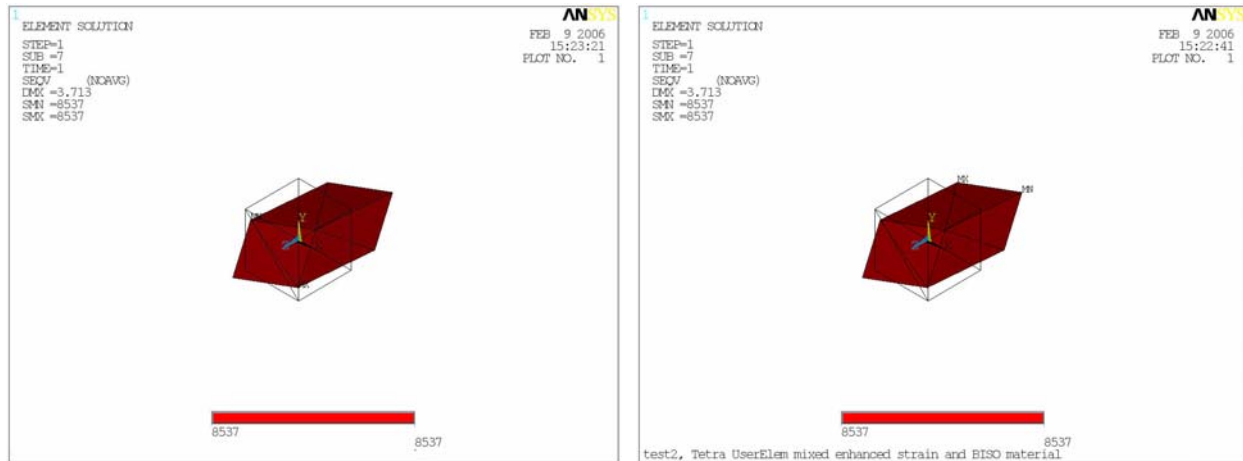
(a)\Constant pressure Tetrahedral (SOLID187)   (b) Stabilized Mixed Tetrahedral

Figure 21. Homogeneous Deformation Test with linear displacement: Equivalent Stress.

6.2 UPSETTING OF A BILLET

To initially assess the performance of the new mixed enhanced strain tetrahedral element under conditions of elasto-plastic finite deformation, a billet upsetting process was analyzed.   In the upsetting problem, the billet was modeled as in Figure 22 and it was subject to a distributed vertical displacement load applied over one third of its top cross-sectional area. This specific upsetting geometry and load was chosen because known results are available in the literature [26]. The overall objective of the forming process being modeled was to achieve a 65% compression of the height of the billet.

In the simulation, a state of plane strain is considered and no contact pairs were defined and the material properties of the billet were given the following values:

Elastic modulus (E): 200GPa   Poison's ratio (ν): 0.3.

Yield stress (σ_y): 250MPa   Tangent Modulus (E_T):1.0GPa

The finite element model used in this simulation has a structured mesh that permits direct comparison with hexahedral element mesh. Results are compared with a hexahedral element with B-bar formulation.
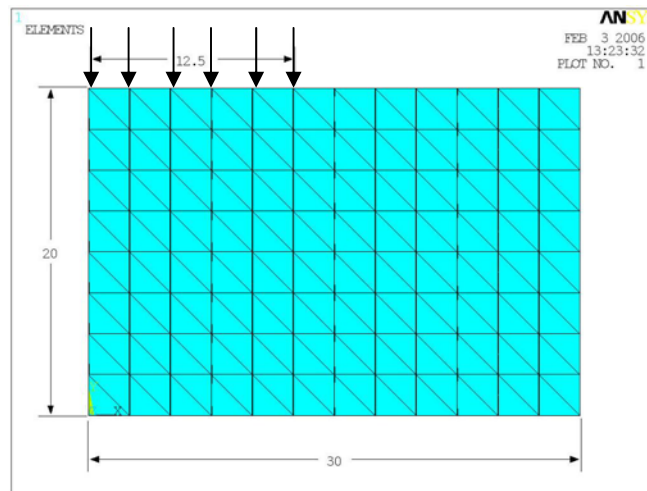
**Figure 22. Finite element model of the upsetting problem**

Figures 23 and 24 contain contour plots of the equivalent stress of the deformed billet and principal stress in the second direction. As shown in the figures, very good agreement was obtained between the predicted deformation and stress results of the hexahedral elements and our new formulation. Examining the contour plots of all three formulations we can note that the stabilized formulation is the only formulation that predicts the correct deformed shape and displacement, as compared to the hexahedral mesh.

The mixed u/p formulation without stabilization predicts close values of equivalent stress but when looking at the deformed shape it can be seen that the displacements are highly underestimated, indicating severe volumetric locking. In fact the deformation of the mixed u/p formulation predicts an upward direction of plastic flow which is totally different from the real one. The pure displacement formulation also shows clear evidence of locking by inspection of the deformed shape and high values of principal stress. The stabilization effect of the mixed enhanced strain formulation is very obvious from the plots of the second principal stress which show a smooth distribution in contrast to the polluted distribution of stresses obtained with the mixed formulation without stabilization.

Even though the results are improved a lot compared with the other formulations, there are still some differences when compared to the hexahedral ones. The only difference in the predicted results relates to the deformation of the billet around the punch corner where the tetrahedral model predicts a smaller slope between the punch face and the free surface than the hexahedral model. In that area the mesh is highly distorted and the compressive stress corresponding to that element is very high as compared to the hexahedral stress. We have to keep in mind though that any sharp corner represents a singularity for the stresses and therefore it is expected that the stresses would have high values which consequently change the contour plot so that the comparison to hexahedral elements seems detrimental to the tetrahedral elements.

Because of these reasons, in Figures 23 and 24, (c) the equivalent stress and second principal stress for hexahedral model was plotted using the same contour range as for the tetrahedral and as it can be seen, our supposition that the singularity at the sharp corner is the only area that differs from the reference plot was confirmed. The stabilized tetrahedral model shows a smooth distribution with values similar to the hexahedral one everywhere except at that corner.
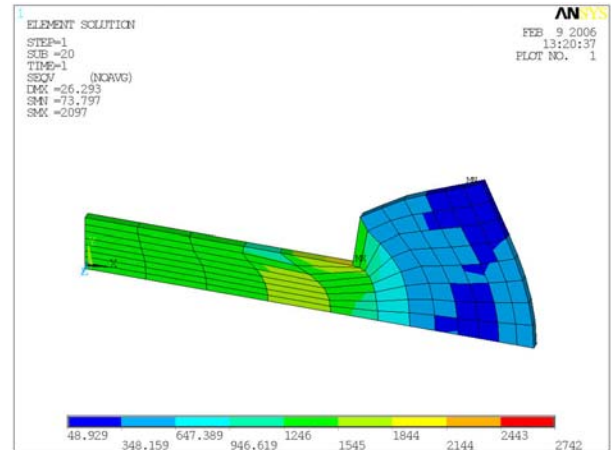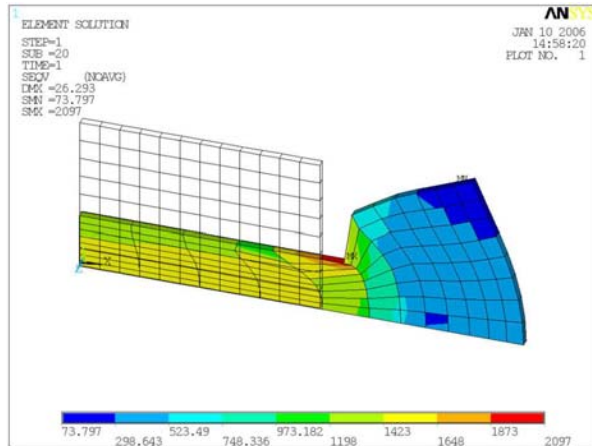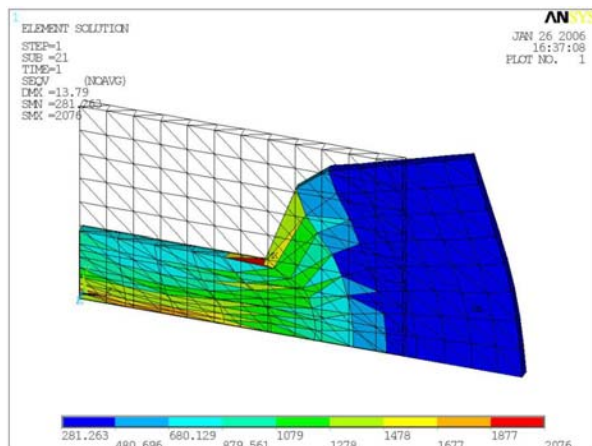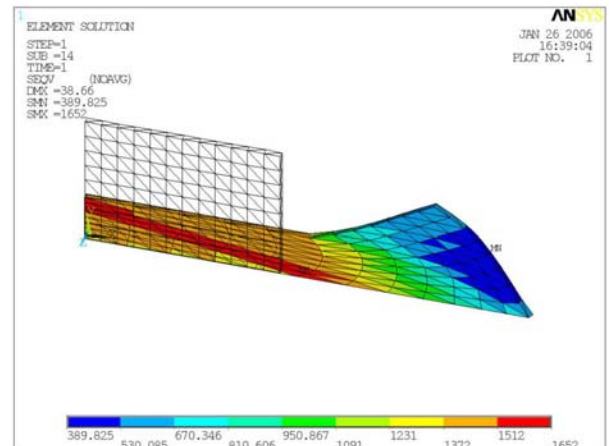
(a)Mixed u/p Hexahedral (automatic contour)　(b) Mixed u/p Hexahedral (same contour range)
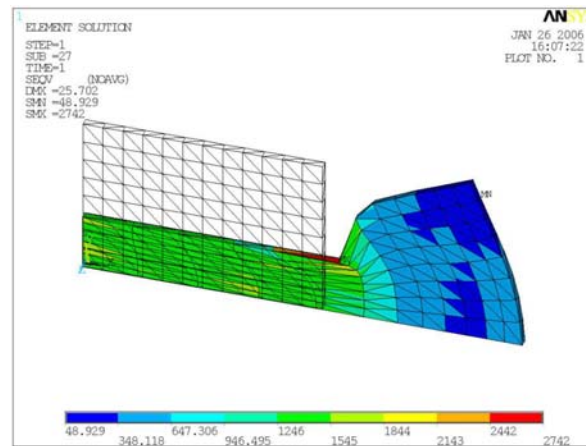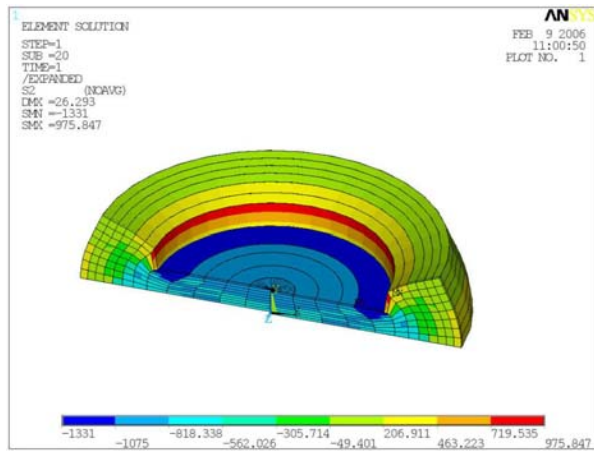
(c) Stabilized mixed u/p Tetrahedral

(d) Mixed u/p Tetrahedral　(e) Pure Displacement Tetrahedral

Figure 23. Upsetting of a billet: Equivalent Stress

(a) Mixed u/p Hexahedral (automatic contour)   (b) Mixed u/p Hexahedral (same contour range)

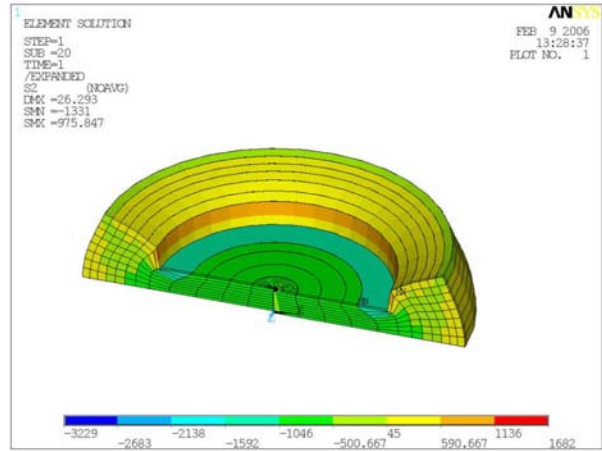(c) Stabilized Mixed u/p Tetrahedral

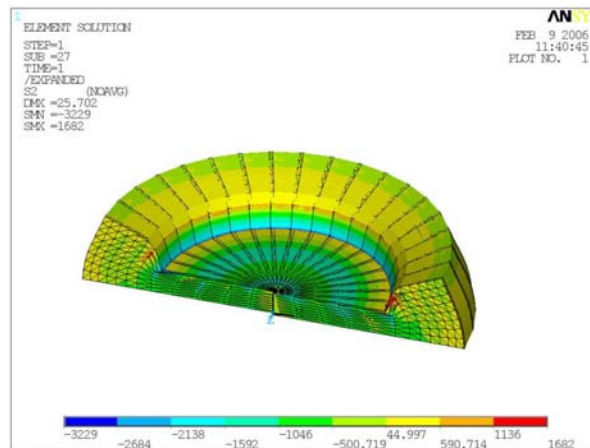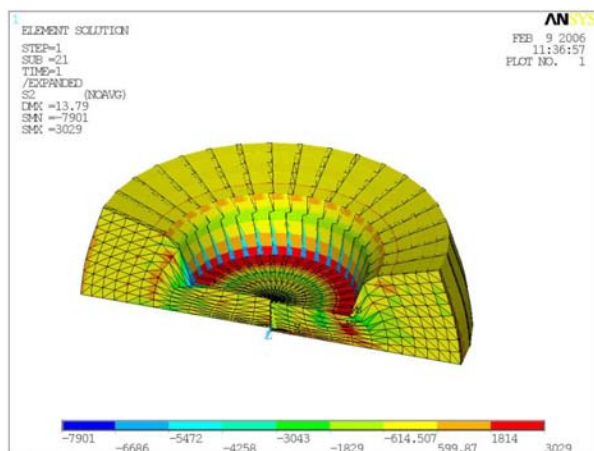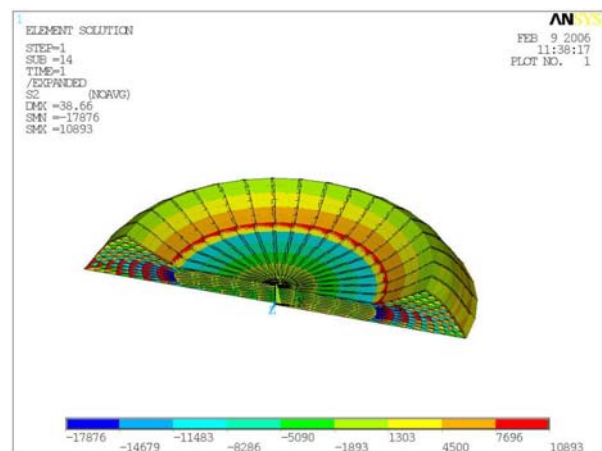(d)Mixed u/p Tetrahedral   (e) Pure Displacement Tetrahedral

Figure 24. Upsetting of a billet: Principal stress in second direction

94

6.3 METAL EXTRUSION

The second forming process used to assess the quality of the new tetrahedral element was a large strain extrusion process that was also studied in the literature [26]. Simulation of metal extrusion is another complicated metal forming problem in which large strains are expected. This process is usually very hard to be carried out to completion without using remeshing procedures. This is due to three causes: the extreme distortion of the elements especially in the angled part of the die, the incompressible nature of the deformation and the existence of the boundary contact conditions.

Description of the model

In the finite element model, the work-piece was defined with a rectangular cross-section with dimensions of 19.5 x 2 mm and an overall length of 45 mm. As shown in Figure 25, the work-piece was forced to pass between two rigid forming tools by imposing a lateral displacement of 45mm in the horizontal direction. The upper tool was defined to be a rigid target surface and its shape was designed to ensure that the final height of the billet was reduced by 50%. A frictionless contact pair was defined between the upper rigid tool and the billet. The bottom contact pair was modeled by imposing symmetry boundary conditions along the centerline of the work-piece. An overall state of plane strain was assumed in the model. For the work-piece, a bilinear isotropic model was defined for the material behavior with the following properties:

Elastic Modulus (E): 200.0GPa   Poisson's ration (v): 0.3,

Yield Stress (σ_y): 800MPa   Tangent Modulus (E_T): 300MPa.

In order to reduce the excessive mesh distortion when the material enters the die and also to reduce the time taken to achieve steady-state conditions, a fillet was created on the right top corner. The mesh that was used is an unstructured mesh.

The reference results are again considered from a finite element model with hexahedral element with B-bar mixed u/p formulation.

Results of equivalent stress are plotted in Figure 26 and equivalent strain in Figure 27.
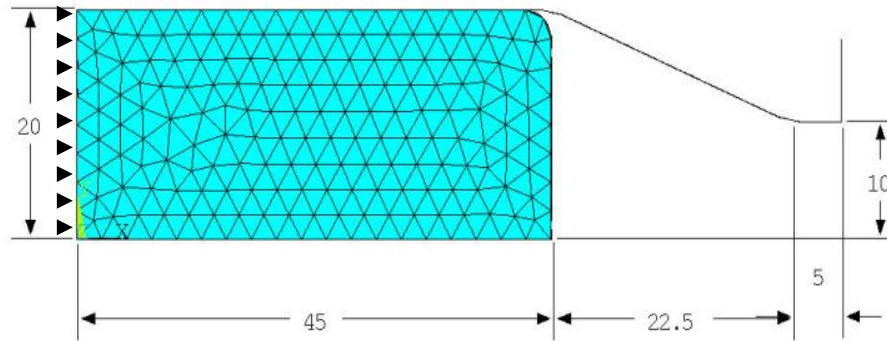
Figure 25. Finite Element model of the metal extrusion

**Results and Discusssions**

From the contours of equivalent stress we can see that the deformation reaches a steady state condition and mesh is homogeneous in this area. As illustrated in the equivalent plastic stress and strain results presented in Figures 26 and 27, the stabilized tetrahedral model was found to have good agreement with the hexahedral model. From a qualitative perspective, the tetrahedral model exhibited a very similar deformation pattern and strain distribution to the hexahedral model throughout the extrusion process.   Quantitatively, the overall displacements results between the two formulations were nearly identical.

In fact, as listed in Table 7 for the nodes with an original height of 20 mm, the average difference in horizontal (u_x) and vertical (u_y) displacements were .4% and 1.1% respectively.

These results clearly indicate the quality of the new tetrahedral formulation. The differences found in minimum and maximum values of the effective stresses and strains can originate also from the difference in mesh used, since the tetrahedral model uses an unstructured mesh as compared to the structured mesh of hexahedral elements even though the number of element divisions per each edge was the same. It is interesting to note that in this case of confined deformation the difference between the stabilized mixed formulation and the mixed formulation without stabilization are not as significant as it was observed in the upsetting process and in linear examples. The distribution of effective stress is smoother than the mixed u/p one. The results of pure displacement formulation are also not so far away but they show even more pollution in the effective stresses and a wrong deformation pattern of the right edge.

Table 7. Extrusion: Comparison between tetrahedral and hexahedral mesh displacements

Initial Horizontal Location (mm) at h=20	Stabilized Tetrahedral Model		Hexahedral Model		Difference in Ux	Difference in Uy
	Ux	Uy	Ux	Uy	(%)	(%)
	mm	mm	mm	mm		
5	45.167	-1.988	45.222	-2.066	0.121	3.755
10	46.067	-4.351	46.102	-4.435	0.075	1.902
15	47.169	-6.834	47.12	-6.849	0.103	0.219
20	49.051	-9.373	49.319	-9.505	0.543	1.385
25	53.442	-9.54	53.675	-9.489	0.434	0.537
30	57.838	-9.504	58.251	-9.513	0.709	0.100
35	62.706	-9.524	63.076	-9.525	0.586	0.015
45	73	-9.669	72.515	-9.565	0.668	1.093
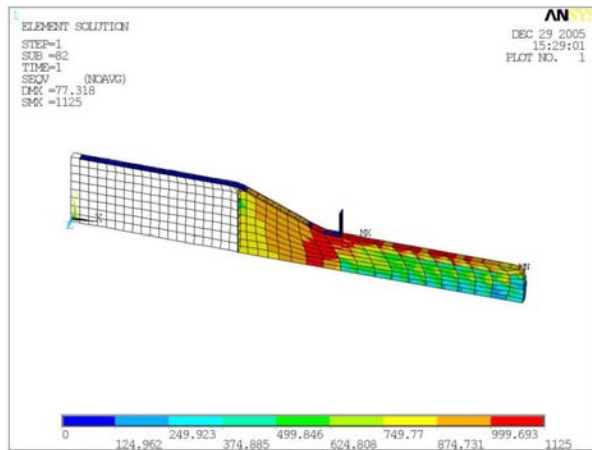
(a) Mixed u/p Hexahedral
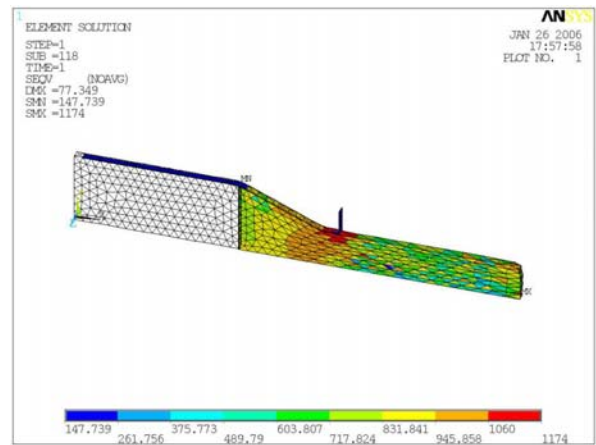
(b) Stabilized Mixed u/p Tetrahedral
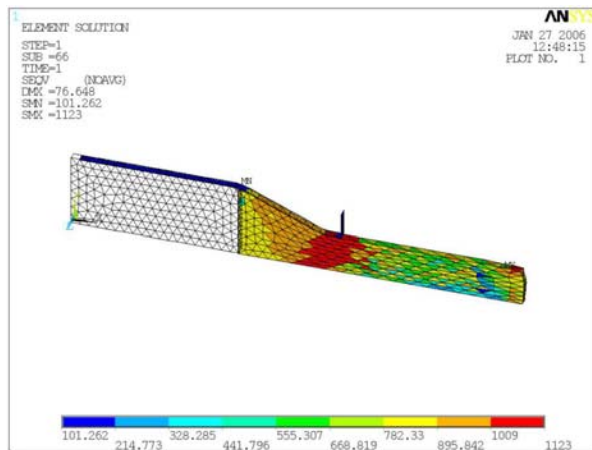
(c) Mixed u/p Tetrahedral

(d) Pure Displacement Tetrahedral

Figure 26. Extrusion process: Equivalent Stress
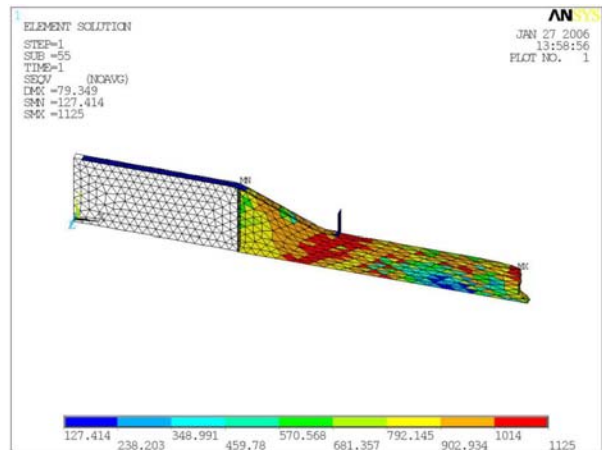
(a) Mixed u/p Hexahedral

(b) Stabilized Mixed u/p Tetrahedral
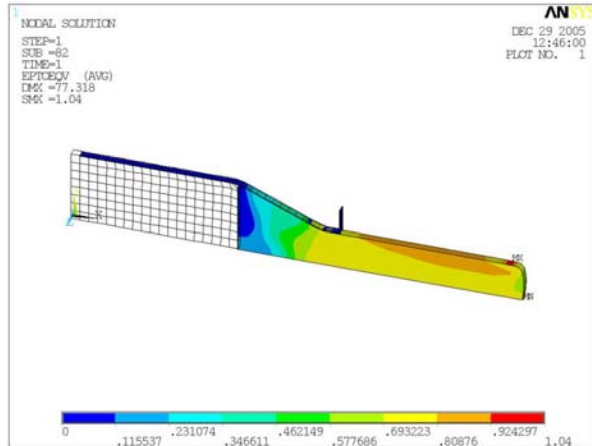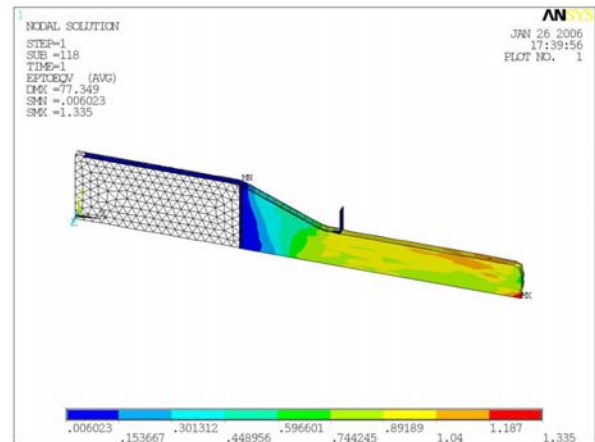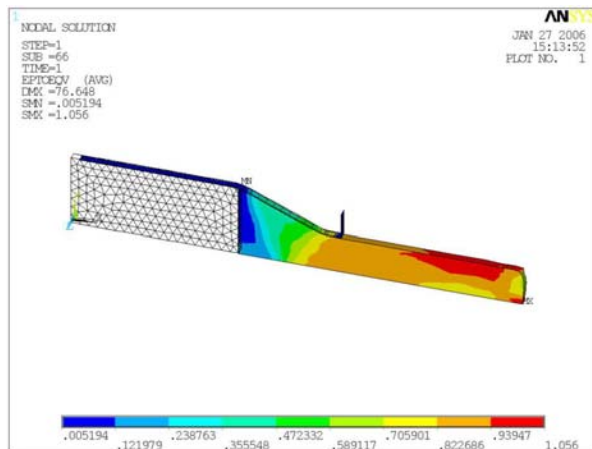
(c) Mixed u/p Tetrahedral
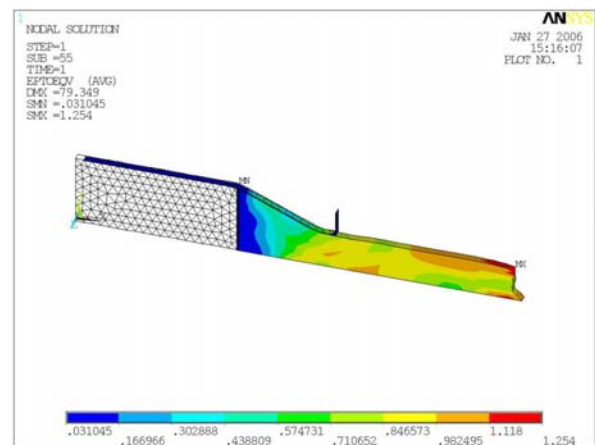
(d) Pure Displacement Tetrahedral

Figure 27. Extrusion process: Equivalent Strain

6.4 HYPERELASTIC CANTILEVER BEAM

This test was designed to assess the performance of the new tetrahedron element in large deformations and large rotations in bending dominant problems where conditions of near incompressibility are present. This example was used by R. Taylor in [47] to verify his enhanced strain formulation for hyperelasticity.

Description of the test

A square cross section cantilever beam with 5 mm length and a whole length of 50 mm is loaded with a displacement along the top left edge in the z direction (see Figure 28). The structured mesh is obtained by generating elements along the three directions from a block made of six tetrahedral elements.
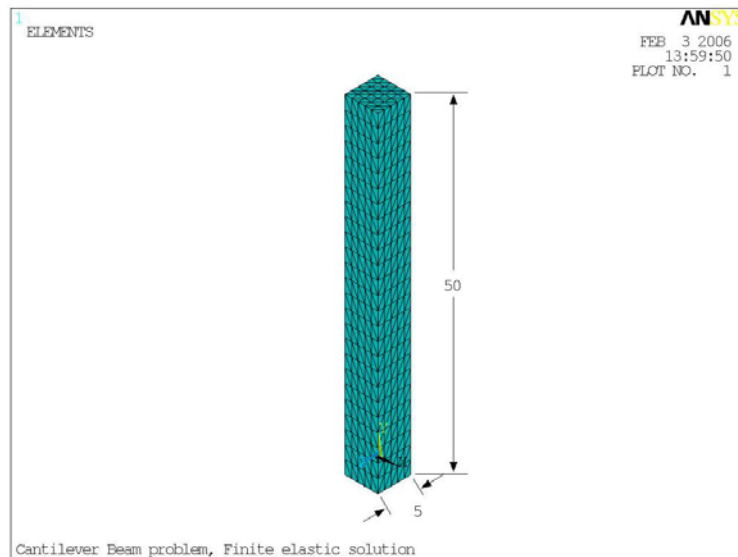
Figure 28. Hyperlastic Cantilever Beam: Finite Element model

The material used is hyperelastic with a Neo-Hookean formulation defined by the following two constants:

G=333.35MPa

d= 1/K = 1.2e-6

The reference finite element model is constructed from mixed u/p hexahedral elements with an enhanced strain formulation because the problem is of a bending dominant type. As done previously the stabilized formulation is presented together with the other two formulations, mixed u/p and pure displacement, for comparison reasons. Contours of equivalent stress, principal stress in the second direction and hydrostatic pressures are shown in Figures 29, 30 and 31. As illustrated in the contour plots, the stabilized enhanced formulation is clearly predicting a deformed shape closest to the hexahedral finite element model (note that the final deformed shape is almost horizontal). The mixed u/p formulation, in contrast, shows a much stiffer response of the beam while the pure displacement formulation shows evidence of locking and incorrectly predicts twisting of the beam instead of bending. In fact, the pure displacement formulation in this case did not even converge, so only results at the last converged substep are shown. The equivalent stress contours of the stabilized tetrahedral are similar with those of hexahedral one and the values of these stresses are within 10 % error. It is noteworthy to mention that even though we have the same number of nodes for both models, the number of tetrahedral elements is six times larger than the number of hexahedral elements. In addition, the tetrahedral elements have 4 degrees of freedom at each node while the hexahedral ones have only three (the pressure is considered constant in this element).

As for the principal stress contour plots in Figure 30, the comparison is even more difficult because it can be observed that even for the hexahedral elements the mixed enhanced strain

formulation (Fig. 30(a)) and the B-bar (Fig. 30(b)) give different results, with the stabilized tetrahedral compressive stress being closer to the compressive stress of the mixed enhanced hexahedral and the tensile stress being closer to the B-bar formulation of the same elements. The hydrostatic pressures are the most sensitive variables when considering locking. A special note has to be made when examining those plots: due to the negative sign considered in the interpolated pressure of the stabilized tetrahedral element as compared to the pressure calculated from stresses of the hexahedral elements, the pressure degree of freedom is plotted with the signs reversed. Therefore when looking at the pressure plots, the minimum pressure of the tetrahedral model is -340 and the maximum pressure is 205. If compared to the hexahedral model, we can see that the maximum pressure is in very good agreement (202) while the minimum pressure shows a peak value. This peak value in the pressures induced by the compressive stresses was noted also by Onate in his results while applying the FIC method [36] and also by Zienkiewicz and Taylor in [49].

Overall the stability is improved since the principal stress and pressure distributions no longer show the spurious oscillations observed in standard and mixed u/p formulations.
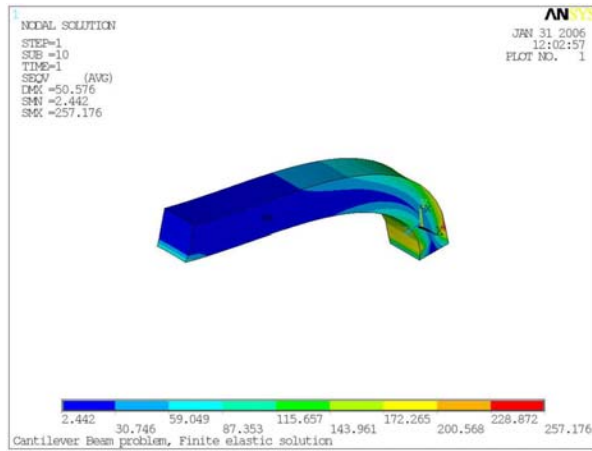
(a)Enhanced Strain Mixed u/p Hexahedral   (b) Stabilized Mixed Tetrahedral
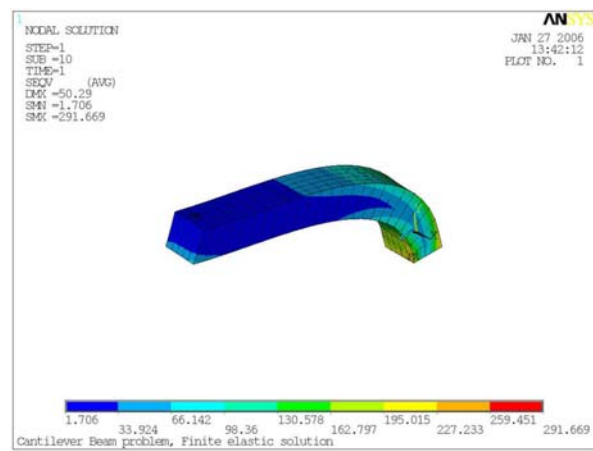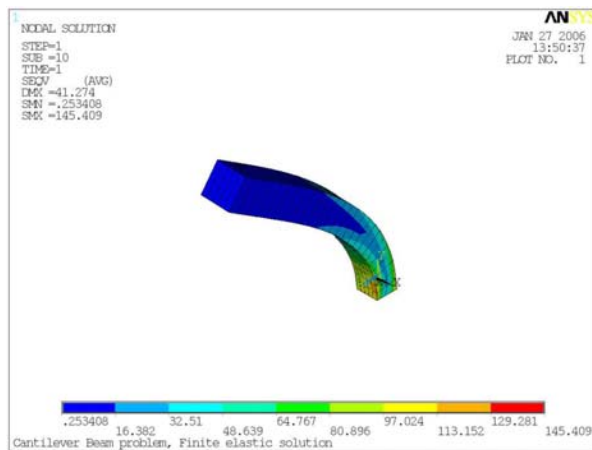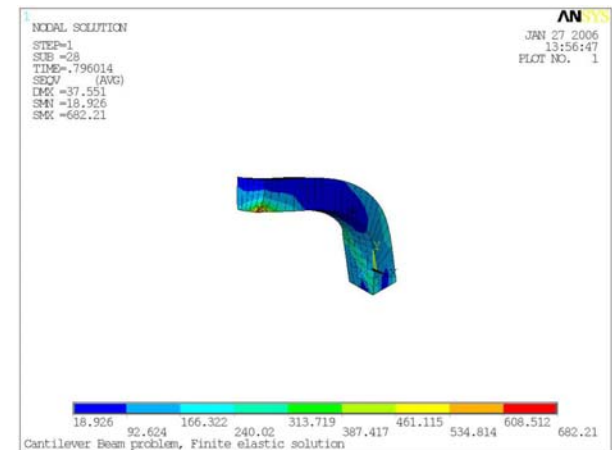
(c) Mixed u/p Tetrahedral   (d) Pure Displacement Tetrahedral (not converged)

Figure 29. Hyperelastic Cantilever Beam: Equivalent Stress
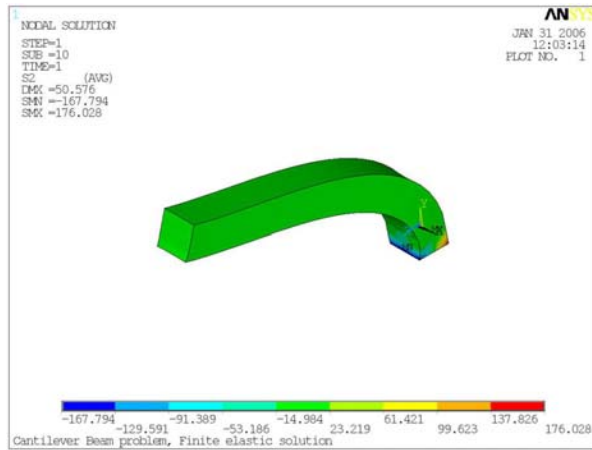
(a) Mixed Enhanced Strain Hexahedral
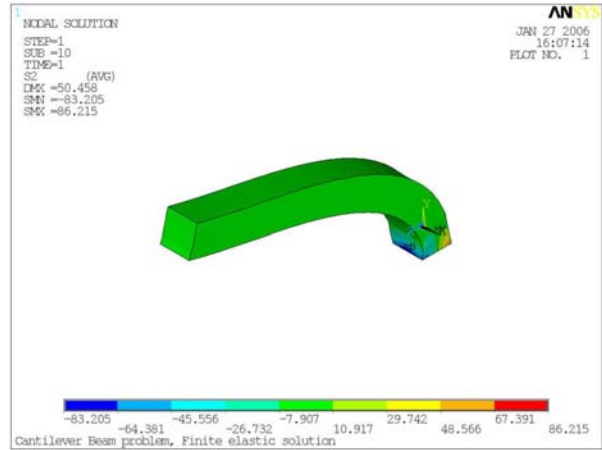
(b) Mixed Hexahedral with B-bar formulation
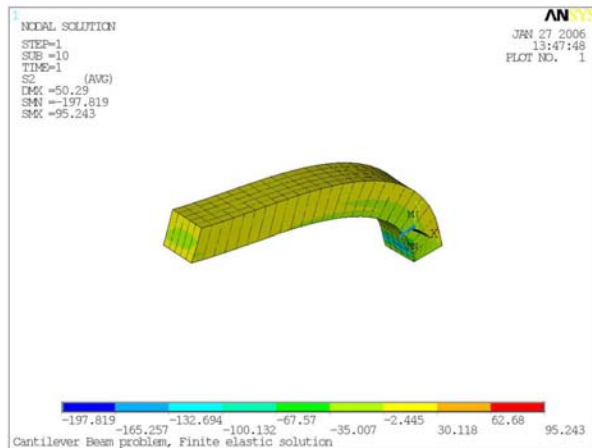
(c) Stabilized Tetrahedral
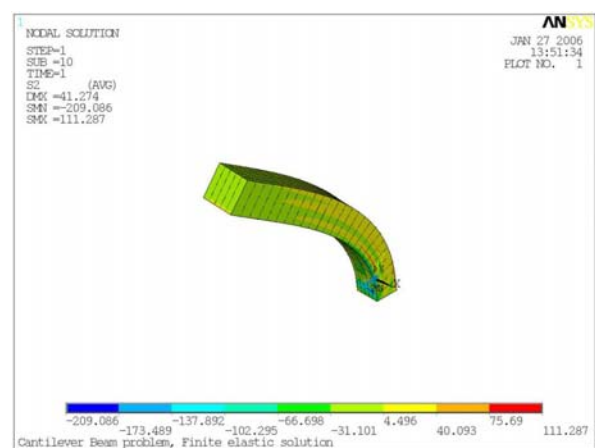
(d) Mixed u/p Tetrahedral
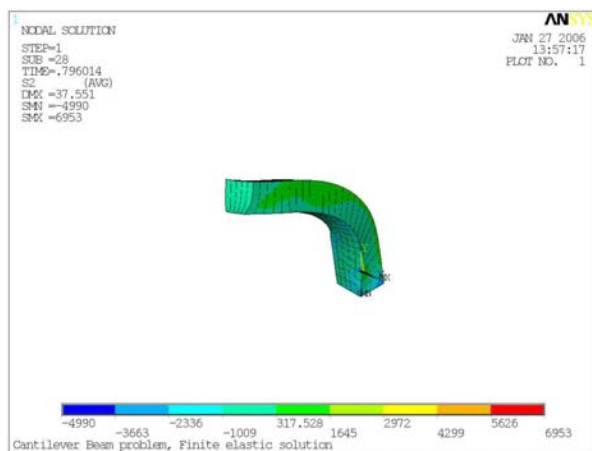
(e) Pure Displacement Tetrahedral (not converged)

Figure 30. Hyperelastic Cantilever Beam: Principal Stress in second direction

104
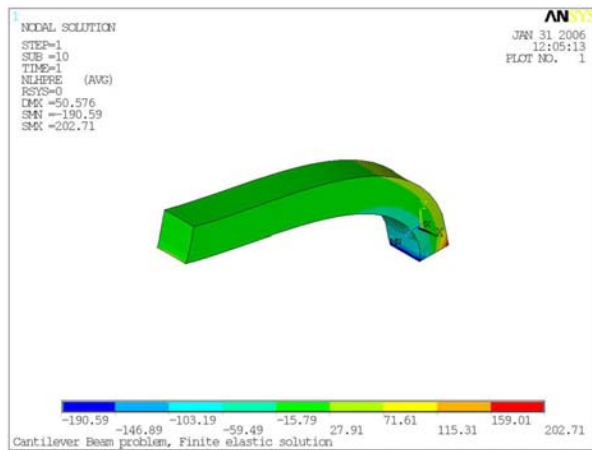
(a) Mixed Enhanced Strain Hexahedral
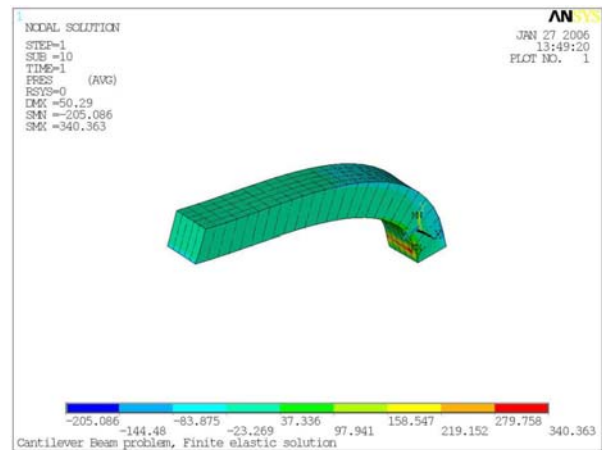
(b) Mixed Stabilized Tetrahedral
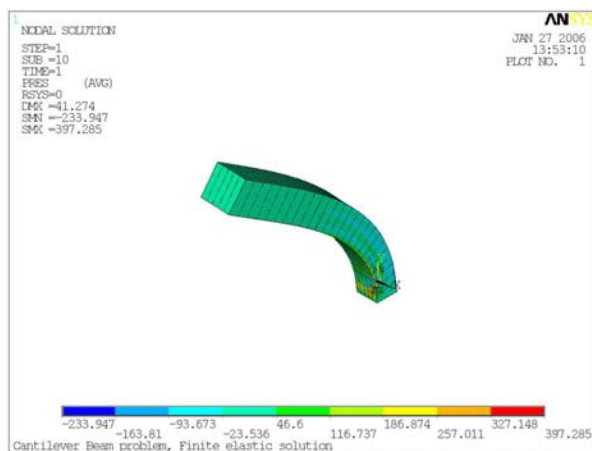
(c) Mixed Tetrahedral
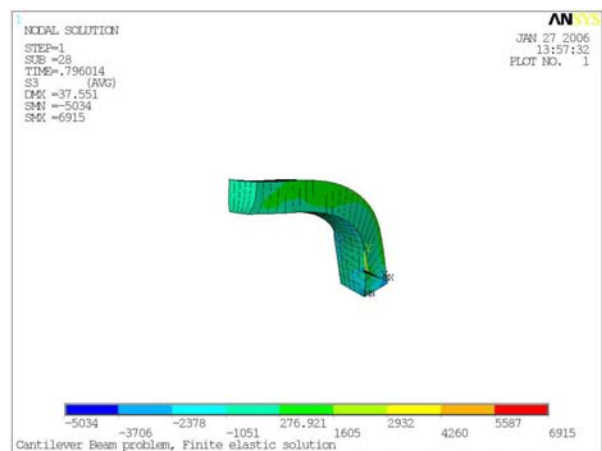
(d) Pure Displacement Tetrahedral

Figure 31. Hyperelastic Cantilever Beam: Hydrostatic Pressure

7.0 CONCLUSIONS

7.1 SUMMARY

Many finite elements, such as the linear tetrahedral element, exhibit the phenomenon of volumetric locking when situations of near incompressibility are encountered during an analysis.

The main goal of the present research was to develop a robust and accurate low-order solid tetrahedral element that exhibits significantly better performance than the existing ones. This was primarily motivated by the absence of an element that could be used to solve general large deformation problems under incompressible conditions that can incorporate a wide range of nonlinear materials. Another motivation lies in the fact that analysts are bringing more geometric details into finite element models, thereby requiring the development of algorithms that can readily interface with CAD models. For these two reasons, the newly developed element will be useful in solving large finite element models with complicated geometries which can not be meshed with standard brick elements. One of the immediate expected fields of applications will be metal forming.

Reviewing the results presented in this dissertation, five different methods of stabilizing the mixed linear displacement/linear pressure tetrahedral element were reviewed in Chapter 2. It was concluded that under specific conditions they are all equivalent. The main question was which one to choose and why. In Chapter 3, a new general formulation applicable to small and large deformation and large rotations was presented.

The new solid tetrahedral element was formulated based on the principle of virtual work and it was stabilized through an enhanced strain derived from a bubble function. Two bubble functions were studied and the results were found to be identical. This approach was chosen among the five choices for the following reasons: it does not require material or mesh dependent parameters, consistent in nonlinear analysis, reasonable stable and computationally efficient. The mixed stabilized formulation together with other two formulations, (a non-stabilized mixed and a standard pure displacement formulation), was implemented through a user-programmable element that interfaces with the commercial finite element software ANSYS. The finite element code uses the pre- and post- processing capabilities as well as the nonlinear solvers of ANSYS. Aspects of the implementation were discussed in Chapter 4.

Several numerical investigations were carried out to verify the element formulation. Some linear tests results were presented and discussed in Chapter 5 and some nonlinear tests with emphasis on simulation of metal forming applications were presented in Chapter 6. The verification of the new formulation was assessed through comparisons with theoretical results when they were available and in most cases by comparisons with a similar analysis carried out with well known stabilized hexahedral element already existing in ANSYS. To assess the improved performance of the mixed stabilized formulation, the results were compared to two other formulations. All numerical examples, both linear and nonlinear, demonstrated the robustness, accuracy and improved performance of the new element in quasi and fully incompressible problems that involve large deformation. In these problems consistent improvement was observed over the mixed u/p without stabilization and the pure displacement formulations. This observation was motivated by the improved stress distributions, improved accuracy of the displacements, and closer results to the stabilized hexahedral elements. Even

though the new element behaved correctly in bending dominant problems in both linear and nonlinear analyses, it still showed shear locking in pure bending problems.

The importance of the new lower order tetrahedral element lies within its ability to provide large deformation analysis capabilities for metal forming problems where the automatic generation of hexahedral elements is not possible, especially when rezoning procedures are applied. Such technology could prove to be an important step in the advancement of simulating metal forming processes that are creating increasingly complex components.

7.2 SUGGESTIONS FOR FUTURE WORK

The robustness of the newly developed element needs to be further explored by performing various analyses using different deformation conditions and a wide range of nonlinear materials.

Four major research directions can be foreseen for a future development of the proposed element.

1. An interesting future work would be the investigation of the new formulation when using anisotropic materials. The formulation should work since no specific assumptions were made on the choice of the material constitutive law.

2. The choice of bubble functions remains an open investigation area, since the only two investigated here produced identical results. Zienkiewicz and Taylor [49] recently used a set of three bubble functions and obtained promising results. This indicates that stabilization can further be improved by the choice of bubble functions.

3. Another issue that was not thoroughly studied in the present study is the influence of the mesh alignment on the results. This was detected in several papers and needs to be further

addressed since it can influence the results obtained after automatic generation of elements during different remeshing techniques.

4. The present formulation was developed for static analyses but it can be extended to transient analyses as well. This can be accomplished because the enhanced term is a strain (not a displacement) which will not affect the inertial terms. It would be interesting to test the performance of the stabilized tetrahedral element in static analyses with body forces.

APPENDIX A

DERIVATION OF THE GEOMETRIC STIFFNESS TERM

The geometric stiffness term represented by the second integral in (3.20) is derived here for its future conversion to the matrix format that is used in the implementation of the element.

$$\overline{C}_{ik}Da_{jk}\delta\varepsilon_{ij} + \overline{C}_{jk}Da_{ik}\delta\varepsilon_{ij} + \overline{C}_{ij}D\delta\varepsilon_{ij} =$$

$$= \overline{\sigma}_{ik}\frac{1}{4}\left(\frac{\partial Du_j}{\partial x_k} - \frac{\partial Du_k}{\partial x_j}\right)\left(\frac{\partial \delta u_i}{\partial x_j} + \frac{\partial \delta u_j}{\partial x_i}\right) + \overline{\sigma}_{ik}\frac{1}{4}\left(\frac{\partial Du_i}{\partial x_k} - \frac{\partial Du_k}{\partial x_i}\right)\left(\frac{\partial \delta u_i}{\partial x_j} + \frac{\partial \delta u_j}{\partial x_i}\right) +$$

$$+ \overline{\sigma}_{ij}D\delta\varepsilon_{ij} = \overline{\sigma}_{ik}\frac{1}{4}\left(\frac{\partial Du_j}{\partial x_k}\frac{\partial \delta u_i}{\partial x_j} + \frac{\partial Du_j}{\partial x_k}\frac{\partial \delta u_j}{\partial x_i} - \frac{\partial Du_k}{\partial x_j}\frac{\partial \delta u_i}{\partial x_j} - \frac{\partial Du_k}{\partial x_j}\frac{\partial \delta u_j}{\partial x_i}\right) +$$

$$+ \overline{\sigma}_{jk}\frac{1}{4}\left(\frac{\partial Du_i}{\partial x_k}\frac{\partial \delta u_i}{\partial x_j} + \frac{\partial Du_i}{\partial x_k}\frac{\partial \delta u_j}{\partial x_i} - \frac{\partial Du_k}{\partial x_i}\frac{\partial \delta u_i}{\partial x_j} - \frac{\partial Du_k}{\partial x_i}\frac{\partial \delta u_j}{\partial x_i}\right) + \overline{\sigma}_{ij}D\delta\varepsilon_{ij} \tag{A1}$$

Interchanging k with j in the first parenthesis and then k with i in the second one we obtain:

$$\overline{C}_{ik}Da_{jk}\delta\varepsilon_{ij} + \overline{C}_{jk}Da_{ik}\delta\varepsilon_{ij} + \overline{C}_{ij}D\delta\varepsilon_{ij} =$$

$$= \overline{\sigma}_{ij}\frac{1}{4}\left(\frac{\partial Du_k}{\partial x_j}\frac{\partial \delta u_i}{\partial x_k} + \frac{\partial Du_k}{\partial x_j}\frac{\partial \delta u_k}{\partial x_i} - \frac{\partial Du_j}{\partial x_k}\frac{\partial \delta u_i}{\partial x_k} - \frac{\partial Du_j}{\partial x_k}\frac{\partial \delta u_k}{\partial x_i}\right) + \tag{A2}$$

$$+ \overline{\sigma}_{ji}\frac{1}{4}\left(\frac{\partial Du_k}{\partial x_i}\frac{\partial \delta u_k}{\partial x_j} + \frac{\partial Du_k}{\partial x_i}\frac{\partial \delta u_j}{\partial x_k} - \frac{\partial Du_i}{\partial x_k}\frac{\partial \delta u_k}{\partial x_j} - \frac{\partial Du_i}{\partial x_k}\frac{\partial \delta u_j}{\partial x_k}\right) + \overline{\sigma}_{ij}D\delta\varepsilon_{ij}$$

Now solve for the last term:

$$\overline{\sigma}_{ij}D\delta\varepsilon_{ij} = \frac{1}{2}\overline{\sigma}_{ij}D\left(\frac{\partial \delta u_i}{\partial x_j} + \frac{\partial \delta u_j}{\partial x_i}\right) \tag{A3}$$

Keeping in mind that in the Updated Lagrange formulation we always calculate the variables at time t+Δt in terms of the known variables at time t, we can write that

$$D\left(\frac{\partial \delta u_i}{\partial x_j}\right) = \lim_{\Delta t \to 0} \frac{\left(\frac{\partial \delta u_i}{\partial^{t+\Delta t}x_j} - \frac{\partial \delta u_i}{\partial^t x_j}\right)}{\Delta t} \tag{A4}$$

By using the chain rule,

$$\frac{\partial \delta u_i}{\partial^{t+\Delta t}x_j} = \frac{\partial \delta u_i}{\partial^t x_k} \cdot \frac{\partial^t x_k}{\partial^{t+\Delta t}x_j} \tag{A5}$$

Also the displacement increment Du_k can be written as the difference between the displacement at time t+Δt and the displacement at time t:

$$^{t+\Delta t}x_k - {}^t x_k = Du_k \Leftrightarrow {}^t x_k = {}^{t+\Delta t}x_k - Du_k \Rightarrow \frac{\partial^t x_k}{\partial^{t+\Delta t}x_j} = \delta_{kj} - \frac{\partial Du_k}{\partial^{t+\Delta t}x_j} \tag{A6}$$

Introducing (A4) and (A5) into (A6) we get:

$$D\left(\frac{\partial \delta u_i}{\partial x_j}\right) = \lim_{\Delta t \to 0} \frac{\left(\frac{\partial \delta u_i}{\partial^{t+\Delta t}x_j} - \frac{\partial \delta u_i}{\partial^t x_j}\right)}{\Delta t} = \lim_{\Delta t \to 0} \frac{\frac{\partial \delta u_i}{\partial^t x_k}\left(\frac{\partial^t x_k}{\partial^{t+\Delta t}x_j} - \delta_{kj}\right)}{\Delta t} =$$

$$= \lim_{\Delta t \to 0} \frac{\frac{\partial \delta u_i}{\partial^t x_k}\left(\delta_{kj} - \frac{\partial Du_k}{\partial^{t+\Delta t}x_j} - \delta_{kj}\right)}{\Delta t} = -\frac{\partial \delta u_i}{\partial^t x_k}\frac{\partial Du_k}{\partial^t x_j} \tag{A7}$$

Similarly, $D\left(\frac{\partial \delta u_j}{\partial x_i}\right) = -\frac{\partial \delta u_j}{\partial^t x_k}\frac{\partial Du_k}{\partial^t x_i}$ \tag{A8}

Introducing (A7) and (A8) back into (A1), reducing the similar terms and using the fact that the Cauchy stresses are symmetric ($\bar{c}_{ij} = \bar{c}_{ji}$) we obtain:

$$\overline{c}_{ik}Da_{jk}\delta\varepsilon_{ij} + \overline{c}_{jk}Da_{ik}\delta\varepsilon_{ij} + \overline{c}_{ij}D\delta\varepsilon_{ij} =$$

$$= \overline{\sigma}_{ij}\frac{1}{4}\left(\frac{\partial Du_k}{\partial x_j}\frac{\partial \delta u_i}{\partial x_k} + \frac{\partial Du_k}{\partial x_j}\frac{\partial \delta u_k}{\partial x_i} - \frac{\partial Du_j}{\partial x_k}\frac{\partial \delta u_i}{\partial x_k} - \frac{\partial Du_j}{\partial x_k}\frac{\partial \delta u_k}{\partial x_i}\right) +$$

$$+ \overline{\sigma}_{ij}\frac{1}{4}\left(\frac{\partial Du_k}{\partial x_i}\frac{\partial \delta u_k}{\partial x_j} + \frac{\partial Du_k}{\partial x_i}\frac{\partial \delta u_j}{\partial x_k} - \frac{\partial Du_i}{\partial x_k}\frac{\partial \delta u_k}{\partial x_j} - \frac{\partial Du_i}{\partial x_k}\frac{\partial \delta u_j}{\partial x_k}\right) -$$

$$- \frac{\overline{\sigma}_{ij}}{4}\left(2\frac{\partial \delta u_i}{\partial 'x_k}\frac{\partial Du_k}{\partial 'x_j} + 2\frac{\partial \delta u_j}{\partial 'x_k}\frac{\partial Du_k}{\partial 'x_i}\right) = \qquad\qquad (A9)$$

$$= \frac{\overline{\sigma}_{ij}}{4}\left(-\frac{\partial Du_k}{\partial x_j}\frac{\partial \delta u_i}{\partial x_k} - \frac{\partial Du_k}{\partial x_i}\frac{\partial \delta u_j}{\partial x_k} + \frac{\partial Du_k}{\partial x_j}\frac{\partial \delta u_k}{\partial x_i} + \frac{\partial Du_k}{\partial x_i}\frac{\partial \delta u_k}{\partial x_j}\right) +$$

$$+ \frac{\overline{\sigma}_{ij}}{4}\left(-\frac{\partial Du_j}{\partial x_k}\frac{\partial \delta u_i}{\partial x_k} - \frac{\partial Du_j}{\partial x_k}\frac{\partial \delta u_k}{\partial x_i} - \frac{\partial Du_i}{\partial x_k}\frac{\partial \delta u_k}{\partial x_j} - \frac{\partial Du_i}{\partial x_k}\frac{\partial \delta u_j}{\partial x_k}\right)$$

Interchanging i with j in the second, seventh and eighth terms and writing the third and the fourth as two terms minus one, then grouping them we obtain the final formula for the geometric stiffness term as:

$$\overline{c}_{ik}Da_{jk}\delta\varepsilon_{ij} + \overline{c}_{jk}Da_{ik}\delta\varepsilon_{ij} + \overline{c}_{ij}D\delta\varepsilon_{ij} =$$

$$= \frac{\overline{\sigma}_{ij}}{4}\left[-\frac{\partial \delta u_i}{\partial x_k}\left(\frac{\partial Du_k}{\partial x_j} + \frac{\partial Du_j}{\partial x_k}\right) - \frac{\partial \delta u_k}{\partial x_i}\left(\frac{\partial Du_j}{\partial x_k} + \frac{\partial Du_k}{\partial x_j}\right)\right] +$$

$$+ \frac{\overline{\sigma}_{ij}}{4}\left[\frac{\partial \delta u_i}{\partial x_k}\left(\frac{\partial Du_k}{\partial x_j} + \frac{\partial Du_j}{\partial x_k}\right) - \frac{\partial \delta u_k}{\partial x_i}\left(\frac{\partial Du_j}{\partial x_k} + \frac{\partial Du_k}{\partial x_j}\right) + 4\frac{\partial Du_k}{\partial x_j}\frac{\partial \delta u_k}{\partial x_i}\right] = \qquad (A10)$$

$$= \overline{\sigma}_{ij}\left[\frac{\partial Du_k}{\partial x_j}\frac{\partial \delta u_k}{\partial x_i} - \frac{2}{4}\left(\frac{\partial \delta u_i}{\partial x_k} + \frac{\partial \delta u_k}{\partial x_i}\right)\left(\frac{\partial Du_j}{\partial x_k} + \frac{\partial Du_k}{\partial x_j}\right)\right] =$$

$$= \overline{\sigma}_{ij}\left(\frac{\partial Du_k}{\partial x_j}\frac{\partial \delta u_k}{\partial x_i} - 2\delta\varepsilon_{ik}D\varepsilon_{jk}\right)$$

APPENDIX B

OUTPUT FILE FOR THE LINEAR HOMOGENEOUS DEFORMATION PROBLEM

Results of strain (EPTO) and stress (S) components for three selected elements of the linear unit cube example subjected to a linearly varying displacement field are listed in the following ANSYS output file together with the analytical results. The new tetrahedral element is here SOLID 285.

```
        ***** ANSYS RESULTS INTERPRETATION (POST1) *****

 ***********************************************************

        TARGET STRAINS
        --------------
  The computed strains for this deformation field
  should be:

  EPTOX = 2.0, EPTOY = 1.0, EPTOZ = 1.5
  EPTOXY = 4.0, EPTOYZ = 1.5, EPTOXZ = 2.0

 ***********************************************************

 ***** POST1 ELEMENT NODAL TOTAL STRAIN LISTING *****


  THE FOLLOWING X,Y,Z VALUES ARE IN GLOBAL COORDINATES

  ELEMENT=        1        SOLID285
    NODE     EPTOX       EPTOY       EPTOZ       EPTOXY      EPTOYZ      EPTOXZ
      10    2.0000      1.0000      1.5000      4.0000      1.5000      2.0000
       9    2.0000      1.0000      1.5000      4.0000      1.5000      2.0000
      11    2.0000      1.0000      1.5000      4.0000      1.5000      2.0000
      12    2.0000      1.0000      1.5000      4.0000      1.5000      2.0000

  ELEMENT=        2        SOLID285
    NODE     EPTOX       EPTOY       EPTOZ       EPTOXY      EPTOYZ
EPTOXZ
       1    2.0000      1.0000      1.5000      4.0000      1.5000      2.0000
```

```
        2    2.0000          1.0000          1.5000          4.0000          1.5000          2.0000
        4    2.0000          1.0000          1.5000          4.0000          1.5000          2.0000
       11    2.0000          1.0000          1.5000          4.0000          1.5000          2.0000


    ELEMENT=         3          SOLID285
       NODE    EPTOX           EPTOY           EPTOZ           EPTOXY          EPTOYZ
EPTOXZ
       11    2.0000          1.0000          1.5000          4.0000          1.5000          2.0000
        4    2.0000          1.0000          1.5000          4.0000          1.5000          2.0000
        1    2.0000          1.0000          1.5000          4.0000          1.5000          2.0000
       12    2.0000          1.0000          1.5000          4.0000          1.5000          2.0000

***** POST1 ELEMENT NODAL STRESS LISTING *****


    THE FOLLOWING X,Y,Z VALUES ARE IN GLOBAL COORDINATES


 ELEMENT=         1          SOLID285
     NODE    SX              SY              SZ              SXY             SYZ             SXZ
       10  0.34000E+07 0.26000E+07 0.30000E+07 0.16000E+07 0.60000E+06
0.80000E+06
        9  0.34000E+07 0.26000E+07 0.30000E+07 0.16000E+07 0.60000E+06
0.80000E+06
       11  0.34000E+07 0.26000E+07 0.30000E+07 0.16000E+07 0.60000E+06
0.80000E+06
       12  0.34000E+07 0.26000E+07 0.30000E+07 0.16000E+07 0.60000E+06
0.80000E+06


 ELEMENT=         2          SOLID285
     NODE    SX              SY              SZ              SXY             SYZ             SXZ
        1  0.34000E+07 0.26000E+07 0.30000E+07 0.16000E+07 0.60000E+06
0.80000E+06
        2  0.34000E+07 0.26000E+07 0.30000E+07 0.16000E+07 0.60000E+06
0.80000E+06
        4  0.34000E+07 0.26000E+07 0.30000E+07 0.16000E+07 0.60000E+06
0.80000E+06
       11  0.34000E+07 0.26000E+07 0.30000E+07 0.16000E+07 0.60000E+06
0.80000E+06


 ELEMENT=         3          SOLID285
     NODE    SX              SY              SZ              SXY             SYZ             SXZ
       11  0.34000E+07 0.26000E+07 0.30000E+07 0.16000E+07 0.60000E+06
0.80000E+06
        4  0.34000E+07 0.26000E+07 0.30000E+07 0.16000E+07 0.60000E+06
0.80000E+06
        1  0.34000E+07 0.26000E+07 0.30000E+07 0.16000E+07 0.60000E+06
0.80000E+06
       12  0.34000E+07 0.26000E+07 0.30000E+07 0.16000E+07 0.60000E+06
0.80000E+06
```

BIBLIOGRAPHY

1. ABAQUS Manual. Hibbitt, Karlsson and Sorensen:1080 Main Street, Pawtucket, RI, 02860, USA, 2003.

2. ANSYS Release 10.0 Theory Verification Manual, Canonsburg, PA, USA :ANSYS Inc., 2005.

3. D.N. Arnold, F.Brezzi, and M. Fortin. A stable finite element for the Stokes equations. *Calcolo*, 21:337-344,1984.

4. Babuška I. Error bounds for finite element methods. *Numer.Math.*, 16:322-333, 1971.

5. C. Baiocchi, F.Brezzi. Virtual bubbles and Galerkin-least-squares type methods. *Comput.Methods Appl. Mech. Engnrg.* 105:125-141, 1993.

6. Klaus-Jurgen Bathe. *Finite element procedures*. Prentice-Hall, Upper Saddle River, NJ, 1996.

7. S.R. Beissel, G.R.Johnson. Large deformation triangular and tetrahedral element formulations for unstructured meshes. *Comput. Methods Appl. Mech. Engnrg.* 187:469-482, 2000.

8. Ted Belytschko, Wing Kam Liu, Brian Moran. *Nonlinear finite elements for continua and structures*. Chichester, England; New York : John Wiley, c2000.

9. F.H.Bertrand, M.R.Gadbois, and P.A.Tanguy. Tetrahedral elements for fluid flow. *Int. J. Numer. Meth. Engng.* 33:1251-1267,1992.

10. F.Brezzi, M.O.Bristeau,L.P.Franca, M.M.Gilbert Rogé. A relationship between stabilized finite element methods and the Galerkin method with bubble functions. *Comput.Methods Appl. Mech. Engnrg.* 96:117-129, 1992.

11. F.Brezzi, J.Pitkäranta. On the stabilization of finite element approximations of the Stokes problem. In W.Hackbusch,editor, *Efficient solution of Elliptic problems, Notes on Numerical Fluid Mechnaics*, vol.10,Vieweg, Wiesbaden, 1984.

12. F.Brezzi, L.P.Franca, T.J.R.Hughes, A.Russo. $b = \int g$. *Comput. Methods Appl. Mech. Engnrg.* 145:329-339, 1997.

13. P.A.J.Van Den Bogert, R.De Boerst, G.T Luiten, and J.Zeilkmaker. Robust finite elements for 3D-analysis of rubber-like materials. *Engineering Computations* 8:3-17, 1991.

14. U.Brink, E.Stein. On some mixed finite element methods for incompressible and nearly incompressible finite elasticity. *Computational mechanics* 19:105-119, 1996.

15. J.Bonet, H. Marriott and O.Hassan. An averaged nodal deformation gradient linear tetrahedral element for large strain explicit dynamics applications. *Commun. Numer. Meth. Engng*; 17:551-561, 2001.

16. J. Bonet and R.D.Wood. *Nonlinear continuum mechanics for finite element analysis.* Cambridge University Press, 1997.

17. M.Cervera, M.Chiumenti, Q. Valverde, C.A. de Saracibar, Mixed linear/linear simplicial elements for incompressible elasticity and plasticity. *Comput. Methods Appl. Mech. Engnrg.* 192:5249-5263, 2003.

18. M. Chiumenti, Q. Valverde, C Agelet de Saracibar, M.Cervera. A stabilized formulation for incompressible plasticity using linear triangles and tetrahedra. *International Journal of Plasticity* 20:1487-1504, 2004.

19. M. Chiumenti, Q. Valverde, C Agelet de Saracibar, M.Cervera. A stabilized formulation for incompressible elasticity using linear displacement and pressure interpolations. *Comput. Methods Appl. Mech. Engnrg.* 191:5253-5264, 2002.

20. R. Codina. Stabilized finite element approximation of transient incompressible flows using orthogonal subscales. *Comput.Methods Appl. Mech. Engnrg.* 191:4295-4321, 2002.

21. C.R.Dohrmann, S.W.Key, M.W.Heinstein and J .Jung. A least-squares approach for uniform straintriangular and tetrahedral finite elements. *Int. J. Numer. Meth. Engrng;* 42:1181-1197, 1998.

22. C.R.Dohrmann, S.W.Key, M.W.Heinstein, J.Jung and W.R. Witkowski. Node-based uniform strain elements for three-node triangular and four-node tetrahedral meshes. *Int. J. Numer. Meth. Engrng;* 47:1549-1568, 2000.

23. L.P Franca, C. Farhat. On the limitations of bubble functions. *Comput.Methods Appl. Mech. Engnrg.* 117:225-230, 1994.

24. L.P Franca, C. Farhat. Bubble functions prompt unusual stabilized finite element methods. *Comput.Methods Appl. Mech. Engnrg.* 123:299-308, 1995.

25. L.P.Franca, S.P.Oliveira. Pressure bubble stabilization features in the Stokes problem. *Comput.Methods Appl. Mech. Engnrg.* 192:1929-1937, 2003.

26. M.S.Gadala and J.Wang. Simulation of metal forming processes with finite element methods. *Int. J. Numer. Meth. Engrng*. 44:1397-1428, 1999.

27. T.J.R Hughes and J. Winget. Finite rotations effects in numerical integration of rate constitutive equations arising in large-deformation analysis. *Short Communications*: 1862-1867,1980.

28. T.J.R. Hughes. *The finite element method: Linear Static and Dynamic Analysis*. Prentice – Hall, Englewood Cliffs NJ, 1987

29. T.J.R. Hughes, L.P.Franca, and M.Balestra. A new finite element formulation for computational fluid dynamics: V. Circumventing the Babuska-Brezzi condition: A stable Petrov-Galerkin formulation of the Stokes problem accommodating equal-order inerpolations. *Comput.Methods Appl. Mech. Engnrg.* 59:85-99, 1986.

30. T.J.R.Hughes. Multiscale phenomena:Green's functions, the Dirichlet-to-Neumann formulation, subgrid scale models, bubbles and the origins of stabilized methods. *Comput.Methods Appl. Mech. Engnrg.* 127:387-401, 1995.

31. O. Klaas, A. Maniatty, M.S.Shephard. A stabilized mixed finite element method for finite elasticity. Formulation for linear displacement and pressure interpolation. *Comput. Methods Appl. Mech. Engnrg*. 180:65-79, 1999.

32. R.M.McMeeking and J.Rice. Finite-element formulations for problems of large elastic-plastic deformation. *Int.J.Solids Structures*, 11:601-616, 1975.

33. Eugenio Oñate. Multiscale computational analysis in mechanics using finite calculus: an introduction. *Comput. Methods Appl. Mech. Engnrg*. 192:3043-3059, 2003.

34. Eugenio Oñate. Possibilities of finite calculus in computational mechanics. *Int. J.Numer. Meth. Engng.* 60; 255-281, 2004.

35. E.Oñate, R.L.Taylor, O,C.Zienkiewicz, J.Rojek. A residual correction method based on finite calculus. Engineering Computations 20(5/6):629-658, 2003.

36. E. Oñate, J.Rojek, R.L.Taylor and O.C.Zienkiewicz. Finite Calculus formulation for incompressible solids using linear triangles and tetrahedra. *Int. J.Numer. Meth. Engng.* 59:1473-1500, 2004.

37. M.Pastor, M.Quecedo, and O.C.Zienkiewicz. A mixed displacement-pressure formulation for numerical analysis of plastic failure. *Computers & Structures*, vol.62, no.1:13-23, 1997.

38. Roger Pierre. Simple C^0 approximations for the computation of incompressible flows. *Comput. Methods Appl. Mech. Engnrg*. 68:205-227,1988.

39. Roger Pierre. Optimal selection of the bubble functions in the stabilization of the P1-P1 element for the Stokes problem. *SIAM Journal on Numerical Analysis*, vol.32, no.4:1210-1224, 1995.

40. M.Quecedo, M. Pastor, O.C.Zienkiewicz. Enhanced linear triangle for plasticity problems in J_2 solids. *Comput.Methods Appl. Mech. Engnrg*. 188:145-163, 2000.

41. J.Rojek, O.C.Zienkiewicz, E.Oñate, R.L.Taylor. Simulation of metal forming using new formulation of triangular and tetrahedral elements. *Metal Forming, Pietrzyk et.al.(eds)©Balkema, Rotterdam, 2000.*

42. J.Rojek, O.C.Zienkiewicz, E.Oñate, E.Postek. Advances in FE explicit formulation for simulation of metal forming processes. Journal of Materials Processing Technology 119:41-47, 2001.

43. Alessandro Russo. Bubble stabilization of finite element methods for the linearized incompressible Navier-Stokes equations. *Comput. Methods Appl. Mech. Engnrg*. 132:335-343, 1996.

44. David Silvester. Optimal low-order finite element methods for incompressible flow. *Comput. Methods Appl. Mech. Engnrg*. 111:357-368, 1994.

45. David Silvester. Stabilized mixed finite element methods. *Numerical Analysis Report No.262*, August 1995.

46. I.M. Smith and D.V. Griffiths. *Programming the finite element method.* John Wiley &Sons, 3rd edition, 1997.

47. R.L.Taylor. A mixed-enhanced formulation for tetrahedral finite elements. *Int. J.Numer. Meth. Engng*. 47:205-227, 2000.

48. P.Thoudtireddy, J.F. Molinari, E.A.Repetto and M.Ortiz. Tetrahedral composite finite elements. *Int. J. Numer. Meth. Engng*. 53:1337-1351, 2002.

49. O.C. Zienkiewicz and R. Taylor. *The finite element method*, vol.1- The Basis, McGraw-Hill, London,5th edition,2000.